ВІСНИК
КИЇВСЬКОГО НАЦІОНАЛЬНОГО УНІВЕРСИТЕТУ ІМЕНІ ТАРАСА ШЕВЧЕНКА

ISSN 1728-2306

РАДІОФІЗИКА ТА ЕЛЕКТРОНІКА 1(25)/2017

Засновано 1999 року

УДК 517

Публікуються результати експериментальних і теоретичних досліджень у галузях фізичної електроніки, фізики плазми, фізики поверхні твердого тіла, емісійної електроніки, кріогенної та мікроелектроніки, нанофізики та наноелектроніки, високотемпературної надпровідності, квантової радіофізики, функціональної електроніки, твердотільної електроніки, мобільного зв'язку, медичної радіофізики, методів отримання діагностичної інформації та її комп'ютерної обробки.

Для науковців, викладачів вищої школи, студентів.

Публикуются результаты экспериментальных и теоретических исследований в областях физической электроники, физики плазмы, физики поверхности твердого тела, эмиссионной электроники, криогенной и микроэлектроники, нанофизики и наноэлектроники, высокотемпературной сверхпроводимости, квантовой радиофизики, функциональной электроники, твердотельной электроники, мобильной связи, медицинской радиофизики, методов получения диагностической информации и ее компьютерной обработки.

Для научных работников, преподавателей высшей школы, студентов.

Experimental and theoretical contributions are published in the following fields: physical electronics, plasma physics, solid-state surface physics, emission electronics, cryogenic electronics, microelectronics, nanophysics and nanoelectronics, high-temperature supercondactive electronics, solid-state electronics, functional electronics, microwave electronics, quantum electronics, mobile communication, medical radiophysics, methods of receipt and computer processing of diagnosis information.

Designed for researches, university teachers, students.

Адреса редколегії	Факультет радіофізики, електроніки та комп'ютерних систем, просп. акад. Глушкова, 4 Г, Київ, Україна, 03127 ☎ (38 044) 526 05 60
Затверджено	Вченою радою факультету радіофізики, електроніки та комп'ютерних систем 14.11.16 (протокол № 3)
Атестовано	Вищою атестаційною комісією України. Постанова Президії ВАК України № 1-05/1 від 10.02.10
Зареєстровано	Міністерством юстиції України. Свідоцтво про державну реєстрацію КВ № 15797-4269Р від 02.10.09
Засновник та видавець	Київський національний університет імені Тараса Шевченка, Видавничо-поліграфічний центр "Київський університет". Свідоцтво внесено до Державного реєстру ДК № 1103 від 31.10.02
Адреса видавця	ВПЦ "Київський університет" (кімн. 43), б-р Т. Шевченка, 14, Київ, Україна, 01601 ☎ (38 044) 239 32 22; факс 239 31 28

BULLETIN

TARAS SHEVCHENKO NATIONAL UNIVERSITY OF KYIV

ISSN 1728-2306

RADIOPHYSICS AND ELECTRONICS 1(25)/2017

Established in 1999

УДК 517

Experimental and theoretical contributions are published in the following fields: physical electronics, plasma physics, solid-state surface physics, emission electronics, cryogenic electronics, microelectronics, nanophysics and nanoelectronics, high-temperature supercondactive electronics, solid-state electronics, functional electronics, microwave electronics, quantum electronics, mobile communication, medical radiophysics, methods of receipt and computer processing of diagnosis information.

Designed for researches, university teachers, students.

Публікуються результати експериментальних і теоретичних досліджень у галузях фізичної електроніки, фізики плазми, фізики поверхні твердого тіла, емісійної електроніки, кріогенної та мікроелектроніки, нанофізики та наноелектроніки, високотемпературної надпровідності, квантової радіофізики, функціональної електроніки, твердотільної електроніки, мобільного зв'язку, медичної радіофізики, методів отримання діагностичної інформації та її комп'ютерної обробки.

Для науковців, викладачів вищої школи, студентів.

Публикуются результаты экспериментальных и теоретических исследований в областях физической электроники, физики плазмы, физики поверхности твердого тела, эмиссионной электроники, криогенной и микроэлектроники, нанофизики и наноэлектроники, высокотемпературной сверхпроводимости, квантовой радиофизики, функциональной электроники, твердотельной электроники, мобильной связи, медицинской радиофизики, методов получения диагностической информации и ее компьютерной обработки.

Для научных работников, преподавателей высшей школы, студентов.

ЗМІСТ

СОДЕРЖАНИЕ

CONTENTS

UDC 539.1.078:621:384.5

I. Dryapachenko, Ph. D.,
O. Kushpij, Postgr.,
V. Ostashko, Ph. D.,
O. Povoroznyk, Ph. D.,
V. Shevel[1], Eng.
Department of Nuclear Reactions,
Faculty of Radiophysics, Electronics and Computer Systems,
Taras Shevchenko National University of Kyiv,
[1]Department of Research Reactor,
Institute for Nuclear Research,
National Academy of Sciences of Ukraine

PRACTICAL NUCLEAR MEDICINE: APPROACH AND REALIZATION WITH USE NEUTRON-PHYSICAL METHODS

In this paper, the authors consider the objective conditions, the necessity and the possibility of systematic, effective application of already tested by them methods of nuclear-physical research on beams of accelerators for the needs of clinical medicine.

Keywords: Accelerator, neutrons, beam therapy, pharmaceutical production, diagnostics

Introduction. This direction of medical-biological research and applications has long been known as nuclear medicine. Already one and a half centuries, nobody has any doubts about the origin of this direction in the *X*-rays of Puluj–Röntgen tubes. We will leaving beyond scope of this article, the of the historical overview of the development of this direction, and only will emphasize that it has always been associated with the most advanced level of development of nuclear physics and biomedical research and their joint use.

The purpose of this work are to draw attention to the possibilities of restoration of previously tested and to implement now at the current level of nuclear physical methods for the medical biological research and their practical application in the diagnosis and treatment of cancer.

Previous experience in the beam oncotherapy with the fast neutrons in Ukraine. If you agree that everything new, as a rule, it is well forgotten, old, then it can start, at least briefly, from what was done forty years ago. According to the initiative and perseverance of the doctor, as we have called him, Victor Letov, at the U-120 cyclotron of the Institute of Nuclear Research of the National Academy of Sciences of Ukraine, it was created a site on the deuterons beam for biomedicine experiments with the fast neutrons. For us, the fundamentalist physicists who had at energy of 15 MeV fast neutron fluxes at that time, it was suggested to participate in these works on the generation and metrology of a stream of the fast neutrons with a twice less of average energy and with order of magnitude higher of intensity. This was done by using a full absorption of a deuteron beam accelerated to energy of 13.6 MeV, in the thick beryllium target [7].

Under objective conditions, the creation of a separate medical-biological site on the cyclotron U-120 (Fig. 1) with several adjacent premises and the head of these works by Professor Vadim Cherednichenko from the Cancer Institute and the doctor of physical and mathematical sciences. Sciences Grigorij Koval, these works acquired a stable algorithm and very soon led to the irradiation of patients with fast neutrons. Up to the Chernobyl Nuclear Power Plant accident in 1986, which "took away" both physicists and physicians, more than two thousand sessions with the fast neutron beam were conducted on this medical-biological complex of the U-120 cyclotron. This statistic includes six hundreds of the real irradiated cancer patients with different types of cancer – the mammary gland, skin, and lungs.

Fig. 1. In the control room Professor Vadym Chernychenko (left) and Chief engineer of the U-120 cyclotron Eugene Belsky (right)

Medical and biological experiments on blood samples and with animals were initiated, which, in turn, prompted further optimization of the nuclear physics technique. It should be emphasized that then it was a question of joining up to the world resonance in nuclear medicine of that time with the use of neutrons, namely, beam therapy for oncotherapy. People on the brink of resistance to the terrible diagnosis were also ready for experimental methods of struggle for life.

The state of affairs in the world. If it is not quite polite but forced skip review of a persistent search by specialists of the improvement of nuclear medicine facilities for thirty years, then specifically with neutrons, this progress led to the rapid development and use of boron neutron capture therapy (BNCT) using the nuclear reaction of ^{10}B (n, α) ^{7}Li.

In 1967 doctor Hiroshi Hatanaka after two years of internship at William Wyatt's lab at the Massachusetts Institute of Technology Hospital, began clinical research and direct application of BNCT in Japan. Then this was done using a collimated stream of epithermal neutrons of the research reactor, where the trepanation of the skull was done in the preparatory surgery, the removal of the available part of the tumor and saturation of its residues with boron-containing drug with the urgent placement of the patient in the chosen geometry near the neutron flux collimator (Fig. 2). One third of patients five years after such a procedure remained alive, and in a few years this share increased to 50 %.

Fig. 2. Scheme of irradiation of the brain tumor by epithermal neutrons of the reactor

In recent years, three centers of BNCT have been put into operation in the country, but not on the basis of the reactor as a source of neutrons, and with using for this (*p*, *n*)-reaction with the energy of accelerated protons little higher than the threshold of this reaction for obtaining low energy neutrons Japan's experience in this area is also interesting because in this high-tech country, large global companies, such as Mitsubishi, Hitachi, embraced the creation of the necessary installations for honor and time at the forefront of science and technology. In other countries, these programs are financed from the state budget. In the world today, there are about a dozen BNCT research centers. Clinical trials have been completed in the United States, Sweden, Finland, the Czech Republic, Argentina, and the European Union (with centered in the Netherlands).

Modern potential opportunities in Ukraine. Returning to our specificity, it is wanted to draw attention to the presence of a unique neutron generator NGP-11 with a current of a beam of deuterons up to two mill amperes in our complex of Institute for Nuclear Research (Fig. 3). This unique installation according to its characteristics, the current of a beam of accelerated hydrogen ions up to 2 mA and a voltage of 250 kV, provides the intensity of the DT-neutron flux to 10^{11} neutrons per second. After commissioning in 1994, apply neutrons were started on this neutron generator, for example, for sterilization of medical materials, processing of polyethylene film, and others like that. It was used for the activation analysis of rocks. Not only from the objective, but, unfortunately, for subjective reasons, work on it has stopped. So far, two or three specialists working with us have successfully operated it twenty years ago. Now we are talking about the possibility of renewal of his work with passport characteristics, which will enable to use it for the needs of nuclear medicine at the world level [5].

Fig. 3. NGP-11 fast neutron generator

Concerning the production of the diagnostic pharmaceutical preparations. With regard to diagnostic problems, then, of course, we mean the possibility of working out radionuclides and the production of pharmaceuticals. Of the 3,000 known natural and artificial radionuclides currently in use, 140 are used in medicine for diagnosis, therapy and disease prevention [4]. Only 10 radionuclides from these 140 are used annually in 90 % of nuclear medicine procedures around the world [9, 6]. First of all, it is Technetium-99, using which every day in the world is conducted from seventy to one hundred thousand scans. Ukraine is now capable of just to import of a dozen or two of the pharmaceutical samples from abroad. This is primarily the localization of tumors in the human body, monitoring cardiac function after a heart attack, mapping the movement of blood in the brain and assisting in surgical intervention [1, 3]. Each year it is approximately 30 million doses with an increase of this amount in the amount of several percent per year [8]. The "power" of each dose of ^{99m}Tc is about 20 mCi at a current price of one dose of about $40. But there is existing already for several years in the Institute for Nuclear Research at on the research reactor WWR-M a well-established technological chain of production of prepackaged dasg samples [10].

The received radiopharmaceutical (Na99mTcO4 solution) passed pre-clinical trials with animals at the Institute of Oncology of the Academy of Medical Sciences of Ukraine. These were packed out in sterile vials (Fig. 4) with an activity of 96.0 MBq / 5 ml. The results of the research have shown the conformity of the characteristics of the preparation with the requirements of normative documents for medicinal preparations.

Fig. 4. Package containing 99 mTs pertechnetate radiopharmaceutical: Na^{99m}TcO4 bottle with solution and transport protective container (body and cover)

Up to now, the main source of nuclides ^{99}Mo / ^{99m}Tc is the fission of ^{235}U reaction by neutrons in a nuclear reactor. The use of high-enriched uranium, as well as low enriched, for this purpose is already being worked out [2]. Similar technologies are also possible using on subcritical installations and with the accelerators of charged particles as a source of neutrons [11].

Conclusion. Over the past thirty years, the irrepressible search and unceasing progress have given nuclear medicine hadrons therapy on synchrotrons, specialized medical cyclotrons, brachytherapy and its "neutron" variant – boron-neutron capture therapy.

It should be considered as the closest to the implementation and long-term perspective for the nuclear-physical methods of treatment of cancer by using the infrastructure of the Institute for Nuclear Research in Kyiv. There is no doubt that, like in other nuclear-physical centers of the world, there is already a whole spectrum of diverse sources of radiation and appropriate infrastructure (premises, biological protection, beam transportation systems, etc.) in the

KINR for authorized maintenance of these works. For example, the nuclear-technological requirements known today for the neutron spectrum – their energy in the range of 2–6 MeV – are determined by the average length of the neutron run in biological tissues, which will be optimal for the necessary neutron thermalization in the required city of the human body.

The further development of these works is necessitated of need by the development and implementation of mobile neutron sources for the distribution of the necessary nuclear medical technologies outside near the powerful, but exclusive, nuclear centers.

REFERENCES

1. Charged particle cross-section database for medical radioisotope production: diagnostic radioisotopes and monitor reactions // IAEA-TECDOC-1211, Vienna, 2001.

2. Medical Isotope Production without Highly Enriched Uranium / Committee of the US National Academies of Science // The National Academies Press, Washington, D.C., 2009.

3. Evaluation of 99mTc-glucarate as a breast cancer imaging agent in a xenograft animal model / P.J. Gambini , P. Cabral et al. // Nuclear Medicine and Biology. – Vol. 38. – P. 255.

4. *Groth S.* Nuclear application in health care-lasting benefits / S. Groth // IAEA Bulletin. – Vienna, 2000. – Vol. 42, № 1.

5. *Grynevych Yu.P*. Practychna onkoterapiya na puchku shvydkykh nejtroniv cyclotrona U-120 / Yu.P. Grynevych, I.P. Dryapachenko // Visnyk Nacionalnoj Akademii nauk Ukrainy. – 2005. – № 10. – P. 39–47.

6. International atomic energy agency. Nuclear technology review / Annex VIII : Production and supply of Molybdenum-99 : IAEA/NTR/2010, Vienna, 2010. – P. 150–167.

7. *Letov V.N.* Fizicheskie i radiobiologicheskie charakteristiki puchka bystrykh nejtronov cyclotrona U-120 / V.N. Letov, V.V. Fesenko, S.M. Ievlev, E.M. Belskij, I.P. Dryapachenko, V.N. Khrapachevskij, V.M. Pasechnik // Medicinskaya radiologiya, 1977. – № 10. – P. 34–40.

8. *Ross C.K.* Predictions regarding the supply of 99Mo and 99mTc when NRU ceases production in 2018 / C.K. Ross and W.T. Diamond // June 2015. http://www.researchgate.net/publication/279309765

9. *Ruth T.* Accelerating production of medical isotopes / T. Ruth // Nature, Vol. 457, January 2009. – P. 29.

10. *Shevel V.N.* // International Nuclear Safety Journal, 2014. – Vol. 3. – N 2. – P. 43–48.

11. *Talamo A.* Radioactive isotope production for medical applications using Kharkov electron driven subcritical assembly facility / A. Talamo, Y. Gohar and N.E. Division // ANL-07/18, Argonne National Laboratory, 2007.

Submitted on 06.12.17

І. Дряпаченко, канд. фіз.-мат. наук,
О. Кушпій, асп.,
В. Осташко, д-р фіз.-мат. наук,
О. Поворозник, д-р фіз.-мат. наук,
В. Шевель[1], інж.,
відділ ядерних реакцій,
[1]відділ дослідницького реактора
Інститут ядерних досліджень
Національна Академія наук України, Київ

ПРАКТИЧНА ЯДЕРНА МЕДИЦИНА: ПІДХІД ТА РЕАЛІЗАЦІЯ З ВИКОРИСТАННЯМ НЕЙТРОННО-ФІЗИЧНИХ МЕТОДИК

Розглянуто об'єктивні умови, необхідність і можливості системної, результативної прикладної реалізації апробованих авторами методик ядерно-фізичних досліджень на пучках прискорювачів для потреб клінічної медицини.

Ключові слова: прискорювач, нейтрони, пучкова терапія, виробництво фармпрепаратів, діагностика.

И. Дряпаченко, канд. физ.-мат. наук,
А. Кушпий, асп.,
В. Осташко, д-р физ.-мат. наук,
О. Поворозник, д-р физ.-мат. наук,
В. Шевель[1], инж.,
отдел ядерных реакций,
[1]отдел исследовательского реактора
Институт ядерных исследований,
Национальная Академия наук Украины, Киев

ПРАКТИЧЕСКАЯ ЯДЕРНАЯ МЕДИЦИНА: ПОДХОД И РЕАЛИЗАЦИЯ С ИСПОЛЬЗОВАНИЕМ НЕЙТРОННО-ФИЗИЧЕСКИХ МЕТОДИК

Рассмотрены объективные условия, необходимость и возможности системной, результативной прикладной реализации ранее апробированных авторами методик ядерно-физических исследований на пучках ускорителей для нужд клинической медицины.

Ключевые слова: ускоритель, нейтроны, пучковая терапия, производство фармпрепаратов, диагностика.

UDC 621.315.592

V. Verbitskiy, Dr. Sci.,
Department of Physical Electronics,
Faculty of Radiophysics, Electronics and Computer Systems,
National Taras Shevchenko University of Kyiv

ANALYSIS OF HETEROGENEOUS THERMOCHEMICAL AND THERMOPHYSICAL PROCESSES OF THE ION DEPOSITION OF TWO-COMPONENT FILMS

One of the problems in modern integrated circuits technology is the creation of proper interconnects between the elements on the chip. If doped polysilicon is used for this purpose, the high frequency response of the circuits turns out to be poor due to electrical resistance being not low enough even for high doping levels. This problem can be solved by an additional layer of titanium silicide above the polysilicon, which creates a much lower resistance in parallel (policide structure formation) and preserves the charged state of the gate stack structure.

Keywords: silicon, titanium, silicide, ion bombardment, heterogeneous reaction.

Introduction. A traditional route to obtain a silicide film involves a high temperature annealing (up to 1070 K) which can alter the dopants distribution in the active region of already existing transistors of the integrated circuit (IC). Therefore, we suggest an alternative technological procedure which does not involve such high temperature thermal exposure. In essence, the silicide film is formed due to titanium ion bombardment of the film's material condensing from the vapors coming from two independent evaporation sources.

The goals of the present work included considering the mechanisms of the ion bombardment influence on the surface of condensing material, determining the major parameters of the silicide formation process, estimating the influence of activation energy on the interatomic interaction during deposition of the two component film.

Experimental. The formation of titanium silicide films is carried out by thermionic deposition from two independent sources. At the same time, the vapors are partially ionized. Our process parameters are the following:

the stream of neutral atoms:

$$n_a = (0.45 \div 1.45) \cdot 10^{16} \text{cm}^{-2}\text{c}^{-1};$$

the ion flow:

$$n_i = (0.1 \div 0.35) \cdot 10^{16} cm^{-2} c^{-1};$$

intensity of ion bombardment:

$$\frac{n_i}{n_a} = 0.07 \div 0.24;$$

energy:

$$E_{iu} = (0.18 \div 1.44) \cdot 10^{-16} J = (1.01 \div 1) \cdot 10^3 eV;$$

pressure in a vacuum chamber:

$$P = (1.3 \cdot 10^5 \div 6.7 \cdot 10^{-7}) mmHg;$$

temperature of the film:

$$T = (400 \div 800)^{\circ} C.$$

The conditions given above are rather typical and can be easily realized using standard process equipment as used in modern microelectronics production technology.

Process Mechanisms. Let us consider the elementary steps of the technological process leading to a thin film of titanium disilicide. A variety of thermochemical processes can occur on the surface of the film, depending on whether ionization of the vapor occurs or is absent. If the fluxes of atoms are neutral, then the following processes are possible: various degrees of oxidation of silicon or titanium, as well as condensation of silicon or titanium. Various degrees of oxidation can produce either monooxides of silicon or titanium or their full stehiometric dioxides. All these possibilities are summarized in (1).

$$\begin{aligned}
&(\text{Si}) > \rightarrow < \text{Si} >, \\
&2 < \text{Si} > + (\text{O}_2) \rightarrow 2 < \text{SiO} >, \\
&2 < \text{SiO} > + (\text{O}_2) \rightarrow 2 < \text{SiO}_2 >, \\
&< \text{Si} > + (\text{O}_2) \rightarrow < \text{SiO}_2 >, \\
&(\text{Ti}) > \rightarrow < \text{Ti} >, \\
&2 < \text{Ti} > + (\text{O}_2) \rightarrow 2 < \text{TiO} >, \\
&2 < \text{TiO} > + (\text{O}_2) \rightarrow < \text{TiO}_2 > \\
&< \text{Ti} > + (\text{O}_2) > \rightarrow < \text{TiO}_2 >
\end{aligned} \quad (1)$$

Note: brackets < > mean that the substance is in a solid state, brackets ( ) designate the substance in a gaseous state. As an example, consider a reaction of the oxidation of silicon:

$$< \text{Si} > + (\text{O2}) > \rightarrow < \text{SiO2} >. \quad (2)$$

In accordance with the general principles of thermochemistry for changing of free energy of this reaction ΔF we can write

$$\Delta F = \Delta F_1 - \Delta F_2. \quad (3)$$

Here the ΔF_1 is the free energy of creating the reaction products, ΔF_2 is the free energy of the initial reactants. On the other hand, the expression for ΔF has the following form:

$$\Delta F = -RT \ln K_p = -4.576 \ln K_p \quad (4)$$

with K_p being the equilibrium constant of the reaction. For this reaction K_p will be equal to $P_{(O2)}$ – the oxygen pressure, at which the reactions of silicon oxidation and decomposition of the oxide are in equilibrium. Taking into account that the free energy of creation of pure substances in thermochemical calculations is taken equal to 0, we can write

$$\Delta F = \Delta F_{SiO2} = 4.576 T \lg P_{O2}. \quad (5)$$

From the previous, it follows that:

$$\lg P_{(O_2)} = \frac{\Delta F_{<SiO_2>}}{4{,}576T}. \quad (6)$$

Taking the value of free energy for silicon dioxide from the standard tables of thermochemical data, we have for the temperature range from 289 K to 1700 K:

$$\lg P_{(O_2)} = -\frac{45500}{T} + 9.5. \quad (7)$$

The generalized dependence of the equilibrium pressure of oxygen on temperature can be represented by a graph in Fig. 1, from which it can be seen that for temperature range from 400 K to 800 K and pressure range from $1.3 \cdot 10^{-5}$ mmHg to $6.7 \cdot 10^{-7}$ mmHg there will be an oxidation reaction of Si, as well as oxidation of Ti. These reactions will block the reactions of silicide formation.

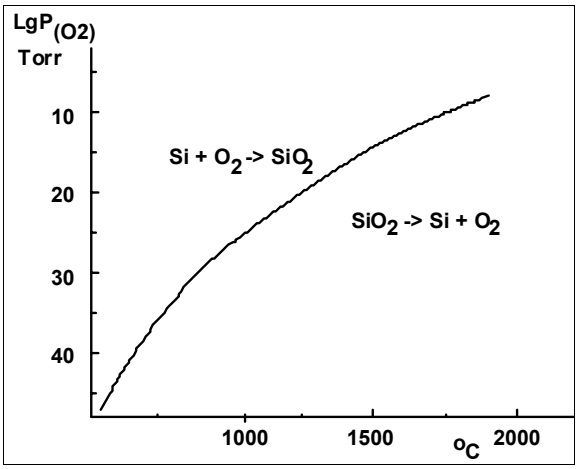

Fig. 1. Pressure vs temperature for oxygen reacting with silicon

In order to avoid blocking pressures (or at least to significantly reduce their influence) the temperature must be increased, possibly close to the melting point of Si ($T_{пл}$ = 1400°C), and the pressure reduced to P~10^{-10}–10^{-12} mmHg. A similar result can be achieved without lowering the pressure or raising the temperature if the atomic flux of Ti is partially ionized and accelerated ions irradiate the growing film. In this case, a high non-stationary local temperature will arise at the sites where the ions hit, which promotes the decomposition of oxides, as well as the desorption of harmful impurities and decomposition products. In addition, ion bombardment itself should facilitate the above processes due to ion sputtering. To estimate the emerging temperatures, it is necessary to determine the effective (averaged) physical parameters of the substance in which local thermal fields appear and the parameters of the process of interaction of the Ti ion with the bombarded substance.

Let the following be the blocking processes of silicide formation

$$< Si > +(O_2) \rightarrow < SiO_2 >,$$
$$2 < TiO > +(O_2) \rightarrow 2 < TiO_2 > \quad (8)$$

where silicon dioxide and titanium dioxide are formed each with a 50 % share. Let's calculate the effective charge Z and the effective mass M of the averaged atom of the mixture of these oxides:

$$Z = \frac{(Z_{Si} + 2Z_0 + Z_{Ti} + 2Z_0)}{6} = \frac{(14 + 2\cdot 8 + 22 + 2\cdot 8)}{6} = 11.3 \quad (9)$$

$$M = \frac{(M_{Si} + 2M_O + M_{Ti} + 2M_O)}{6} = \frac{(28.1 + 2\cdot 16 + 47.9 + 2\cdot 16)}{6} = 23.33 \quad (10)$$

If an ion of Ti (Z = 22, M = 47.9) falls along the Z axis on the surface of a certain substance with Z=11.3 and M =23.3 then according to the formula for energy loss, we have

$$(\frac{dE_i}{dZ}) = 0.278 \cdot \frac{Z_{Ti}\cdot Z}{(Z_{Ti}^{\frac{2}{3}} + Z^{\frac{2}{3}})^{\frac{1}{2}}} \cdot \frac{M_{Ti}\cdot N}{M_{Ti} + M} \cdot \frac{eV}{nm}, \quad (11)$$

where $N \approx 5\cdot 10^{22} cm^{-3}$. Then, one can write $(\frac{dE_i}{dZ})_n = 650\frac{eV}{nm} = 650\cdot 10^7 \frac{eV}{cm}$, and as we can see, the $(\frac{dE_i}{dZ})_n$ has the dimension of force. Respectively for the range of ion in matter, we have

$$R_n = \frac{E_{iO}}{(\frac{dE_i}{dZ})_n} = \frac{10^3 eV}{650\frac{eV}{nm}} = 1.54\cdot 10^{-7} cm,$$

where E_{iO} is the initial energy of the Ti ion ($E_{iO} = 10^5 eV$). Since the lattice constant of the substance (for example, Silicon) has a value of roughly 5 nm, the ion with energy $E_{iO} = 1000 eV$ actually penetrates into the film to a depth of the order of several atomic layers. In this case it is provided that the main losses are the elastic interaction of the ion with the atomic electric charges.

Let us estimate the interaction time of the Ti ion with the substance of the film, for which we use the law of conservation of momentum with the condition that the ion in the film will be decelerated and stop completely (reflections, scattering into vacuum, etc. are excluded).

$$F\,\Delta t = M_{Ti}\,\Delta V, \quad (12)$$

where F – braking force; $F = (\frac{dE_i}{dz})_n$ Δt – braking time; ΔV – loss of speed during the energy exchange. Then

$$\Delta t = \frac{(2E_{i0}\cdot M_{Ti})^{1/2}}{(\frac{dE_i}{dZ})_n} \approx 5\cdot 10^{-14} s. \quad (13)$$

Thus, in the local region near the surface of our film, which has a size of $1.54\cdot 10^{-7}$ cm there will be an influx of energy in the keV range during the time of $5\cdot 10^{-14}$ s (the time commensurate with the period of thermal vibrations of the lattice). If we accept that kT is equal to 10^3eV and the energy Φ of the chemical bond in SiO_2 or TiO_2 as well as the energies of physical (chemical) adsorption of O_2, O, N, H_2, OH, CH and so on, do not exceed several electron-Volts or even a fraction of eV, then the probability of destruction of the indicated bonds and subsequent desorption is

$$W \sim e^{-\frac{\Phi}{KT}} = e^{-\frac{1}{10^8}} = 1. \quad (14)$$

A more specific estimate of the local temperature arising in the zone of action of a single ion is possible from the solution of the corresponding heat equation:

$$T(x,y,z,t,\zeta,\eta,\chi) = \frac{Q}{C\rho}(\frac{1}{2\cdot(\pi\cdot a^2\cdot t)^{1/2}})^3 \times \exp(\frac{-\{(x-\zeta)^2+)(y-\eta)^2+(z-\chi)^2\}}{4\cdot a^2\cdot t}) + T_0 \quad (15)$$

where T is the temperature (in Celsius) at a point (x, y, z) at the moment of time t, caused by a point heat sink Q, that is located at the point of the medium (ξ,η,χ) at the zeroth point of time. Further, here: $a^2 = \frac{\lambda}{C\rho}$, and (α, C, ρ) are film's material properties: thermal conductivity, specific heat and density, T_O is the initial temperature of the film. If an instantaneous point source is placed at the origin of coordinates $\xi,\eta,\chi = 0$, then the expression is simplified to the following:

$$T(x,y,z) = \frac{Q}{C\rho}(\frac{1}{2\cdot(\pi\cdot a^2\cdot t)^{1/2}})^3 \times \exp(\frac{-(x^2+y^2+z^2)}{4\cdot a^2\cdot t}) + T_0 \quad (16)$$

Since we assumed that SiO_2 and TiO_2 oxides are formed in the one to one ratio under the low-vacuum and

low-temperature conditions, then it is necessary to determine the average thermos-physical characteristics of such material at an average temperature T_O being equal to 550°C (823 K). In accordance with the reference data for SiO_2 and TiO_2 we have:

$$\lambda_{SiO_2} = 0.005 cal \cdot cm^{-1} \cdot s^{-1} \cdot gr^{-1};$$

$$c_{SiO_2} = 0.231 cal \cdot g^{-1} \cdot gr^{-1};$$

$$\rho_{SiO_2} = 2.3 g \cdot cm^{-3};$$

$$a^2_{SiO_2} = 9.41 \cdot 10^{-3} cm^{-2} \cdot s^{-1} (theory);$$

$$a^2_{SiO_2} = 6 \cdot 10^{-3} cm^{-2} \cdot s^{-1} (\exp erimental);$$

$$\lambda_{TiO_2} = 0.0088 cal \cdot cm^{-1} \cdot s^{-1} \cdot gr^{-1};$$

$$\rho_{TiO_2} = 4.2 g \cdot cm^{-3};$$

$$a^2_{TiO_2} = 0.0099 cm^{-2} \cdot s^{-1} (theory);$$

The averaged thermos-physical characteristics are:

$$\rho = (\rho_{SiO_2} + \rho_{TiO_2})/2 = 3.25 g \cdot cm^{-3};$$

$$\lambda = (\lambda_{SiO_2} + \lambda_{TiO_2})/2 = 0.0069 cal \cdot cm^{-1} \cdot s^{-1} \cdot gr^{-1};$$

$$a^2 = (a^2_{SiO_2} + a^2_{TiO_2})/2 = 0.00965 cm^{-2} \cdot s^{-1};$$

The calculation of the temperature for the above given thermos-physical characteristics of the film at Q taken as 10^3eV ($0.38 \cdot 10^{-16}$ cal), and time interval Δt taken as $5 \cdot 10^{-14}$s gives the following results:

$$T(0,0,\Delta t) = 112500 + T_0 = 113050^\circ C;$$

$$T(0,0,Rn/2,\Delta t) = 8882.6 + T_0 = 9432.6\ ^\circ C;$$

$$T(0,0,Rn,\Delta t) = 0.518 T_0 = 550^\circ C;$$

Thus, instantaneous temperatures of several tens of thousands of degrees and significant spatial temperature gradients are observed in the ion-film interaction zone. It should be noted that in this case we are not talking about temperature as a characteristic of an equilibrium thermodynamic process. The point is that we use spatial (Rn) and temporal (Δt) intervals of ~$1.54 \cdot 10^{-7}$ cm and ~$5 \cdot 10^{-14}$s correspondingly, as well as the temperature values of ~10^5 Celsius, under which the traditional concept of heat conduction, heat capacity, density of a substance, etc. are being used. The obtained temperatures to some extent characterize only the energy of the procuring processes. Therefore, estimates similar to those given above can only be used for general orientation. It follows from the carried calculations that the irradiation by ions of the film's material under the influence of considerable nonstationary temperatures and spatial temperature gradients, the oxidation reactions (1) can become inverse:

$$< SiO_2 > \rightarrow < Si > + (O_2)$$

$$< TiO_2 > \rightarrow < Ti > + (O_2)$$

with the release of gaseous products (in this case oxygen), thereby eliminating or reducing the factors that block the process of silicide formation.

Let us consider the process of interaction of incident Ti ions with a substrate's substance at the atomic level. We will dwell on the mechanical oscillations of the averaged atom of the substrate under the action of an instantaneous impact. The equation of motion of the atom has form:

$$M \cdot \ddot{Z} + H \cdot \dot{Z} + K \cdot Z = I \cdot \delta(t - \tau), \quad (17)$$

where Z – the deviation of an atom by a mass M from its equilibrium position, H – the coefficient of friction (if there is a dissipation), K – the elasticity coefficient of the restoring force (this force is assumed to be proportional to the deflection of the atom), I – momentum of the incident ion, and $\delta(t-\tau)$ is the Dirac's delta-function. The initial conditions are:

$$Z|_{t=t0} = 0. \quad (18)$$

The impact occurs at the moment τ, and the observation time from t_0 to infinite future. At the moment between t_0 and τ there was no movement of the atom, therefore Z remains zero for all such moments. Integrating the differential equation we obtain:

$$M(Z|_{\tau+0} - Z|_{\tau-0}) + K \cdot \int_{\tau-0}^{\tau+V} Z dt = I \cdot \int_{t-0}^{\tau+V} \delta(t-\tau) dt. \quad (19)$$

Next we have:

$$\dot{Z}|_{\tau+0} = \frac{1}{M} \text{ and } Z_{\tau+0} = 0. \quad (20)$$

Thus at times greater than τ the external excitation force is absent and it is necessary to find the solution of the homogeneous equation:

$$M \cdot \ddot{Z} + H \cdot \dot{Z} + K \cdot Z = 0$$

under the initial conditions (20). The general solution of this equation has form:

$$Z = C_1 e^{b_1 t} + C_2 e^{b_2 t}, \quad (21)$$

where b_1 and b_2 are the roots of the characteristic equation:

$$Mb^2 + Hb + K = 0, \quad (22)$$

$$b_{1,2} = \frac{-H \pm \sqrt{H^2 - 4MK}}{2M}. \quad (23)$$

Substituting the boundary conditions (20) into (21), we obtain:

$$\begin{cases} C_1 \cdot e^{b_1 \tau} + C_2 e^{b_3 \tau} = 0 \\ C_1 \cdot b_1 \cdot e^{b_1 \tau} + C_2 . b_2 \cdot e^{b_2 \tau} = M^{-1} \end{cases},$$

$$C_1 = \frac{I}{M(b_1 - b_2)} \cdot e^{-b_1 \tau};\ C_2 = \frac{-I}{M(b_1 - b_2)} \cdot e^{-b_2 \tau}. \quad (24)$$

Thus, the solution of the equation has the form:

$$\begin{cases} 0, t_0 < t < 0 \\ Z = \dfrac{I}{M(b_1 - b_2)} \cdot [e^{b_1(t-\tau)} - e^{b_2(t-\tau)}], 0 < t < \infty \end{cases}. \quad (25)$$

Or at the limit of $\tau \to 0$:

$$\begin{cases} 0, t_0 < t < 0 \\ Z = \dfrac{I}{M(b_1 - b_2)} \cdot [e^{b_1 t} - e^{b_2 t}], 0 < t < \infty \end{cases}. \quad (26)$$

If the friction is negligible, which is the case when H^2 is smaller than 4MK, we have:

$$b_{1,2} = -\frac{H}{2M} \pm J\sqrt{\frac{K}{M} - \frac{H^2}{4M^2}} = -\gamma \pm j\omega, \quad (27)$$

$$\gamma = \frac{H}{2M},\ \omega = \sqrt{\frac{K}{M} - \frac{H^2}{4M^2}}.$$

Then it follows:

$$Z = \frac{I}{M} \cdot \frac{e^{-\gamma t}}{\omega} \cdot \frac{e^{j\omega t}}{2j} \cdot \frac{e^{j\omega t} - e^{-j\omega t}}{2j} = \\ = \frac{I}{M} \cdot \frac{e^{-\gamma t}}{\omega} \cdot \sin \omega t \quad (28)$$

where ω is the circular frequency of the natural vibrations of an atom, as determined by the absorption spectrum (in the case of SiO_2, the value of λ is ca. 4 μm. In this case, the fluctuation period Δt is equal to $1.38 \cdot 10^{-14}$ s. The function $Z(t)$ gives a description of the natural oscillations of the averaged atom of mass M elastically attached to other similar

atoms in the environment with friction, if an ion deceleration pulse was transmitted to this atom at the zero point in time. In our case, this is Ti ion with momentum equal to

$$I = \frac{dE}{dZ}\Delta t = 650 \times 10^7 eV \cdot cm^{-1} \cdot 5 \cdot 10^{-14} s .$$

In the absence of friction (for simplicity) γ = 0 and for the amplitude of the natural oscillations, we have:

$$A = \frac{I}{M \cdot \omega} = 2.75 \cdot 10^{-8} cm .$$

If we take into account that the atom with mass M (23.33) is transferred from ion with mass M_{Ti} (47,9) not by the whole pulse, but only its part

$$\alpha = \frac{2M}{(M + M_{Ti})} = 0.6$$

then the deviation (amplitude) is: $A = 0.6 \times 2.75 \cdot 10^{-8} cm$.

Thus, under the influence of an instantaneous impact, the atom shifts from the equilibrium position to 1.6 Angstrom, almost 30 % of the period of the crystal lattice, which can lead to the rupture of the bonds (physical, chemical, etc.) of such an atom with the medium and desorption into the surrounding space.

Let us estimate the energy of the vibrational motion of an atom. At any moment of time, if there are no braking processes, it is the sum of the kinetic and potential energy:

$$E = \frac{MV^2}{2} + \frac{MZ^2}{2} = \frac{1}{2}(MZ^2 + KZ^2) . \qquad (29)$$

Further, due to obvious equality

$$Z = \frac{\alpha I}{M\omega} \cdot \sin \omega t \qquad (30)$$

We have:

$$\dot{Z} = \frac{\alpha I}{M} \cdot \cos \omega t ,$$

$$\dot{Z}^2 = (\frac{\alpha I}{M})^2 \cdot \cos^2 \omega t , \qquad (31)$$

$$Z = (\frac{\alpha I}{M\omega})^2 \cdot \sin \omega t .$$

So, with K and M being an effective stiffness and an effective mass of the oscillator and assuming no friction, we arrive at the following expression for E:

$$E = \frac{1}{2}[M(\frac{\alpha t}{M})^2 \cdot \cos^2 \omega t + \\ + \frac{K}{2\omega} \cdot (\frac{\alpha I}{M})^2 \cdot \sin^2 \omega t] = \frac{1}{2} \cdot \frac{(\alpha I)^2}{M} \qquad (32)$$

That is, the energy of oscillations of an atom in the absence of friction is constant

$$E = \frac{1}{2}\frac{\alpha^2 I^2}{M} = const . \qquad (33)$$

For our conditions, this energy is equal to 776 eV, corresponding to a temperature of ~10^7 K. The considerable energy of the atomic oscillations, in our opinion, will help to break the bonds of the atom with the film's medium formed on the surface of the target. It should be noted that the estimates obtained above are obtained under the condition that the transfer of energy from the ion to an atom occurs at the expense of a direct (central) elastic impact. It is more likely that energy losses are due to several (dozens of) indirect impacts. This can significantly reduce (by 1–2 orders of magnitude) the energy of atomic vibrations, although it remains more than sufficient to destroy interatomic bonds.

Conclusion. Our analysis of the heterogeneous processes during ion deposition of the binary thin films indicates that even small ion energies (up to 100 eV) can stimulate the silicide formation by shifting the atoms as far as 0.16 nm within the crystalline grating (up to 30 % of the crystal periodicity) leading to breaking of chemical bonds, displacement and desorption of the deposited atoms including the undesired impurities on the film's surface.

REFERENCES

1. *Sade G.* Titanium silicide formation in bilayer barrier structure / G. Sade, J. Pelleg, V. Ezersky // Microelectronic Engineering, 1997. – Vol. 33, Is. 1–4. – P. 317–323.

2. *Tung R.T.* Epitaxial silicide interfaces in microelectronics / R.T. Tung, S. Ohmi // Thin Solid Films, 2000. – Vol. 369, Is. 1-2. – P. 233–239.

3. *Zhang S., Östling M.* Metal Silicides in CMOS Technology: Past, Present, and Future Trends / S. Zhang, M. Östling // Critical Reviews in Solid State and Materials Sciences, 2003. – Vol. 28, Is. 1. – P. 1–129.

Submitted on 06.12.17

В. Вербицький, д-р фіз.-мат. наук,
кафедра фізичної електроніки,
факультет радіофізики, електроніки та комп'ютерних систем,
Київський національний університет імені Тараса Шевченка

АНАЛІЗ ГЕТЕРОГЕННИХ ТЕРМОХІМІЧНИХ ТА ТЕРМОФІЗИЧНИХ ПРОЦЕСІВ ІОННОГО НАПОРОШЕННЯ ДВОКОМПОНЕНТИХ ПЛІВОК

Однією з проблем сучасної технології інтегральних електронних схем є створення високоякісних міжелементних з'єднань на кристалі. При використанні полікремнію високочастотний відгук схеми виявляється незадовільним через високий електричний опір, навіть для високих рівнів легування. Ця проблема може бути розв'язана шляхом створення додаткового шару силіциду титану зверху полікремнію, що створює додатковий значно нижчий опір, підключений паралельно (формування поліцидної структури), а також зберігає зарядовий стан структури затворного стеку.

Ключові слова: кремній, титан, силіцид, іонне бомбардування, гетерогенна реакція.

В. Вербицкий, д-р физ.-мат. наук,
кафедра физической электроники,
факультет радиофизики, электроники и компьютерных систем,
Киевский национальный университет имени Тараса Шевченко

АНАЛИЗ ГЕТЕРОГЕННЫХ ТЕРМОХИМИЧЕСКИХ И ТЕРМОФИЗИЧЕСКИХ ПРОЦЕССОВ ИОННОГО НАПылЕНиЯ ДВОхКОМПОНЕНТныХ ПЛёНОК

Одной из проблем современной технологии интегральных электронных схем есть создание высококачественных межэлементных соединений на кристалле. В случае использования поликремния, высокочастотный отзыв схемы оказывается неудовлетворительным из-за высокого электрического сопротивления даже для высоких уровней легирования. Эта проблема может быть решена путём создания дополнительного шара силицида титана поверх поликремния, что создаёт дополнительное параллельно подключённое, значительно более низкое сопротивление (формирование полицидной структуры), а также сохраняет зарядное состояние структуры затворного стека.

Ключевые слова: кремний, титан, силицид, ионное бомбардирование, гетерогенная реакция.

UDC 533.951.2, 533.9.02

A. Goncharov, Dr. Sci.,
V. Tsiolko, Ph. D.,
A. Dobrovol'skii, Ph. D.,
V. Bazhenov, Ph. D.,
I. Litovko[1], Ph. D.
Institute of Physics, National Academy of Sciences of Ukraine, Kyiv,
[1]Institute of Nuclear Researches, National Academy of Sciences of Ukraine, Kyiv

NEW GENERATION PLASMADYNAMICAL SYSTEMS WITH FAST ELECTRONS

Brief review of an ongoing research and development of the novel generation plasmaoptical tools based on the axial-symmetric cylindrical electrostatic plasma lens configuration and the fundamental plasmaoptical principles of magnetic electron isolation and equipotentialization magnetic field lines is presented. As an related to this system, the tool based on the hollow cathode effect is also considered. Practical application of the proposed plasmaoptical tools with fast electrons for essential improvement of deposited film surface quality by means of efficient removal of microdroplet fraction from dense metal plasma flows formed by erosion vacuum arc sources is considered theoretically and demonstrated experimentally.

Keywords: plasmadynamics, plasmaoptics, plasma lens, hollow cathode, gas discharge, fast electron flow.

Introduction. High-current neutralized charged particle beams (positive, negative ions and electrons) and energetic ion-plasma flows are used widely for basic research and high-technology applications, for example, in heavy fusion research, high current linear accelerators, spacecraft control systems, high dose ion implantation for material surface modification and ion-plasma treatment.

The fundamental concept of the new generation plasma devices is based on application of cylindrical plasma lens (PL) configuration and plasma-optical principles of magnetic insulation electrons and maintain the magnetic field lines as equipotentials ("equipotentialization") for the control of electrostatic fields introduced into the plasma medium for manipulating non-magnetized ions. This plasma-optical concept was first described by Morozov [10, 11]. These early contributions also clarified the essential advantages of electrostatic plasma lens as compared with the more traditional electrostatic and magnetic lenses. Note also the experiments have demonstrated plainly that the optical strength of the plasma lens can be up to two orders of magnitude greater than for an Einzel lens and up to four orders of magnitude greater than for a magnetic lens under the same experimental conditions. This lens is well-explored tool for focusing high-current, large area, energetic heavy ion beams [3, 5], where the concern of beam space charge neutralization is critical. The crossed electric and magnetic fields inherent to the plasma lens configuration provide the suitable method for establishing a stable plasma discharge at low pressure. Using plasma lens configuration in this way, a number of low maintenance, cost effective and high reliability plasma generation devices using permanent magnets and possessing considerable flexibility towards spatial configuration were developed [6]. These kinds of devices are part of a larger class of plasma devices (plasma accelerators, magnetrons, jet propulsions, magnetically insulated diodes) that use a discharge in crossed electric and magnetic fields with closed electron drift for the production, formation and manipulation of high current beams and ion-plasma flows. In these conditions, the variation of the magnetic field line configuration within device volume and the distribution of electric potential enable the formation and control of high current ion beams while maintaining their quasi-neutrality. This makes attractive the practical applications of such devices. They can be operated as stand-alone instrumentation, for example for liquid crystal alignment on large-area substrates, or as part of an integrated processing system together with magnetron sputtering, for example, for deposition of spectrally-selective coatings on industrial glass. These devices can be applied both for fine ion cleaning, polishing and activation of substrates before deposition, including synthesis new nanomaterials and exotic coatings.

One particularly interesting result of these basic researches was observation of the essential positive potential at the floating substrate. This suggested to us the possibility of an electrostatic plasma lens for focusing high-current beams of negatively charged particles, electrons and negative ions, based on the use of the dynamical cloud of positive space charge under magnetic isolation electrons [7, 8]. The experimental results demonstrate an attractive possibilities application positive space charged plasma lens with magnetic electron insulation for focusing and manipulating wide aperture high-current no relativistic electron beams. For relatively low-current mode, for which electron beam space charged less than positive space charged plasma lens, it realizes electrostatic focusing of passing electron beam. In case of high-current mode when electron beam space charge is much more, than space charge plasma lens, the lens operates in plasma mode to create transparent plasma accelerating electrode and compensate space charge propagating electron beam.

We describe also the original approach for effective additional elimination of microdroplets in a dense flow of cathodic arc plasma [9]. This approach is based on application of the cylindrical plasma lens configuration for introducing at volume of propagating along axis's dense low temperature plasma flow convergent radially energetic electron beam is generated self-consistently by ion–electron secondary emission from electrodes of plasmaoptical tool. The theoretical estimations and experimental demonstrations that have been carried out at the Institute of Physics NASU provide confidence and optimism that proposed idea for removal and clearing the micro droplet component from dense, low-temperature metal plasma has the high practical potential for elaboration novel state-of-the-art plasma processing for the filtering of microdroplets (or their reduction to the nanoscale) from the dense plasma formed by erosion plasma sources like vacuum arc and laser produced plasma, without losses of plasma production efficiency.

Basic plasmaoptical principles. The fundamental plasma optical principles are based on using of magnetically insulated cold electrons (i. e., transverse mobility << parallel mobility) to provide space charge neutralization of the focused high-current ion beam and maintain the magnetic field lines as equipotentials ("equipotentialization"). This means that value of the magnetic field is those, that the following inequalities are correct $\rho_{He} << D << \rho_{Hi}$, where ρ_{He} and ρ_{Hi} are the electron and ion Larmor radiuses, D is typical system size.

The electrostatic plasma lens is an axially-symmetric plasma-optical device with a set of cylindrical ring electrodes located within the magnetic field region, with magnetic field lines connecting ring electrode pairs symmetrically about the lens mid-plane (Fig. 1).

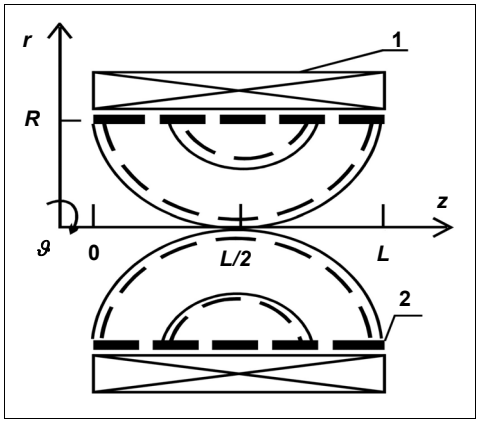

Fig. 1. Schematic of the plasma lens: 1 – magnetic coils; 2 – cylindrical electrodes; dashed lines – equipotentials; solid lines– magnetic field lines

The condition of equipotential magnetic field lines of length $l >> R$, the lens radius, passing through the axial region of the system and crossing the outermost electrodes (which are grounded) follows from a model in which the lens volume is uniformly filled with cold background electrons of density n_e and energetic beam ions of density $n_b = \frac{I_b}{eQv_b\pi R^2}$, where eQ is the ion charge, with e the electronic charge and Q the ion charge state (1, 2, 3,...), v_b is the beam ion velocity, and R is the beam radius. This condition can be given as [3]:

$$n_e - \frac{I_b}{eQv_b\pi R^2} = \pm\frac{\varphi_L}{e\pi R^2}, \qquad (1)$$

where φ_L is the maximum electric potential on the ring electrodes. The plus sign corresponds to beam focusing and the minus sign to beam defocusing − the dispersive operational regime of the lens. Here, we assume Q to be the mean ion charge state, for simplicity. In order that equipotential magnetic field lines to be generated, an electron density is needed that is sufficient to compensate both the space charge due to the beam and the vacuum electric potential within the lens volume. It can be seen from the equation that beam focusing can be obtained for low ion beam density − this is similar to the Gabor lens. In this case, the ion beam density does not play a role and the electrons are used only for space charge compensation and transformation of the external vacuum electric field in order to make the electric field lines transverse to the magnetic field lines for focusing low current positive ion beams. For a high current beam when, if un-neutralized, the beam could blow up under its own space-charge forces, neutralization can be provided by electrons of sufficient density held within the beam by its space charge. This regime occurs when the beam potential parameter I_b / v_b exceeds significantly the maximum externally applied lens voltage, $I_b / v_b >> \varphi_L$. In the high beam current regime, quasi-neutral plasma is formed within the lens volume consisting of cold magnetized electrons drifting across the magnetic field lines and fast beam ions that are affected to first approximation only by the radial electrostatic field of the lens. Note that the equipotentialization condition follows from the steady-state hydrodynamic equation of motion of cold electrons, which in this case is

$$\mathbf{E} = -\frac{1}{c}(\mathbf{v_d} \times \mathbf{H}), \qquad (2)$$

where $\mathbf{v_d}$ is the drift velocity of cold electrons, **H** is the magnetic field within the lens volume, and c is the velocity of light. The macroscopic electrostatic field **E** can exist only in the presence of closed electron drift and an "insulating" magnetic field. Then the electric field is perpendicular to the magnetic field, leading to magnetic field lines that are equipotentials.

The focal length F of this kind of electrostatic plasma lens is given by

$$F = \frac{\theta\varphi_b R}{2\varphi_L}, \qquad (3)$$

where φ_b is the ion beam accelerating potential (i. e., φ_b is the ion source extractor voltage) and the energy of the beam ions is $E_b = eQ\varphi_b$, φ_L is the maximum electric potential on the ring electrodes, and θ is a geometric parameter about unit. Importantly, note that the focal length of the plasma lens does not depend on the ion charge-to-mass ratio; this is a consequence of the purely electrostatic optical system, as previously mentioned.

Plasmaoptical filter of microdroplets based on plasma lens configuration with crossed electric and magnetic field. As said above, we suggest for the first time a new more practical approach for the effective removal of the microdroplets, as well as its conservation and incorporation into the plasma stream produced by erosion plasma sources (vacuum arc or laser produced plasma). This approach is based on application of the cylindrical plasma lens configuration for introducing in a volume of propagating along axis dense low temperature plasma flow convergent toward axis energetic electron beam produced by ion-electron secondary emission from electrodes of plasma optical tool. The first experiments and theoretical estimations [4, 9] have demonstrated the workability an idea of application the new plasma-optical tool based on plasma lens configuration with convergent and oscillating fast electrons for effective additional evaporation, destroying and clearing of liquid metal droplets in a passing intense flow of dense metal plasma. The simplified schematic of a new plasma-optical system utilizing an electron beam for effective elimination of microdroplets in passing arc metal plasma flow is shown in Fig. 2. Here **C** is the cathode, **A** is the anode, **D** is the aperture, **MC** is the magnetic coil, **M** are the magnetic field lines, **Δ** is the spatial layer, in which the strong radial electrical field is supported, $\mathbf{C_1}$ is the hollow cylinder, from which internal surface generated electrons of secondary ion-electron emission.

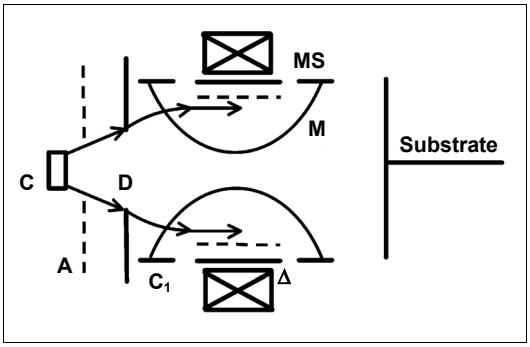

Fig. 2. Schematic of clearing microdroplets from a vacuum arc plasma flow

The application of a negative potential results in the formation of a spatial layer $\Delta << \rho_e \equiv \frac{eE_r}{m_e\omega_{He}^2}$ with a large electrical field E_r. This field is mainly directed along the radius. Width of near surface layer Δ with the large electrical field is rather small, $\Delta << D$. Hence the negative electrical potential φ_0 is concentrated into the narrow layer.

The system is in a magnetic field H_0 of a short coil. The value of the magnetic field is those, for which the following inequalities are performed

$$\rho_{He} << D << \rho_{Hi}. \quad (4)$$

Here ρ_{He} and ρ_{Hi} are the electron and ion Larmour radiuses. Note, here it means that

$$\rho_{He} = \frac{\left(\frac{2e\varphi_0}{m}\right)^{\frac{1}{2}}}{\omega_{He}}.$$

In the volume of magnetic field the electrons are magnetized and ions are not magnetized. When the arc plasma flow is incident on the magnetic field of a short coil, the magnetic field penetrates into the flow. The electron mobility across a magnetic field is strongly suppressed. The electron movement along magnetic field is free up to region of electric potential jump. Under these conditions the magnetic field lines are equipotential up to region of electric potential jump. I.e. the magnetic field lines are equipotential inside flow. Inside the flow an electric potential is distributed, which penetrate into the flow or which is formed as a result of the flow polarization. Then in space, filled with plasma, the electrical field is created, the form of which is approximately similar the structure of magnetic field lines. Because the electrons of the ion plasma flow are magnetized, they in the field of the short coil are displaced to its axis, damping expansion of the flow due to electric field E_p of plasma flow polarization. Thus, with increase of the magnetic field the near axis density of ion flow increases. I.e. the magnetic field controls the flow electrons, and they in turn keep ions from radial expansion due to E_p. The electric field E_p of plasma flow polarization, which prevents the arc plasma flow from the expansion in plasma-optical system, can be estimated by the following way. For estimation we use a model that plasma flow of radius R, which moves with velocity v_i through the plasma-optical system of length L is focused by E_p to the point. Then, one can use for evaluation the balance of centrifugal force and electrical focusing force

$$\frac{Mv_i^2}{R_f} = qE_p. \quad (5)$$

Here q, M are the charge and mass of ions; v_i is the velocity of the flow ions, R_f is the radius of flow curvature. Using the ε_i = 40 eV, R = 3.5 cm, we can obtain

$$qE_p \approx 6{,}6 \text{ eV / cm}. \quad (6)$$

The electrical field E_r in the layer Δ accelerates flow ions to an internal surface of the hollow cylinder. The negative voltage U = 1÷3 kV is supplied on cylindrical electrodes. As a result of secondary ion – electron emission the beam of high-energy electrons with velocity $v_b \approx \left(\frac{2e\varphi_0}{m_e}\right)^{\frac{1}{2}}$ and current density ($j_b = \gamma j_{is}$, γ is the rate of secondary ion-electron emission) is formed in a thin layer $\Delta << \frac{v_b}{\omega_{He}}$ (ω_{He} is the electron cyclotron frequency). This electron beam, self-consistently injected from the lateral inner cylindrical surface to the flow axis, is an additional effective source of energy for effective elimination of micro-droplets. During time of micro-droplet motion through system L/v_d with velocity v_d = 10 ÷ 100 m/s the electron beam pumps large energy $\Delta\varepsilon_b$ into system.

Let us estimate width of the layer near cylindrical electrode with large electrical field E_r, equating two ion currents to the wall: ion current in the layer (3/2 dependence) and ion Bohm current

$$j_b = 0{,}4\left(2T_e / M_i\right)^{\frac{1}{2}} n_0 = j_{is} = \left(1/9\pi\right)\left(2e/M_i\right)^{\frac{1}{2}} \varphi_0^{\frac{3}{2}} \Big/ \Delta^2. \quad (7)$$

Here n_0, T_e are the plasma electron density and temperature. From here one can derive the width Δ of the layer with large electrical field

$$\Delta / r_{de} = \left(e\varphi_0 / T_e\right)^{\frac{3}{4}} \left(10^{\frac{1}{2}}\right) \Big/ 3 >> 1. \quad (8)$$

$$\Delta << \rho_e \equiv eE_r \Big/ m_e\omega_{He}^2. \quad (9)$$

Let us show that the collision frequency ν_{be} of high-energy electrons with plasma electrons satisfies inequality

$$\nu_{be} << v_b / D. \quad (10)$$

Really from

$$\nu_{be} \approx 7.7\times10^{-6}\varepsilon_b^{-3/2} n_e \lambda_{ee} \quad (11)$$

for ε_b = 1 keV, $\lambda_{ee}\approx10$, $n_e = 10^{12}\text{cm}^{-3}$ one can derive $\nu_{be} \approx 2.6\times10^3\ \text{s}^{-1}$. For v_b / D one can derive $v_b/D \approx 4.4\times10^8\ \text{s}^{-1}$ for D = 7 cm. One can see that high-energy electrons many times cross the dense arc plasma flow during free movement, without taking into account the collective processes. Thus, high-energy electrons are accumulated in volume and slowly transfer energy for the micro-droplet evaporation.

Now we compare the system radius $D/2$ and dimension $R_b = \pi v_b / \omega_{He}$ of radial oscillations of high energy electrons in crossed fields

$$R_b = \pi\sqrt{2\varepsilon_b / m_e} \Big/ \omega_{He} = \pi\sqrt{2\varepsilon_b m_e}\left(c/eH_0\right). \quad (12)$$

For ε_b = 1 keV, H_0 = 400 Oe one can derive R_b = 0.84 cm. It means that dimension of radial oscillations of high energy electrons is smaller in comparison with the system radius. Thus, at the beginning the electrons, injected from the cylindrical electrode, are concentrated in a radial layer near the cylindrical electrode. It provides the energy pump by beam of high-energy electrons just to the area where the micro-droplets are located. Namely, since the angular distribution of micro-droplets is broader than of the ions, the micro-droplet fraction at the periphery of the plasma flow larger. It is good for their evaporation by radially injected electron beam from the cylindrical wall. However, the high energy electrons cross the cross-section of arc plasma flow due to their collisional mobility. It provides evaporation of micro-droplets throughout the cross-section of the arc plasma flow.

Mechanisms of crushing and evaporation of the droplets. For determining possible mechanisms of crushing and evaporation of the droplets, one should analyze channels of energy income and loss at the droplets. Besides high energy electrons, energy can come to the droplet from electrons and ions of arc discharge plasma. This energy is spent for heating, crushing and evaporation of

the droplets, however, in addition to that it can be spent for thermal emission and also can be brought away by electrons of secondary and thermal emissions. Besides, drift of electrons in crossed fields, as well as radial oscillations of electrons, also can serve as an additional mechanism of droplet evaporation.

By contributions of separate processes to energy balance, one can consider roles of certain processes under particular conditions. An equation of energy balance at the droplet can be written, as follows:

$$Q_{\Sigma} = \frac{L}{v_d}\left[\begin{array}{c} I_e(r_d)(T_e - e\varphi_d) - gI_b(r_d)e\varphi_d + \\ +I_i(r_d)(\varepsilon_{ii} + \varepsilon_v + \varepsilon_i + e\varphi_d) + I_b(r_d)(\varepsilon_b - e\varphi_d) \end{array}\right] -$$

$$-\frac{L}{v_d}\left[gI_b(r_d)e\varphi_d + I_{th}(T_d, r_d)e\varphi_d + \alpha\sigma T_d^4\right], \quad (13)$$

$$Q_{\Sigma} = Q_1 + Q_2 + Q_3, \quad (14)$$

where $Q_1 = cm_d(T_2 - T_1)$ is energy spent for heating the droplet from initial temperature T_1 to temperature of efficient evaporation T_2; m_d is droplet mass, c is specific heat capacity; $Q_2 = r\delta m_{dr}$, (r is specific evaporation heat) is energy spent for evaporation of a fraction δm_{dr} of the droplet, which evaporated prior to reaching the substrate; Q_3 is energy spent for ionization of a fraction of evaporated atoms from the droplet;

$I_e(r_{dr}) \approx 4\pi {r_d}^2 n_{0e} v_{the} \exp(-e\varphi_d / T_e)$ is current of electron flow to the droplet, n_{0e}, T_e, v_{the} are density, temperature and thermal velocity of the flow electrons, respectively;

$I_i(r_{dr}) \approx \pi {r_d}^2 n_{0i} v_{0i}$ is current of ion flow to the droplet, n_{0i}, v_{0i} are density and directed velocity of the flow ions, respectively;

$I_b(r_{dr}) \approx 1{,}6\pi\gamma {r_d}^2 n_{0i} v_S$ is current of high energy electrons to the droplet;

ε_i = 20 ÷ 80 eV is mean kinetic energy of directed ion flow;

$\varepsilon_b = e\varphi_0$ is energy of high energy electrons, φ_0 is electric potential jump near inner surface of cylindrical electrode;

ε_v is condensation energy;

ε_{ii} is ionization energy of the flow ions;

k is Boltzmann constant;

$r_{dr} \approx 1$ μm, T_{dr}, $\varphi_{dr} = (T_e/e)\ln\left(4(m_i/m_e)^{1/2}(T_e/2\varepsilon_i)^{1/2}\right)$

are radius, temperature and electrical potential of the droplet, respectively;

α is irradiation ability;

σ is Stephan–Boltzmann constant;

g is secondary electron-electron emission coefficient;

$I_{th}(T_{dr}, r_{dr})$ is thermal emission current;

L is the system length;

v_{dr} = 10 ÷ 100 m/s is velocity of the droplets

$$I_b(r_{dr}) \approx \left(4\pi {r_d}^2\right)0{,}4\gamma n_i v_S = 1{,}6\pi\gamma {r_d}^2 n_{0i} v_S .$$

One can estimate role of particular processes in crushing the droplets. The estimations performed for the droplets having 1 μm radius and 10 m/s velocity show that major energy comes to the droplet from high energy electrons.

Let us assume that the whole electron beam energy is spent without losses to droplet evaporation and accompanying thermal radiation. If more energy is used for thermal radiation than for droplet evaporation, the energy balance equation (13) can be approximately written as follows

$$j_b\varepsilon_b(2\pi RL)(L/v_d) \approx (\alpha\sigma T_d^4)(4\pi r_d^2)n_d(\pi R^2 L)(L/v_d). \quad (15)$$

Here left side term of equality corresponds to energy pumped to the system by electron beam during a time of droplet flight through the system. Right side term corresponds to energy spent by the droplet having temperature T_d to thermal radiation for the same time. j_b and ε_b are flow density and electron beam energy; $j_b = 0{,}4\gamma\sqrt{2}(T_e/M_i)^{\frac{1}{2}} n_0$; R and L are radius and length of the plasma-optical system; T_d, v_d, r_d and n_d are temperature, velocity, radius and density of the droplets; α is irradiation ability. For liquid copper α = 0,13÷0,15. We use mean value α = 0,14. For the following parameters: σ = 5.6705 10^{-8} W/m^2 = 5,6705 10^{-5} Erg/cm^2, ε_b = 1 keV, r_d = 1 μm, n_0 = 10^{12} cm^{-3}, T_e = 3 eV, R = 3,5 cm, n_d = 2.5 cm^{-3} we obtain

$$T_d = \left[0.4\gamma\sqrt{2T_e/m_i}\, n_0 \Big/ \alpha\sigma(2\pi r_d^2)n_d R\right]^{1/4} \approx 0{,}7\ 10^7 \text{ K}. \quad (16)$$

It is essentially higher than the temperature of copper boiling. Following from that, the beam pumps enough energy to the system for evaporation of the droplets, even taking into account their thermal radiation.

Actual T_d is less due to the following:

– the beam does not have sufficient time to transfer all the energy when it is present in the system;

– droplet dimensions may be more than 1 μm;

– droplet density in the flow may be more than n_d = 2,5 cm^{-3};

– not the whole applied to central electrode voltage is concentrated near cylindrical surface in a form of jump.

We show respectively that even at temperature of boiling the droplets their thermal radiation is less than energy pumped to the system by the beam of high energy electrons. For that purpose we take ratio β of thermal radiation energy of all droplets during their flight through the system to energy pumped to the system for the same time by the beam of high energy electrons

$$\beta = (\alpha\sigma T_d^4)(4\pi r_d^2)n_d(\pi R^2 L)(L/v_d) / j_b\varepsilon_b(2\pi RL)(L/v_d) =$$

$$= (\alpha\sigma T_d^4)(2\pi r_d^2)n_d R / j_b\varepsilon_b \quad (17)$$

For T_d = 2840,15 K (copper boiling temperature) from (17) we obtain:

$$\beta = (\alpha\sigma T_d^4)(2\pi r_d^2)n_d R / j_b\varepsilon_b = 1{,}4\ 10^{-7}. \quad (18)$$

Here it also follows that the beam pumps sufficient energy to the system for evaporation of the droplets even taking into account their thermal radiation.

Let us determine quantity of atoms in typical liquid copper droplet with dimensions r_d = 1 μm.

$$N = (4/3)\pi N_A \rho r_d^3 / m_{\mu} \approx 3{,}4\cdot 10^{11}. \quad (19)$$

For decrease of losses of the flow metal ions to secondary ion-electron emission one can use slow isotropic ions created in result of droplet evaporation and ionization of formed atoms. These newly created ions are accelerated near the wall by electric potential jump and provide electron beam formation in result of secondary ion-electron emission.

Experimental studies of dense metal plasma flow passing through the plasmaoptical filter. The experiments were performed at setup schematically shown in Fig. 3. A repetitively-pulsed cathodic arc (also called vacuum arc) plasma gun (items 1, 2, 3, 5 of Fig. 3) was used to produce an energetically-streaming copper plasma. The plasma lens (PL) configuration is of length 14 cm and aperture 8 cm, and includes three cylindrical electrodes (items 4, 5) in a magnetic field formed by permanent magnets 7 and magnetic circuit 8. The lens outer electrodes are grounded by design, and the

central electrode is biased at up to –3 kV. The plasma stream 9 exiting the lens is then monitored by a sectioned cylindrical current collector device 10.

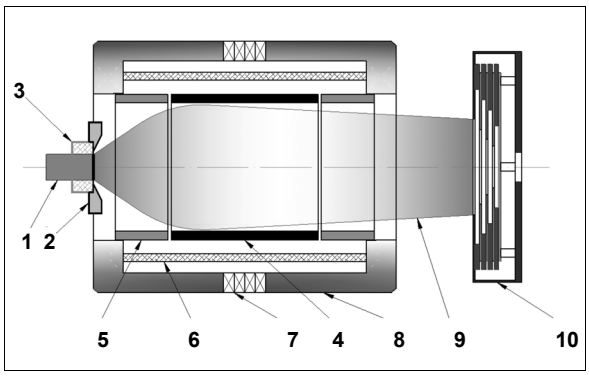

Fig. 3. Schematic of the experimental setup

Plasma is formed from the cathode material; here the cathode is copper (a 6 mm diameter rod), to form a copper plasma. The arc current was up to 100 A, with pulse duration 100–300 μs and repetitively pulsed at 1–5 pulses per second. The base vacuum chamber pressure was 1.5×10^{-6} Torr, and argon gas could optionally be added. The ion current associated with the plasma flow was measured by a sectioned collector, item 10 of Fig. 3, consisting of 4 individual ring-shaped collectors. The entrance aperture of collector is screened with a high transparency metal grid. The collector segments were biased negatively to repel electrons and thus measure ion current, and the current to each ring was measured by a Pearson current transformer.

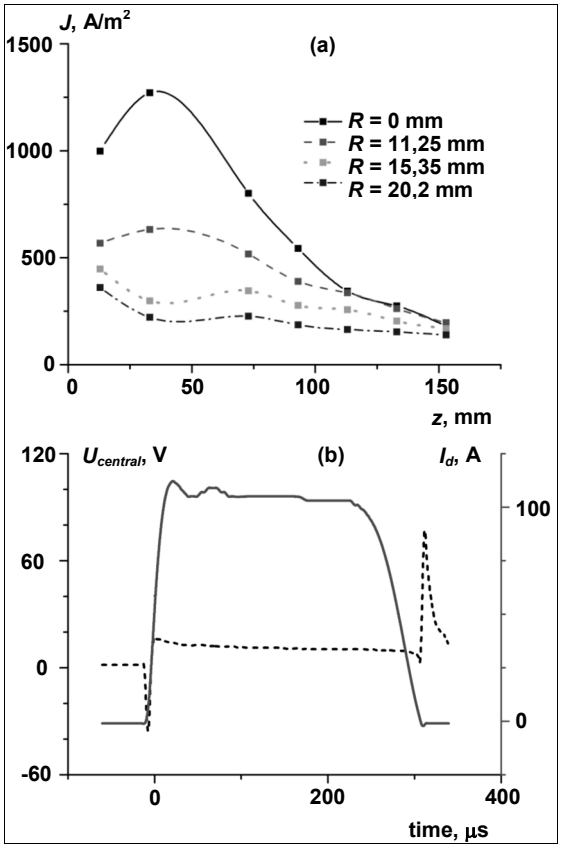

Fig. 4. Distribution of current density for different radius under floating potential on central electrode, I_d = 100 A, pressure 1,5 x 10^{-6} Torr, H = 360 Gs: a) current density; b) potential on central electrode (~ 10 V, dashed curve) and arc discharge current (~ 100 A, solid curve)

The results of our investigations of this system are shown in Figs. 4, 5 [2]. The data shown are the result of averaging over 6 plasma pulses (the point of zero is exit of PL). It should be noted the propagating ion plasma flow in free space lead to strong flow divergence. At the same time, the presence of crossed *EH* fields improves essentially the passing flow through system under different working gas pressure and applied potential to central lens electrode. Moreover, one can see the lens demonstrates plainly focusing properties in these experimental conditions. Especially clearly this effect is manifested in case of floating potential at the central lens electrode (see Fig. 4a). We believe this effect is due to self- consistent mode formed in an electrostatic plasma lens under propagating wide-aperture, high-current, low energy metal ion plasma flow produced by cathodic-arc discharge at low pressure. In Fig. 4b one can see the formation of positive self- sustained potential about 10 V that applied to central electrode under passing ion-plasma beam.

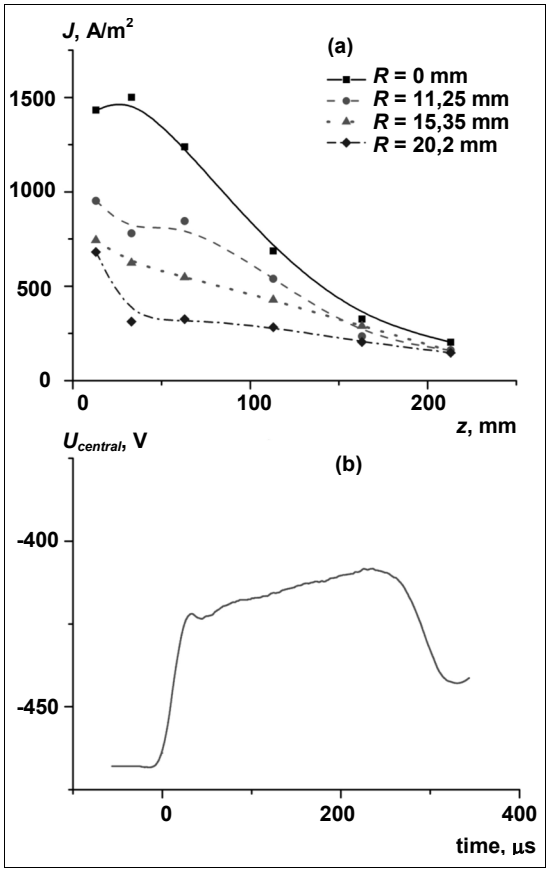

Fig. 5. Distribution of current density for different radius under –500 V on central electrode, I_d = 100 A, pressure 1,5 x 10^{-6} Torr, H = 360 Gs: a) current density; b) potential on central electrode

Also, one can see (Fig. 5) that under negative applied potential on the central lens electrode in volume PL focusing of passing ion plasma flow at the exit of PL is observed too. This effect can be understood due to generation of fast electrons by secondary ion electron emission on inner surface the central lens electrode. These electrons can be accumulated at the axis and provide focusing ions due to electric field E_p of plasma flow polarization.

Investigations of the plasmadynamical filter effect on the quality of obtained metal coatings. As it was already noted, plasmaoptical filter is the system of crossed electric and magnetic fields. Electromagnetic field of com-

plex configuration is formed inside the filter depending on experimental conditions. Placement of the filter with respect to the plasma source can be either with certain gap between the filter and the source, or without it. In the first case plasma flow is formed outside the system of filter fields, whereas in another case it occurs practically in the filter volume. In both cases buffer gas can be present in the system at certain amount for improvement or arc discharge formation. Sign of potential at the filter electrodes, magnetic field strength and geometry, presence and pressure of buffer gas can influence the result of filter operation. Influence of these parameters on the filter operation was studied in the laboratory experiment. Particularly, influence of presence and absence of buffer gas on deposited coating has been verified, Fig. 6.

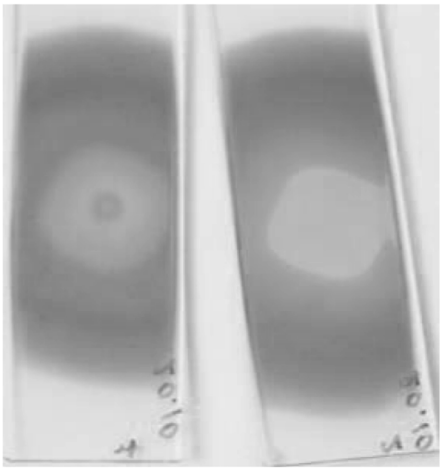

1 2

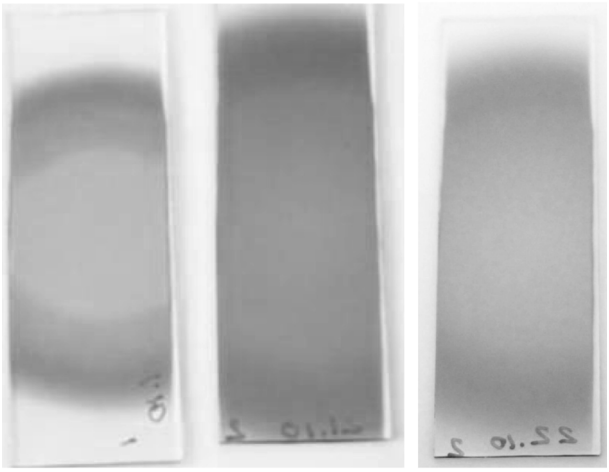

3 4 5

Fig. 6. Samples of deposited copper films under different conditions of the plasma flow formation. Arc discharge pulse duration 280 μs, I_d = 100 A 1 and 2 pressure in the chamber 2 x 10^{-6} Torr, 1 – potential is not supplied to central electrode; 2 – -2 kV at central electrode; 3 and 4 argon pressure in the chamber 4 x 10^{-4} Torr, 3 – potential is not supplied to central electrode, 4 – -2 kV at central electrode; 5 – argon pressure 1 x 10^{-4} Torr and –2 kV at central electrode

One can see from pictures of deposited copper coatings at Figs. 6 1 and 2 that at buffer gas absence clearly distinctive central region is formed, and negative potential supply to central electrode changes behaviour of the plasma transport through the filter. Particularly, the film occupies larger square and visually more uniform. One can see from pictures 3–5 that buffer gas feed also changes conditions of plasma flow transport through the filter. Relatively big buffer gas pressure of 4 x 10^{-4} Torr also increases deposited film square and uniformity. Applying the same potential of –2 kV to central electrode further increases the coating square and uniformity, however at that in the filter volume its own discharge with up to 30 A current and up to 500 V operating voltage is ignited. The last circumstance influences behaviour of optical emission from the filter volume.

If one would decrease buffer gas pressure down to 1 x 10^{-4} Torr, own discharge is not ignited, and the coating square and uniformity are higher than that in cases 1 or 3.

Earlier we have shown that there are certain differences also in current distribution along radius of the plasma flow passed through the filter volume. Different conditions of the filter operation form different distributions of the current density along the system radius. Thus we have one more confirmation of obtained results.

In Figs. 7–9 one can see the scanning electron microscope (SEM) photos (square of images 250x330 μm) demonstrating the experimental results of the surface quality after copper deposition onto stainless steel samples under different experimental conditions (the filter being turned on and off). Comparison of the photos clearly demonstrates effect of reducing microdroplet quantity and dimensions, at that the best result is achieved with the filter operating in plasma lens regime, that is, with magnetic field and high negative voltage applied to the central electrode.

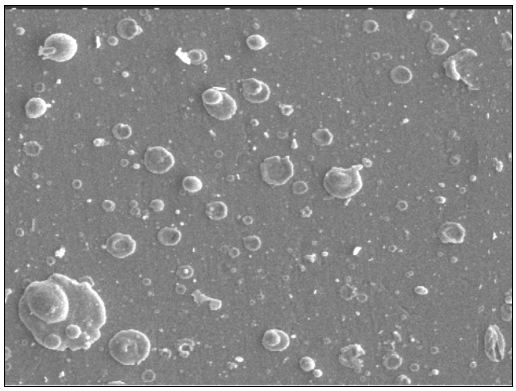

Fig. 7. SEM photo of copper microdroplets with the filter being turned off

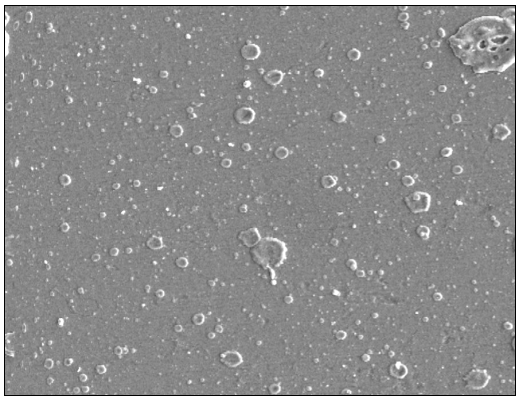

Fig. 8. SEM photo of copper microdroplets with the filter being turned on without magnetic field (U = –1000 V, H = 0 Gs)

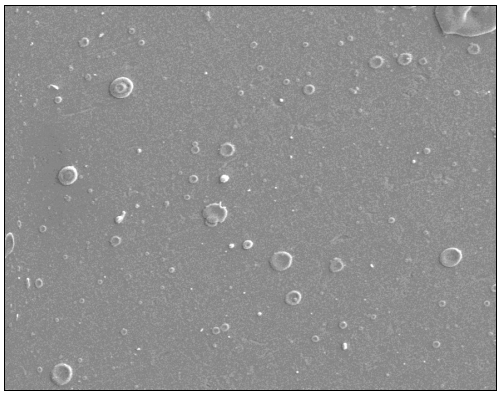

Fig. 9. SEM photo of copper microdroplets with the filter being turned on with magnetic field (*U* = –1000 V, *H* = 360 Gs)

For study of statistical distribution of the droplets by size, surface of deposited coatings was studied by means of optical microscope. The samples were obtained by copper film deposition onto glass substrates. The film deposition was performed with the filter being completely turned off, for the filter without magnetic field and for the filter with magnetic field (plasma lens configuration). In the case without magnetic field, the system of filter electrodes, depending on pressure in the chamber, creates conditions for occurrence of either non-self maintained discharge, or self-maintained one of hollow cathode type.

Modern software such as Gwyddion with free code (gwyddion.net) allows processing obtained pictures at personal computer. For avoiding influence of service information on the software operation, each picture was preliminary processed in picture editor. All service information was removed. After that the image was imported to the software with definition of actual X and Y dimensions and relative height units. Since in subsequent the data were calculated only in the sample plane, actual height values are inessential. Actual height values of the creations at the surface were not determined. After background removal, mask with defined threshold was applied and equivalent radius values of the spots marked by the mask were calculated. The mask was chosen in a way that it should cover majority of visible creations without touching overall background. For each case several pictures of the surface with the same square were taken. Typical distributions over a number of the spots with particular dimensions for each regime of the filter operation are presented in Figs. 10–12. One can see from presented histograms that number of droplets essentially decreases in both cases of the filter use. Maximum size of droplets reaching the sample surface also decreases. Incomplete removal of microdroplets surely requires further researches aimed to optimization of the filter parameters.

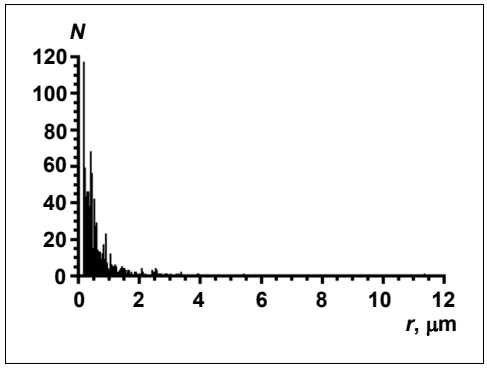

Fig. 10. Distribution for the case of filter being turned off

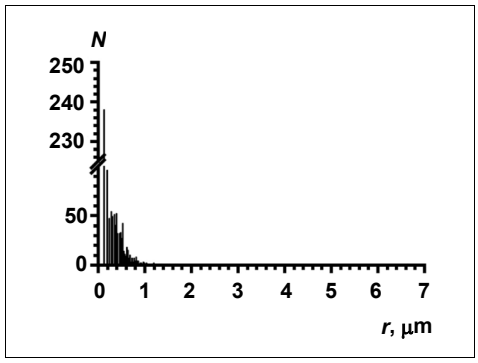

Fig. 11. Distribution for the case of filter without magnetic field and *U* = –2 kV at central electrode

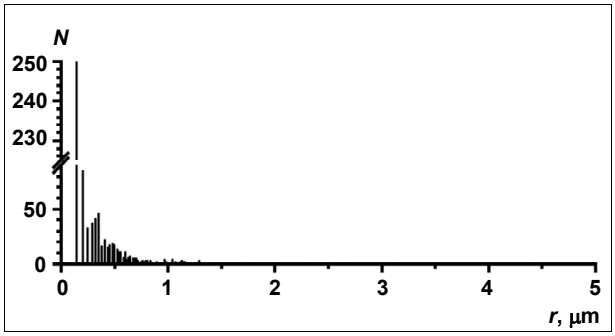

Fig. 12. Distribution for the case of filter with magnetic field *H* = 360 Gs and *U* = -2 kV at central electrode

As one can see from the Fig. 11, effect of reducing microdroplet fraction is also observed in the plasmaoptical system without magnetic field. Actually, the system under such conditions represents well known hollow cathode configuration, which also produces fast electron flow. Mechanism of fast electron effect enhancement in this case is due to multiple oscillations of the electrons across the cathode cavity. An important feature of such system is magnetic field absence which enables easy scaling of the plasmadynamical filter dimensions for fulfilling particular requirements of practical use. Due to that, works have been initiated on research and development of plasmadynamical filter based on hollow cathode effect [1].

Plasmadynamical filter of microdroplets based on hollow cathode discharge configuration. Experiments were performed at the setup similar to shown in Fig. 3, but without magnetic field use. Plasma stream was formed by vacuum arc discharge with titanium cathode. The arc current was about 100 A, with pulse duration 100–1000 μs and repetitively pulsed at 1–5 pulses per second. The base vacuum chamber pressure was $1.5 \times 1\ 0^{-6}$ Torr, and argon gas could optionally be added. The filter unit was represented by stainless steel cylinder with internal diameter D_{in} = 120 mm and length L = 220 mm which served as the discharge hollow cathode.

Pulsed power supply unit for hollow cathode discharge operation was constructed on a basis of single cycle thyristor based inverter, and was composed of two modules: recharge and discharge ones.

Recharge module is elaborated on a basis of single phase full wave rectifier circuit composed of step-up transformer and a bridge of four diodes. One diagonal of the bridge is connected to secondary winding of step-up transformer, and another diagonal – to load resistance, which in our case was represented by storage capacitor. Voltage regulator (autotransformer) in primary winding circuit of the transformed allowed smooth regulation of output voltage of the module from zero up to 700 V. Current measurement

was provided by low-inductance shunt with signal output to oscilloscope or computer. Steady voltage of capacitive storage was measured by microampermeter with resistive voltage booster. Voltage kinetics was measured by means of resistive voltage divider with 1:1000 ratio also with signal output to oscillograph or computer. Outputs to the oscilloscope were protected by transorb diodes. The module operates using commercial net voltage without intermediate conversion, and has advantages of design simplicity and high reliability.

Discharge module is composed of thyristor, reverse current diode, high voltage pulsed transformer, measuring and protective circuits. Step-up pulsed transformer had transformation ratio of about 30.

Power supply unit operates as follows. Capacitive energy storage is charged from single phase net up to required voltage level via voltage regulator (autotransformer), step-up transformer and rectifier. At control pulse supply to thyristor, voltage from the capacitor creates an output via pulse step-up transformer to the hollow cathode. The discharge current is limited by an impedance of discharge circuit ($R_{wave} \approx 1500$ Ohm), active resistance of secondary winding of pulse transformer ($R_{Tr} = 172$ Ohm) and active resistance of the discharge ~ 300–400 Ohm. Since the discharge circuit impedance exceeds its active resistance by a factor of about three, the discharge process of the capacitor has single full sine wave character. Besides, since of power supply unit output resistance essentially exceeds the discharge one, the power supply module operates in current source regime. Maximum current which could be supplied to the discharge was about 5 A. Repetition rate of current/voltage pulses was 0.2–2 Hz. Maximum idle output voltage of the source $U_{N\text{-}L} = 10$ kV.

Hollow cathode discharge with the use of pulsed powering possessed the following peculiarities:

– it was not ignited without arc discharge plasma flow even at maximum voltage from pulsed power supply of 10 kV;

– it was ignited only by trailing edge of arc discharge plasma flow;

– it exhibited steady operation at argon pressure range $3*10^{-4} – 2*10^{-3}$ Torr.

It should be noted that power supply used by us was of current source type. Thus, with voltage $U_{N\text{-}L}$ increase at the discharge ignition we actually predetermined current value provided by the source to the discharge, and U_{HC} voltage followed this current, as required. Dynamic current-voltage characteristic (CVC) of the discharge (Fig. 13) demonstrates discharge voltage dependence on the current which is typical for the discharges with hollow cathode effect, that is, with presence of CVC region where discharge voltage is practically independent on discharge current. One can see from Fig. 14 that maximum electric power in the discharge reaches about 9 kW, or ≈ 3.5 W/cm^3. Electric energy introduced into the discharge in our experiments was varied in range 20–25 J.

Increase of argon pressure in the discharge system leads to more stable and reproduced discharge operation regime. However, simultaneously with pressure increase the discharge voltage decreases (at the same current value), and, consequently the discharge power also decreases. Comparison shows that argon pressure increase from з $3*10^{-4}$ to $1*10^{-3}$ Torr results in:

– essential decrease of the discharge voltage U_{HC} (at the same current $I_{HC} = 3.5$ A voltage U_{HC} decreases from 2.5 kV to 1.25 kV);

– weak dependence of voltage U_{HC} on current I_{HC} – at maximum current I_{HC} increase from ≈ 2 A to ≈ 5 A the discharge voltage remains practically unchanged. One can also clearly see that from dynamic CVC behaviour presented in Fig. 15.

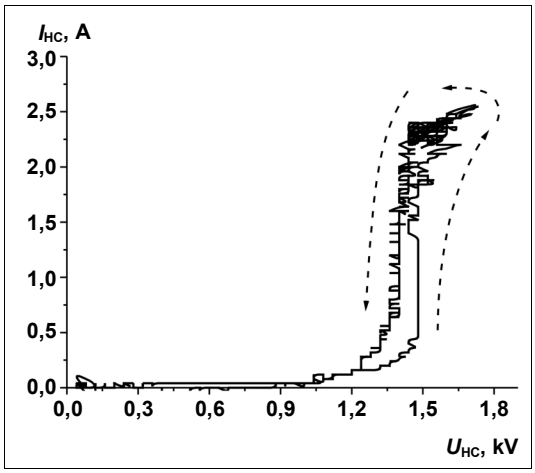

Fig. 13. Dynamic CVC of hollow cathode discharge. Cathode $D_{in} = 120$ mm, argon pressure $3*10^{-4}$ Torr

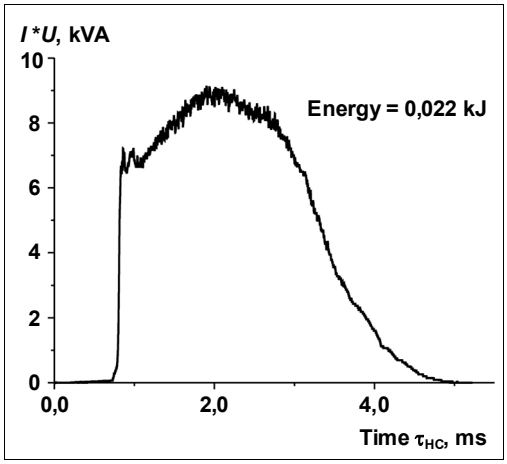

Fig. 14. Kinetics of electric power introduced into the discharge. Cathode $D_{in} = 120$ mm, argon pressure $3*10^{-4}$ Torr

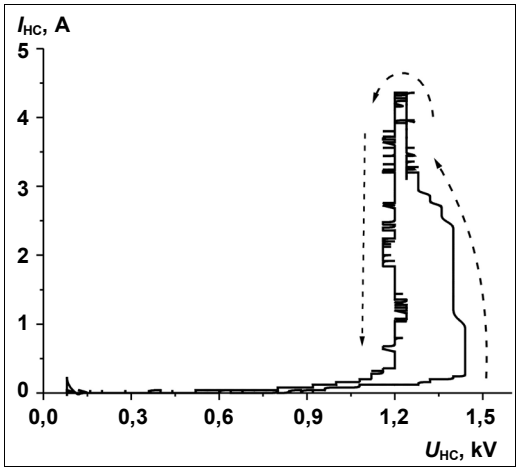

Fig. 15. Dynamic CVC of hollow cathode discharge. Cathode $D_{in} = 120$ mm, argon pressure $1*10^{-3}$ Torr

Increase of argon pressure also results in decrease of maximum electric power in the discharge down to ≈5 kW (2 W/cm^3) and energy introduced to the discharge down to 14 J (Fig. 16). As we have seen above, external characteristics of hollow cathode discharge (voltage U_{HC}, power in the discharge) change essentially enough at argon pressure variation in the system. Let us consider now, how this pressure variation influences the plasma parameters – electron temperature, plasma density and potentials. Typical kinetics of discharge current I_{HC} and probe current I_p are presented in Fig. 17. Jumps at the fronts of I_{HC} and I_p current kinetics are due to presence of vacuum arc discharge plasma in the cathode cavity. Minima at I_{HC} and I_p dependencies correspond to system transition to actual hollow cathode discharge glow. Measurements of probe characteristics was done for two τ_{HC} time points – at about 250 μs from beginning of I_{HC} and I_p growth (that is, during transition process) and 1250 μs (at maximum of discharge current I_{HC}).

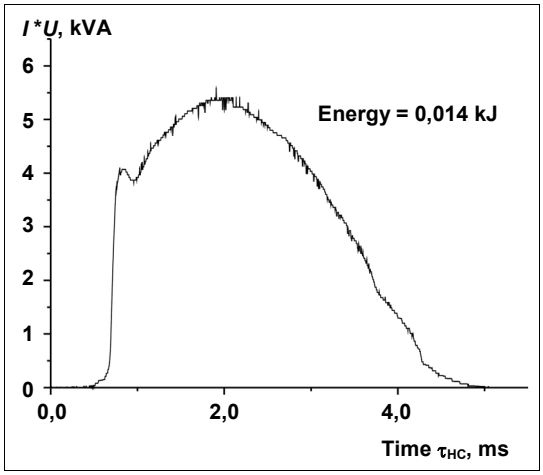

Fig. 16. Kinetics of electric power introduced into the discharge. Cathode D_{in} = 120 mm, argon pressure 1*10^{-3} Torr

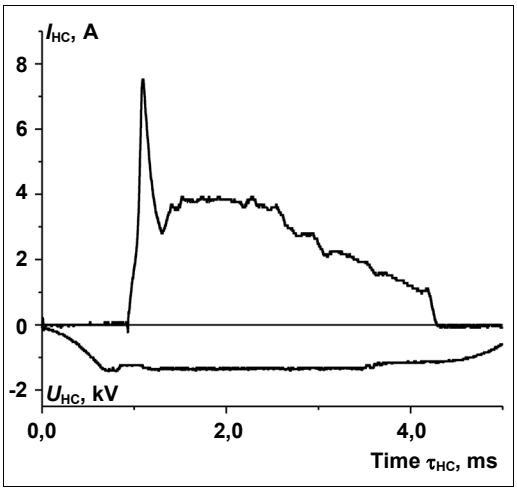

Fig. 17. Typical kinetics of discharge current I_{HC} and probe current I_p. Cathode D_{in} = 120 mm, argon pressure 1*10^{-3} Torr

Fig. 18 presents dependence of probe current I_p logarithm on probe voltage U_p for time point 250 μs and argon pressure 1e-3 Torr. One can see that:

– electron temperature reaches 7–8 eV;

– plasma density is about 1.5*10^{11} cm^{-3};

– plasma potential U_{pl} deviates from anode potential by a difference from –1 V to –12 V.

In advance it can be noted that plasma of transition process is in some sense a mixture of arc discharge plasma and plasma of initial stage of hollow cathode discharge glow.

Figs. 19 and 20 present results of probe measurements of hollow cathode discharge plasma for two argon pressure values – 1*10^{-3} and 5*10^{-4} Torr. In both cases during the measurements the discharge current I_{HC} was maintained at a level of 4.0–4.5 A, whereas U_{HC} voltage was 1.2–1.3 kV at pressure 1*10^{-3} Torr and 1.5–1.6 kV at 5*10^{-4} Torr. That is, electric power in the discharge at lower pressure value was by ≈25–30 % higher than that at higher pressure value. One can see from the figures that argon pressure decrease twice results in electron temperature T_e increase from 14 to 19 eV.

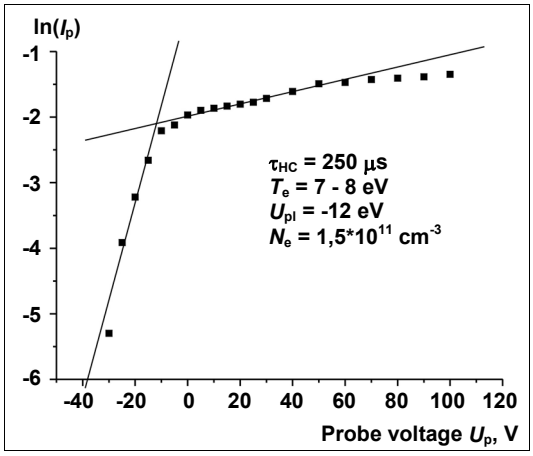

Fig. 18. Dependence of probe current I_p logarithm on probe voltage U_p. Cathode D_{in} = 120 mm, argon pressure 1*10^{-3} Torr. Time point of the measurement 250 μs after discharge ignition, plasma parameters are shown in the figure

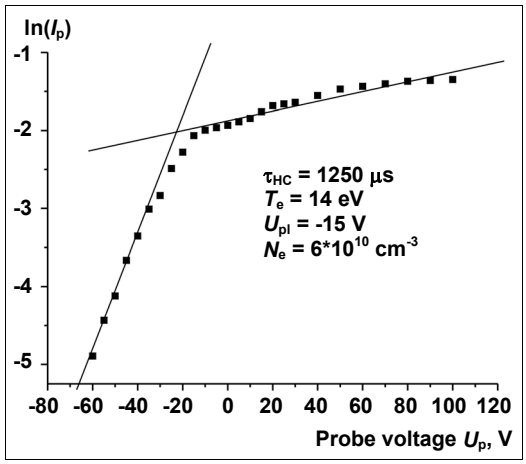

Fig. 19. Dependence of probe current I_p logarithm on probe voltage U_p. Cathode D_{in} = 120 mm, argon pressure 1*10^{-3} Torr. Time point of the measurement 1250 μs after discharge ignition, plasma parameters are shown in the figure

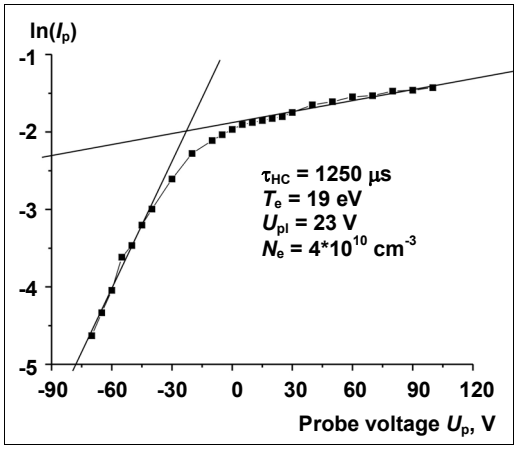

Fig. 20. Dependence of probe current I_p logarithm on probe voltage U_p. Cathode D_{in} = 120 mm, argon pressure 3*10^{-4} Torr. Time point of the measurement 1250 μs after discharge ignition, plasma parameters are shown in the figure

It should be noted that accomplished experiments in a whole have shown that argon pressure decrease from (1–1.5)*10^{-3} to (4–5)*10^{-4} Torr results in T_e increase from 13–14 eV to 19–21 eV. Mentioned decrease of argon pressure in the system also leads to plasma density decrease from 6*10^{10} cm^{-3} to 4*10^{10} cm^{-3}, that is, approximately by factor of 1.5. It should be also noted that the pressure decrease causes further deviation of hollow cathode discharge plasma potential U_{pl} from anode potential – from –15 V to –23 V. This fact gives indirect evidence to formation of potential fall in aperture hole between arc discharge anode and hollow cathode discharge plasma.

Conclusion. In result of accomplishing research and development works in the Institute of Physics NASU, existing experimental setup with copper plasma source and plasmadynamical microdroplet filter of plasma lens type was essentially upgraded, and modern setup with titanium plasma source and the microdroplet filter based on hollow cathode discharge was elaborated. Both setups operated in pulsed periodical regime at low working gas pressure and demonstrated essential reduction of microdroplet fraction in metal plasma flows from vacuum arc sources.

For the first time, self-focusing of low-energy dense multi-component ion-plasma flow formed by erosion plasma source was realized and, as well, possibility of focusing low-energy dense ion-plasma flow by polarization field formed in a volume of the flow is demonstrated. Presence of fast electrons in the plasma-optical filter volume is shown when the filter electrode is under negative potential.

Base models of physical processes in the plasma flow passing through the plasma-optical filter that could result in microdroplet destruction are proposed, and analytical estimations are accomplished.

These results open up novel attractive possibilities of further development, improvement and applications of erosion plasma sources for synthesis of high quality thin films and coatings with given functional features. This work is in progress. We have an intention of further study of optimum conditions for radical decrease of microdroplet fraction in the streaming plasma flow.

Acknowledgments. The authors would like to thank Prof. V. Maslov (KIPT) for fruitful and stimulating discussions and theoretical assistance. This work is supported in part by the grants P13/16-17, PL/17 (NAS of Ukraine).

REFERENCES

1. *Bazhenov V.Yu., Dobrovol'skii A.M., Goncharov O.A.,* et al. // Problems of Atomic Science and Technology, 2016. – Vol. 106, № 6. – P. 183–186.
2. *Bugaev A., Dobrovolskiy A., Goncharov A.,* et al. // Journal of Applied Physics, 2017. – Vol. 121. – P. 043301.
3. *Goncharov A.* // Rev. Sci. Instrum., 2013. – Vol. 84. – P. 021101.
4. *Goncharov A.A.* // Rev. Sci. Instrum., 2016. – Vol. 87, – P. 02B901.
5. *Goncharov A.A., and Brown I.G.* // IEEE Trans. Plasma Sci., 2004. – Vol. 32. – P. 80–83.
6. *Goncharov A.A., and Brown I.G.* // IEEE TPS, 2007. – Vol. 35. – P. 986–991.
7. *Goncharov A., Dobrovolskiy A., Dunets S.,* et al. // IEEE TPS, 2011. – Vol. 39. – P. 1408–1411.
8. *Goncharov A.A., Dobrovolsky A.N., Dunets S.N.,* et al. // RSI. – 2012. – Vol. 83. – P. 02B723.
9. *Goncharov A., Maslov V. and Fisk A.* // Proceedings of the 55th Annual Technical Conference of the Society of Vacuum Coaters. – Santa Clara, CA, April 28 – May 3, 2012. – P. 441–444.
10. *Morozov A.I.* // Dokl. Acad. Nauk. USSR. – 1965. – Vol. 163, № 6, – P. 163–167.
11. *Morozov A.I.* Introduction to Plasmadynamics / A.I. Morozov . – M. : Fismatlit, 2008.

Submitted on 27.04.17

О. Гончаров, д-р фіз.-мат. наук,
В. Ціолко, канд. фіз.-мат. наук,
А. Добровольський, канд. фіз.-мат. наук,
В. Баженов, канд. фіз.-мат. наук,
І. Літовко[1], канд. фіз.-мат. наук,
Інститут фізики НАН України, Київ
[1]Інститут ядерних досліджень НАН України, Київ

ПЛАЗМОДИНАМІЧНІ СИСТЕМИ НОВОГО ПОКОЛІННЯ ЗІ ШВИДКИМИ ЕЛЕКТРОНАМИ

Наведено короткий огляд поточних досліджень і розробок плазмооптичних пристроїв нового покоління на основі аксіально-симетричної конфігурації електростатичної плазмової лінзи та фундаментальних плазмооптичних принципів магнітної ізоляції електронів і еквіпотенціалізації магнітних силових ліній. Як пориднену систему розглянуто також пристрій на основі ефекту порожнистого катода. Теоретично досліджено та експериментально продемонстровано практичне застосування запропонованих плазмодинамічних пристроїв зі швидкими електронами для суттєвого покращення якості поверхні покриттів завдяки ефективному усуненню мікрокрапельної фракції із щільних потоків металевої плазми, створеної ерозійними вакуумно-дуговими джерелами.

Ключові слова: плазмодинаміка, плазмооптика, плазмова лінза, порожнистий катод, газовий розряд, потік швидких електронів.

А. Гончаров, д-р физ.-мат. наук,
В. Циолко, канд. физ.-мат. наук,
А. Добровольский, канд. физ.-мат. наук,
В. Баженов, канд. физ.-мат. наук,
И. Литовко[1], канд. физ.-мат. наук,
Институт физики НАН Украины, Киев,
[1]Институт ядерных исследований НАН Украины, Киев

ПЛАЗМОДИНАМИЧЕСКИЕ СИСТЕМЫ НОВОГО ПОКОЛЕНИЯ С БЫСТРЫМИ ЭЛЕКТРОНАМИ

Представлен краткий обзор текущих исследований и разработок пламооптических устройств нового поколения на основе аксиально-симметричной конфигурации электростатической плазменной линзы и фундаментальных плазмооптических принципов магнитной изоляции электронов и эквипотенциализации магнитных силовых линий. В качестве родственной системы рассмотрено также устройство на основе эффекта полого катода. Теоретически рассмотрено и экспериментально продемонстрировано практическое применение предложенных плазмодинамических устройств с быстрыми электронами для существенного улучшения качества поверхности покрытий благодаря эффективному устранению микрокапельной фракции из плотных потоков металлической плазмы, созданной эрозионными вакуумно-дуговыми источниками.

Ключевые слова: плазмодинамика, плазмооптика, плазменная линза, полый катод, газовый разряд, поток быстрых электронов.

UDC 677.027

O. Ivanyuta, Ph. D.,
S. Kratko, stud.,
Faculty of Radiophysics, Electronics and Computer Systems,
Taras Shevchenko National University of Kyiv

MODERNIZATION SYSTEMS OF PASSIVE DISGUISE

Methods of masking was considered distortion as visible silhouette objects by causing the special distorting colouring, mixing to conduct their authentication or direction motion and their modernization. A method and structural decision of modernization was offered the existent masking systems is offered in wide dynamic and spectral ranges. The problem of disguise – de camouflage is decided by the operative change of printing by a radio engineering net on basis without corps light-emitting diodes.

Keywords: mobile camouflage system, optical range, techniques of camouflage, concealment, decoys.

Introduction. The camouflage and systems of masking are aimed at increase of survivability of military systems, they are responsible for the first two elements of protection in the equation "isn't seen, not found, not gunned, not killed". Camouflage comes from the French word camoufler meaning "to blind or veil." The decision of many questions, related to visibility, requires difficult theoretical researches and long measuring and supervisions at times. Masking tactics application, for example use of features of terrain, implementation of the correct camouflage to mix system with a background (surrounding) and to tear traps in the region, promotes increase of complexity of the task on detection of purpose by any opponent of services in, for example, the following literature [1, 2].

Dazzle paint schemes were employed in both world wars to confuse and obfuscate range, scale and type estimates by enemy submariners peering through systems supervision (Fig. 1). Among different perspective technologies spectral and adaptive controlled materials stand in the upper part of the list though their development still is at the initial stages. A dummy Spitfire: key aspect was to throw a realistic looking shadow. As for a visible range, here we see quite advanced systems it belongs to such systems as the polymeric light-emitting diode and other systems on the basis of conductivity. It gives good hopes for interesting applications which could lead to the active camouflage systems imitating a background on a system surface that could be very interesting especially in city regions. Though the technology still shall develop and develop, especially it concerns displays, data handling and the power of batteries. Holography, optical fiber, lowering of signatures, the adaptive camouflage and optical camouflage are more and more promising technologies

Fig. 1. Paint schemes were employed to confuse and obfuscate range, scale and type estimates through systems supervision [1]

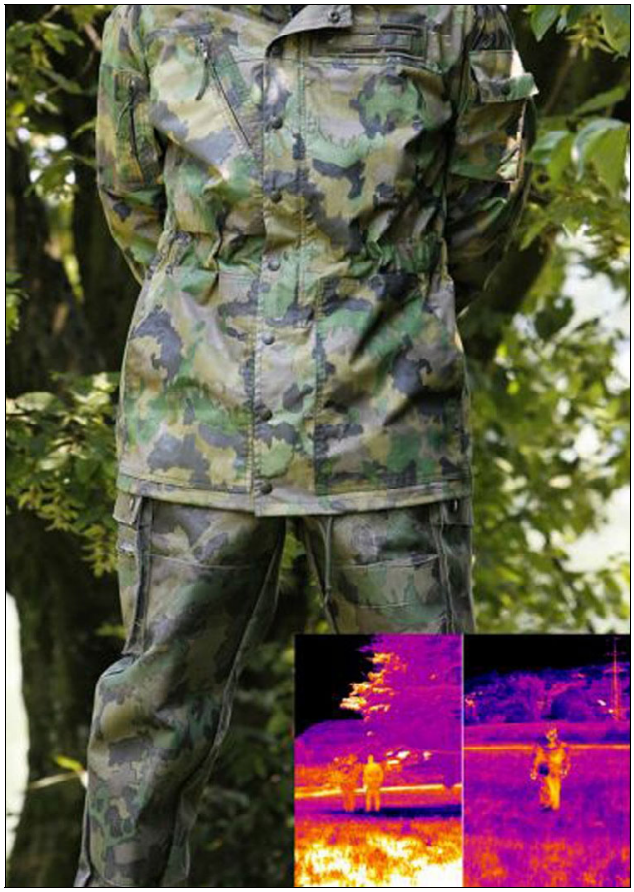

Fig. 2. Wareman in a form with the elements of disguise in an optical range, and in infra-red (in to the rights lower corner)

whereas many other technologies with the purpose to make a subject invisible are considered; it doesn't mean "to invent an invisible covering", but merge of object to its background as is possible in the bigger range of a range in Fig. 2 and Fig. 3 [2].

thermodynamic equilibrium with absolutely black body at this temperature, is called as thermal equilibrium radiation. Equilibrium thermal radiation is uniform, isotropic and isn't polarized, transfer of energy in it's absent and all its characteristics depend only on temperature of absolutely black body radiator. Initially green I was in the preferable color as the majority of wars were carried to be carried in Europe where the grass and trees were the prevailing natural elements. Further the partitioning templates with two, three or more flowers entered game and those armies which deployed the soldiers in different scenarios started diversifying the camouflage.

Fig. 3. Image of locomotive tank in an infrared range, got by heat vision, placed on a pilotless aircraft. On a colour gamut to define real it is a tank or inflatable model of tank

Experimental. The electromagnetic radiation which is in This Army Tactics, Techniques, and Procedures (ATTP) is intended to help company-level leaders understand the principles and techniques of camouflage, concealment, and decoys (CCD) [3, 4]. To remain viable, all units must apply CCD to personnel and equipment. Ignoring a threat's ability to detect friendly operations on the battlefield is short-sighted and dangerous. Friendly units enhance their survivability capabilities if they are well versed in CCD principles and techniques. In NATO it wasn't reached agreements on standards on patterns and flowers though the document AEP – 31 is the recommendation about the applied colors of a so-called spotty camouflage for military equipment. In the present terms of radio electronic secret service a camouflage cover already is not effective without possibility of operative manipulation of its colour gamut, and protecting from the radiation of objects, that are into it in Fig. 4. The current tendency is a transition from colors on the basis of solvents to products on a water basis in connection with the strict nature protection legislation which require lowering of volatile organic components. That fact that night vision glasses of new generation work in the range lower than 1,2 μm, forces vendors of fabrics to use new colorants which could be effective in the range of 1,8 ÷ 2,0 μm [2]. Opportunity to change characteristics shows how strongly Leps coverings from Intermit differ from the standard colors in a short-range infrared spectrum developed for counteraction to systems of night vision of the 70 th years which however, are still widespread. Soldiers must be aware that an enemy can detect, identify, and acquire targets by using resources outside the visual portion of the EM spectrum. Many threat forces were trained and equipped by the former Soviet Union. Its long-standing battlefield doctrine of camouflage is a living legacy in many former Soviet-client states. Enemy forces that are trained in maskirovka possess a strong fundamental knowledge of CCD principles and techniques. Friendly forces must be very careful to conduct CCD operations so that a well-trained enemy will not easily recognize them. On a picture 5 a difference is retimed in the cal radiance house in the background, which is painted the special paint (paint with a low radiate ability which weakens only (static mode)), and house on a foreground which is not painted. That is the substantial failing in the plan of decamouflage?

Fig. 4. Secret service a camouflage cover already is not effective without possibility of operative manipulation of its colour gamut, and protecting from the radiation of objects, that are into it [2]

An enemy uses many different types of electronic surveillance equipment. Sensor systems are classified according to the part of the EM spectrum in which they operate. Fig. 2–3 shows the EM spectrum and some typical enemy sensors operating within specific regions of the spectrum. An enemy uses detection sensors that operate in the active or passive mode:

Active sensors emit energy that reflects from targets and is recaptured by the emitting or other nearby sensor, indicating the presence of a target. Examples of active sensors are searchlights and radar.

Passive sensors do not emit energy; they collect energy, which may indicate the presence of a target. Examples of passive sensors are the human eye, night-vision devices (NVDs), IR imaging devices, acoustic sensors, and photographic devices. Visual sensors work in the parts of the EM spectrum that are visible to the human eye. Enemy soldiers' eyes are the principle sensors on a battlefield. They may be aided by binoculars, telescopic sights, and image intensifiers. Civilian populations, enemy agents, recon teams, and patrols are visual-sensor systems from the enemy's intelligence viewpoint.

Results and discussion. Not a lot of information is available about the coverings of the Intermat company reducing a purpose radar scattering cross-section which, according to the company, provide lowering for 97 % in the X-range (the frequency range of 5,2 ÷ 11 GHz) (Fig. 5). It means that the detection range for a radar decreases more than half, as the equation non-linear. After drying thickness of a film makes about 1,5 mm and is compatible to anti-thermal coverings. Both formulas can be connected in uniform substance for the

purpose of support of lowering of thermal and reflection power. In case of deployment of machines in operations adaptation of their camouflage diagrams is necessary worldwide they corresponded to the unrolled regions. When sending to operational theatres on the long terms the decision on repainting of technique is made.

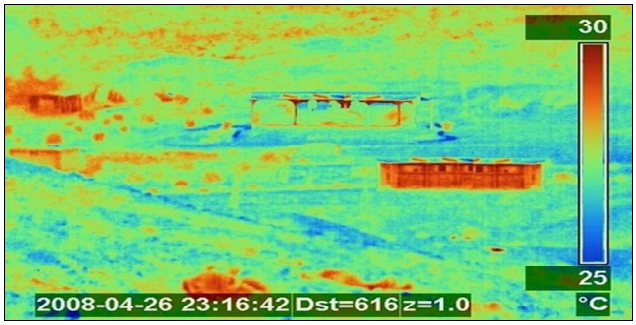

Fig. 5. Difference in the caloradiance of house in the background, which is painted the special pain (paint with a low radiate ability which weakens only (static mode)), and house on a foreground which is not painted

However, as transportation of heavier machines on TVD is excessively expensive, many armies aim to leave them there as it is possible not to change more long and respectively their painting. Easy machines on the other hand are exposed to rotation together with subdividing which can be torn for a period of up to 9 months. In this case the machine collaring with use of constant color according to the new diagram, that is desert, a three-collared pattern or completely white diagram of the UN, can become expensive pleasure as this necessary operation shall repeat in case of each re-deployment.

The material Ulcas also provides protection against radar investigation in the range of the frequencies of 1 ÷ 100 GHz. Steady against chemical influence, Ulcas it can be used at temperatures from – 20 °C to + 80 °C and has mass less than 250 g/m^2. Changing the geometrical form of the machine and reducing its thermal and radar signatures (even in movement), it, for example, also reduces chances of receiving shock from the shell attacking on top. This company makes use of the experience in paint and varnish coverings for production of anti-thermal and anti-radar camouflage networks, coverings and films, also as awnings and a personal camouflage. Its Arcus networks weaken radar signals in the range of 58 ÷ 100 GHz, especially in a segment of 8 ÷ 40 GHz, with the variable level of weakening of component 10 ÷ 35 dB. Besides, all fabrics are processed by anti-thermal coverings and can be made on any camouflage template. The company makes awnings, and also suits for snipers from "air-penetrating" anti-thermal fabric with a density 60 g/m^2 [2–4].

The mobile camouflage system of MCS (Mobile Camouflage System) from the same company is based on similar three-dimensional material, but its configuration is set up under machine type for further improving of division in visible, thermal and radar ranges. By operation in hot climate of MCS it can be integrated with HTR Cool cam where HTR means Heart Reduction (heat release lowering). Working at the expense of a combination of insulation and reflection of solar radiation, the system prevents heating up of a surface of the machine under the sun, and, as a result reduces temperature inside. Also multispectral Shadow Umbrella allowing not only working in open manholes in solar time, but also guaranteeing full masking against air reconnaissance even is offered when the crew manholes leaves open.

The dynamic range of disguise is supposed by integration on-the-spot of object of local elements with a variable amplification or weakening of radiation in the set range of frequencies factor. In Fig. 6 it is possible to see the attempt of realization of the similar system which works in the mode of 3-D (that works in a visible, thermal and radiolocation spectrum). IR sensors detect the contrasts in heat energy that targets radiate on the battlefield and display the contrasts as different colors or shades. Because longer wavelength IR radiation is more susceptible to atmospheric absorption than NIR radiation, IR sensors are less affected by typical concentrations of fog or conventional smoke.

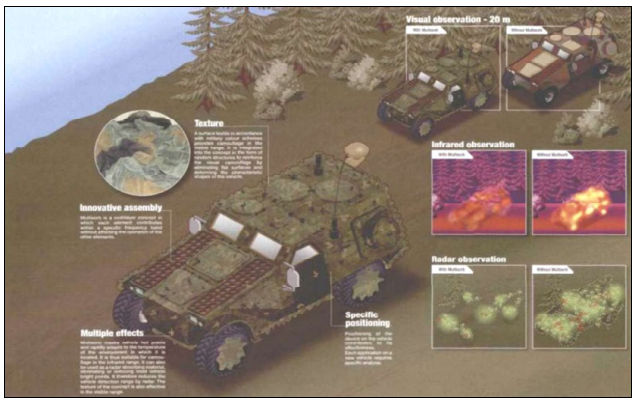

Fig. 6. The dynamic range of disguise is supposed by integration on-the-spot of object of local elements with a variable amplification or weakening of radiation in the set range of frequencies factor [3]

Differences in thermal mass and surface properties (reflectivity) of man-made and natural materials result in target-to-background contrasts. These contrast levels change dramatically over a daily cycle. For example, operating vehicles and generators, heated buildings and tents, and soldiers are usually hotter than their background. Also, equipment exposed to direct sunlight appears hotter than most natural backgrounds. At night, however, equipment might appear cooler than its background if it is treated with special emissivity coatings. In other words, military equipment, particularly metallic equipment, generally heats up and cools off more quickly than its background. Sophisticated, passive IR sensors (such as the Forward-Looking Infrared System [FLIRS]) can be mounted on aircraft. FLIRS sensors provide aircrews and enemy ground forces with real-time IR imagery that is displayed on video monitors. Due to film processing, however, these systems are subject to time delays in obtaining the data. Newer versions of this sensor produce non -film-based images. The UV area is the part of the EM spectrum immediately below visible light. UV sensors are more important in snow-covered areas, because snow reflect s UV energy well and most white paints and man-made objects do not reflect UV energy very well. Photographic intelligence systems with simple UV filters highlight military targets as dark areas against snow-covered backgrounds. These backgrounds require specially designed camouflage that provides a high UV reflectance. As local elements with a variable amplification factor it is possible to use usual light-emitting diodes, computer-integrated in texture of protective material (wares), for example camouflage from microcircuits of type PLIS (programmable logical integrated circuits) in Fig. 7. Radar uses high-frequency radio waves to penetrate atmospheric impediments such as fog, mist, and smoke.

Radar works by transmitting a very strong burst of radio waves and then receiving and processing the reflected waves. In general, metal objects reflect radar waves well, while radar waves are either weakly reflected by or pass through most other objects. The shape and size of a metal object determine the strength of the reflected signal. A large, metal object generally reflects more signal than a small object. Therefore, large, metal objects can be detected from greater distances. Threat forces make a great effort to search for, detect, and locate the sources of US radiocommunications. They use various direction-finding techniques to locate opposing emitters. Once an emitter is detected, an enemy can take a number of actions, ranging from simply intercepting the transmissions to jamming or targeting the emitter for destruction.

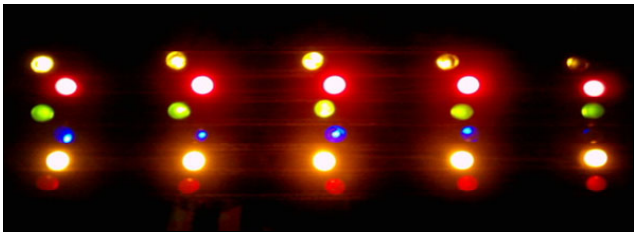

Fig. 7. The eltment camouflage with program – apparate sewing microcircuits of type programmable logical integrated circuits

Target acquisition can be accomplished by a variety of sensors that operate throughout the EM spectrum. This poses a challenge in CCD planning and employment–determining which enemy sensor(s) that CCD operations should be designed to defeat. Unfortunately, no single answer is correct for all situations. Unit commanders without specific guidance from higher echelons assess their tactical situation and plan CCD operations accordingly. If intelligence data indicate that an enemy will use visual sensors for recon and target acquisition, then visual countermeasures must be employed in Fig. 8. For IR or radar sensors, countermeasures that are effective in those spectra must be employed. If a multispectral or spectral threat is anticipated, CCD operations are conducted to protect a unit in its most vulnerable EM bandwidths. Very few available camouflage materials or techniques provide complete broadband protection. Movement attracts the enemy's attention and produces a number of signatures (tracks, noise, hot spots, dust). In operations that inherently involve movement (such as offensive operations), plan, discipline, and manage movement so that signatures are reduced as much as possible (Fig. 9).

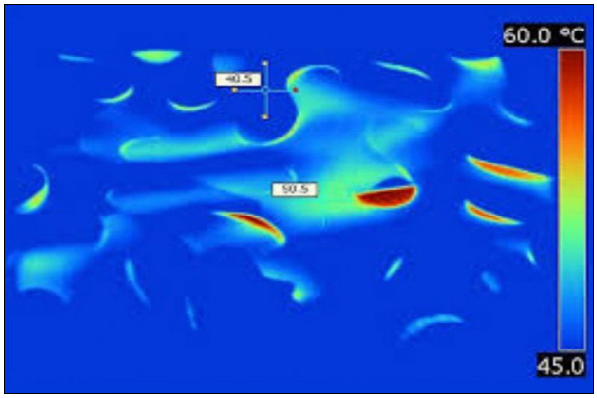

Fig. 8. The networks can work in visible, radiolocation and infra-red spectrums and guarantee weakening of thermal selection even at a contact with a hot surface

Fig. 9. Wareman in a form with the elements disguise in positivity camouflage[4]

By analogy creations of term dazedly on the basis of radio engineering net from materials (metals with large resistance) it is possible to create a radio engineering net (successive-parallel connections on the basis of modern light-emitting diodes which can change a wave-length (frequency of radiation) in a wide range from infrared to the ultraviolet range (250–3000 nm) The fundamentals of CCD do not change between environments. The seven rules for avoiding detection and the seven recognition factors that are listed in chapter 3 and the three CCD principles–preventing detection, improving survivability, and improving deception capabilities–still apply. However, the guidelines for their application change. Different environments require thoughtful, creative, and unique CCD techniques. This chapter discusses different CCD techniques that have proven effective in three special environments–desert, snow-covered areas, and urban terrain (Fig. 10).

The physical characteristics of urban areas enhance CCD efforts. The dense physical structure of these areas generates clutter (an abundance of EM signatures in a given area) that increases the difficulty of identifying specific targets. Urban clutter greatly reduces the effectiveness of a threat's surveillance sensors, particularly in the IR and radar wavelengths. Urban terrain, therefore, provides an excellent background for concealing CPs, reserves, combat-service-support complexes, or combat forces. The inherent clutter in urban terrain generally makes visual cues the most important consideration in an urban CCD plan.

Fig. 10. Wareman in a form with the elements disguise in activity camouflage [5]

The regular pattern of urban terrain; the diverse colors and contrast; and the large, enclosed structures offer enhanced concealment opportunities. Established, hardened road surfaces effectively mask vehicle tracks. Depending on the nature of the operation, numerous civilian personnel and vehicles may be present and may serve as clutter. This confuses an enemy's ability to distinguish between military targets and the civilian population. Underground structures (sewers, subways) are excellent means of concealing movement and HVTs.

When augmented by artificial means, man-made structures provide symmetrical shapes that provide ready-made CCD. The CCD for fighting positions is especially important because of the reduced identification and engagement ranges (100 meters or less) typical of urban fighting. Limit or conceal movement and shine. These signatures provide the best opportunity for successful threat surveillance in urban terrain. Careful placement of equipment and fighting positions remains important to provide visual CCD and avoid detection by contrast (thermal sensors detecting personnel and equipment silhouetted against colder buildings or other large, flat surfaces).

Conclusions. At last, the purpose of traps is rather not concealment of some objects, and it is rather a tangling of the opponent. They provide an effective method on deception of hostile prospecting means and means on information collection and, therefore, reduce efficiency of fire of the opponent. In order that they were probable, traps shall work out a signature which is compatible in all required ranges to the ranges of original system which they represent, that is tan gently visible, short-range IR spectrum, the vision and radar signatures.

Deception in war is the art of misleading the enemy into doing something, or not the enemy into doing something, or not doing something, so that his strategic doing something, so that his strategic or tactical position will be weakened or tactical position will be weakened. Deception needs to be part of the plan. It must appear believable.

Drawing attention can get you killed. Deception is part of every level; visual, SigInt, ElInt, ComINT [5].

REFERENCE

1. [Electronic resource]. – URL: http://stjag.ru/index.php/en/?option=com_k2&view=item&id=31088.
2. [Electronic resource]. – URL: http://army-news.ru/2014/06/obzor-zarubezhnyx-produktov-v-sfere-kamuflyazha-i-maskirovki/
3. [Electronic resource]. – URL: http://www.us.army.mil
4. [Electronic resource]. – URL: http://www.train.army.mil
5. [Electronic resource]. – URL: www.apd.army.mil

Submitted on 16.02.17

О. Іванюта, канд. ф.-м. наук, С Кратько, студ.
факультет радіофізики, електроніки та комп'ютерних систем
Київський національний університет імені Тараса Шевченко

МОДЕРНІЗАЦІЯ СИСТЕМ ПАСИВНОГО МАСКУВАННЯ

У статті розглянуті методи маскування як елементи спотворення силуетів видимих предметів. Вони створюють забарвлення спеціальних форм, щоб проводити ідентифікацію елементів або напрямок їх руху. Були запропоновані методи і структура напрямів модернізації до існуючих вже маскуючих систем в широкому динамічному та спектральному діапазонах. Показано, що завдання маскування – демаскування може бути вирішене оперативною зміною принту засобами радіотехніки на основі систем із без корпусними світлодіодами.

Ключові слова: рухлива маскувальна система, оптична амплітуда, методи камуфляжу, маскування, приманки.

А. Иванюта, канд. ф.-м. наук, С Кратько, студ.
факультет радиофизики, электроники и компьютерных систем
Киевский национальный университет имени Тараса Шевченко

МОДЕРНИЗАЦИЯ СИСТЕМ ПАССИВНОЙ МАСКИРОВКИ

В статье рассмотрены методы маскировки как элементы искажения силуэтов видимых предметов. Они отображают окраску специальных форм, чтобы проводить идентификацию элементов или направления их движения. Были предложены методы и структура направлений модернизации к существующим уже маскирующим системам в широком динамическом и спектральном диапазонах. Показано, что задачи маскировки – демаскировки может быть решена оперативным изменением принта средствами радиотехники на основе систем с бескорпусными светодиодами.

Ключевые слова: подвижная маскировочная система, оптическая амплитуда, методы камуфляжа, маскировки, приманки.

UDC 621.315.592

S. Levitskiy, Ph. D.
M. Fomin, Stud.,
Department of Radio Engineering and Radio Electronic Systems,
Faculty of Radiophysics, Electronics and Computer Systems,
National Taras Shevchenko University of Kyiv

PECULIARITY OF THE LC-OSCILLATOR IN SATURATION REGIME

In this paper has been determined a specific mechanism phenomenon nonisochronism. This phenomenon was described concerning to our oscillator – a inductive three points oscillator on bipolar npn - transistor with a common emitter.

Keywords: LC-oscillator, saturation regime, nonisochronism.

Introduction. In the simulation of LC-oscillators by the Multisim – program it was been observed that when the self-excitation oscillator is entering in the saturation regime, the frequency of its oscillations is slightly reduced (Fig.1). It is a well known phenomenon of nonisochronism, when increasing of the amplitude of oscillation causes in nonlinear systems to reduce there frequency [1, 2]. Potential U_{Km} becomes greater than the voltage supply V1, the voltage at the collector-base transition changes its sign, and the collector becomes somewhat more negative from the base, so that the collector-base transition of the transition opens.

Then the collector current begins to flow in a reverse direction opposite to that which would have to come from the emitter. And there in oscillograms of the collector. The task of this work was to determine the specific mechanism of this phenomenon concerning to our oscillator – a inductive three points oscillator on bipolar npn-transistor with a common emitter (Fig. 2).

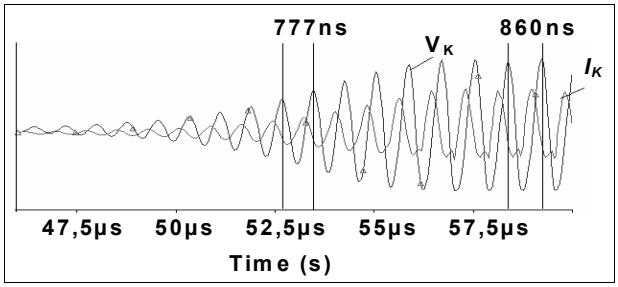

Fig. 1. Reducing of frequency generating of voltage on the collector

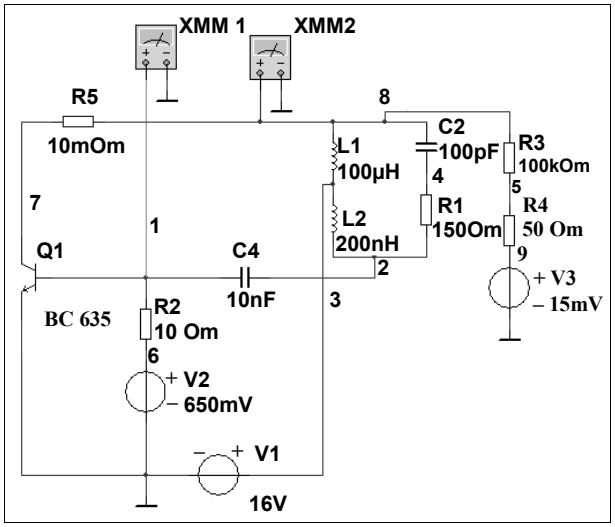

Fig. 2. Inductive three points oscillator on bipolar *npn*-transistor with a common emitter

The phenomenon of saturation in this oscillator is that with the growth of oscillations amplitude, when the collector current is observed a ejection (Fig. 3), which may even exceed the direct collector current.

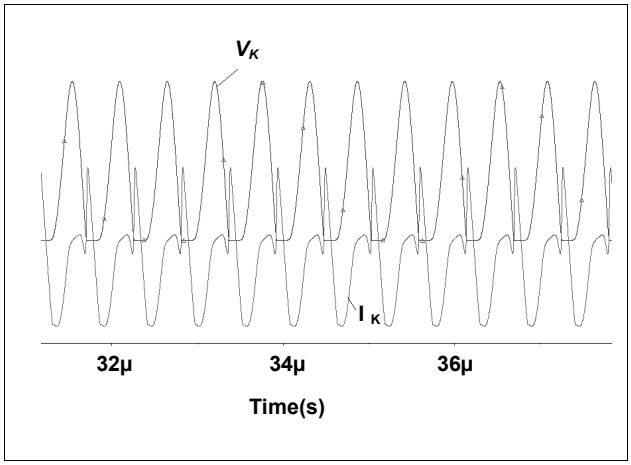

Fig. 3. Current and voltage of collector

As this ejection takes place not just at the moment of maximum collector current (and minimum voltage on the collector, as it would be), is due to the fact that the collector current I_K of the transistor causes inertia lags behind in time of collector voltage V_K [3, 4]. While its negative ejection must be confined to the date of the entering of the transistor in the saturation mode.

So, in some saturation moments the carriers are injected into the base simultaneously on both sides - both the emitter and collector of. This leads to a temporary large increase of the space charge in the base, which can not be dissolved during the period of oscillation.

The managing performance of the base is weaken, the work pace of the transistor decreases and the generated frequency will be somewhat reduced. That is is really observed by modeling these processes. Switching of Schottky diodes between the collector and the base removed this effect, and the generated frequency was increased.

REFERENCES

1. *Anisimov I.O.* Kolivannya ta hvili. – K. : "Kiyivskiy universitet", 2009.
2. *Butenin, N.V., Neymark Y.I., Fufaev I.A.* Vvedenie v teoriyu nelineynyih kolebaniy. – M. : Nauka, 1987.
3. *Levitskiy S.M.* Osnovi radIoelektroniki. – K. : "Kiyivskiy universitet", 2007.
4. *Kuklin. L.P.* Generatory sinusoidalnyih kolebaniy i nelineynyie preobrazovaniya signalov. – M. : MFTI, 2010.

Submitted on 23.02.17

С. Левитський, д-р, фіз.-мат. наук,
М. Фомін, студ.,
кафедра радіотехніки та радіоелектронних систем,
факультет радіофізики, електроніки та комп'ютерних систем,
Київський національний університет імені Тараса Шевченка

ОСОБЛИВОСТІ РОБОТИ *LC*-АВТОГЕНЕРАТОРА В РЕЖИМІ НАСИЧЕННЯ

Визначено конкретний механізм явища неізохронності. Це явище було описано щодо нашого осцилятора – індуктивної триточки, генератора на біполярному прп-транзисторі з загальним емітером

Ключові слова: LC-автогенератор, режим насичення, неізохронність.

С. Левитський, д-р, физ.-мат. наук,
Н. Фомин, студ.,
кафедра радиотехники та радиоелектронних систем,
факультет радиофизики, электроники и компьютерных систем,
Киевский национальный университет имени Тараса Шевченко

ОСОБЕННОСТИ РОБОТЫ LC-АВТОГЕНЕРАТОРА В РЕЖИМЕ НАСЫЩЕНИЯ

Определен конкретный механизм явления неизохронности. Это явление было описано по отношению к нашему осциллятору – индуктивной трёхточке, генератора на биполярном прп-транзисторе с общим эмиттером.

Ключевые слова: LC-автогенератор, режим насыщения, неизохронность.

UDC 612.799.1; 53.06

Eu. Martysh, Dr. Sci.,
Yu. Veremii, Ph. D.,
Medical Radio Physics Department,
Faculty of Radiophysics, Electronics and Computer Systems,
Taras Shevchenko National University of Kyiv

COMPARATIVE ANALYSIS OF METHODS AND DEVICES IN COSMETIC EPILATION

Modern hair removal techniques as laser hair removal, electro-epilation, chemical hair removal are known in modern cosmetic surgery. The main type of modern electro-epilation is thermolysis, a process where the hair is destroyed thermally, by sharp heating with high frequency alternating current. Thermolysis is used for all types of hair, but requires perfect technique, since it has a relatively high probability of obtaining significant burns. This method also has a large number of contraindications and serious complications. Most of them are connected with basic acting factor of both methods – heat shock. Cold atmospheric plasma provides selectively applying chemical energy to a target location on an external body surface, such as skin tissue for hair removal or prevent or inhibit hair growth.

Keywords: hair removal, electrotherapy, laser hair removal, microdischarge, low-temperature plasma, cold plasma treatment.

Introduction. Such modern hair removal techniques as laser hair removal, electro-epilation, chemical hair removal are known in modern cosmetic surgery. With a professionally conducted course of procedures, all these techniques allow achieving a certain result. The main type of modern electro-epilation is thermolysis, a process where the hair is destroyed thermally, by sharp heating with alternating current (frequency from 9 to 14 MHz). Thermolysis is used for all types of hair, but requires perfect technique, since it has a relatively high probability of obtaining significant burns [8].

Laser hair removal is a leading modern method of combating unwanted hair. Under the influence of light radiation, the hair follicle heats up and collapses. The effect of the procedure depends largely on the professionalism of the doctor and the laser device chosen. There are also a large number of contraindications and serious complications. These are: skin burns, folliculitis, allergic reactions and others [6]. It can be argued that the absolute majority of the shortcomings of the two main methods of epilation discussed above come from heat shock. It is the basic acting factor of these methods. It is well-known that cold atmospheric plasma (CAP) is attracting considerable attention due to their capability in biomedical applications because most bio organisms are very vulnerable to thermal shock [4].

CAP device causes hair loss or prevent or inhibit hair growth with plasma providing a control means for controlling the flow of the gas source. Also it provides the means for controlling the run time, voltage and current of the electrode. CAP is provided for selectively applying chemical energy to a target location on an external body surface, such as skin tissue e.g., the removal of pigmentations, scars, tattoos, etc., and for other surgical procedures on the skin, such as tissue rejuvenation, cosmetic surgery, hair removal and/or transplant procedures. The superiority of plasmas in comparison to previous medical standards remains to be clarified, especially in physiologic and economic terms.

In the paper shown brief review modern methods of cosmetic epilation and offered the alternative method with using cold atmospheric plasma.

Hair. Each strand of hair is made up of the medulla, cortex, and cuticle (Fig. 1). The innermost region, the medulla, is not always present and is an open, unstructured region. The highly structural and organized cortex, or middle layer of the hair, is the primary source of mechanical strength and water uptake. The cortex contains melanin, which colors the fiber based on the number, distribution and types of melanin granules. The shape of the follicle determines the shape of the cortex, and the shape of the fiber is related to how straight or curly the hair is. The cuticle is the outer covering. Its complex structure slides as the hair swells and is covered with a single molecular layer of lipid that makes the hair repel water. The diameter of human hair varies from 0.017 to 0.18 mm.

Hair growth begins inside the hair follicle. The only "living" portion of the hair is found in the follicle. The hair that is visible is the hair shaft, which exhibits no biochemical activity and is considered "dead". The base of a hair's root (the "bulb") contains the cells that produce the hair shaft. Other structures of the hair follicle include the oil producing sebaceous gland which lubricates the hair and the arrector pilimuscles.

Most common interest in hair is focused on hair growth, hair types and hair care. Attitudes towards different hair, such as hairstyles and hair removal, vary widely across different cultures and historical periods, but it is often used to indicate a person's personal beliefs or social position, such as their age, sex, or religion [2].

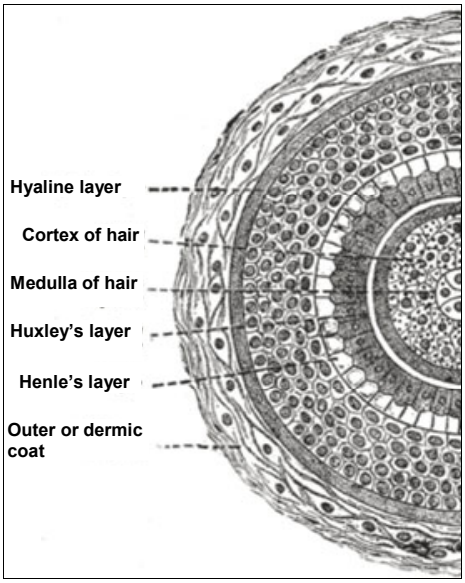

Fig. 1 Hair structure

Cosmetic electrotherapy. Cosmetic electrotherapy is a range of beauty treatments that uses low electric currents passed through the skin to produce several therapeutic effects. There are four main types of treatment, that differ in the type of current they use including:

Galvanic treatment;

Neuromuscular electrical stimulation (NMES);

Micro-current electrical neuromuscular stimulation (MENS);

High-frequency treatment.

High-frequency treatment (HFT) (Fig. 2) uses low-current high-frequency alternating currents, delivered via a glass electrode. Because the high frequency current converts some of the oxygen in the air into ozone, the treatment has a germicidal action, and is also drying and warming. Consequently, the treatment is used to aid healing and also to help desquamation (the skin's natural exfoliation) and stimulate sweat and sebaceous glands.

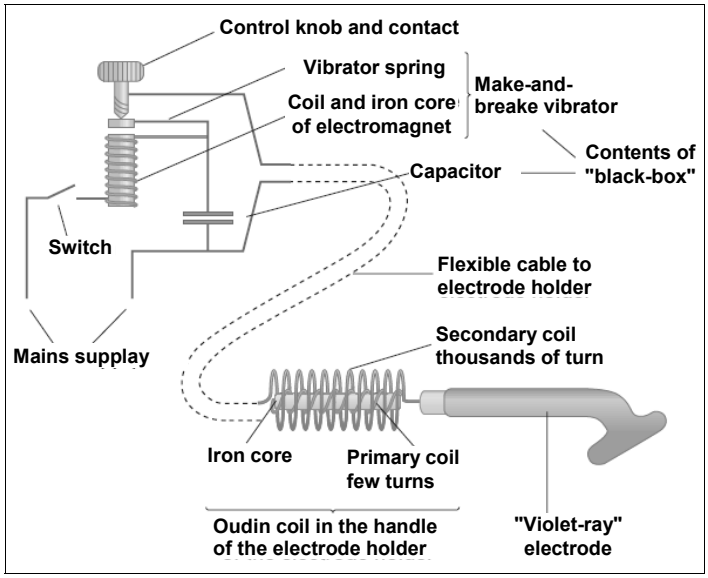

Fig. 2. High-frequency treatment device

At up to 250,000 Hz frequency, the hollow glass electrode behaves like a glow discharge tube and is sometime called a "violet ray" or "violet wand" (though the colour depends on the gas in the glass). Similar devices are used in hair depilatory.

HFT procedures involve threading a thin wire into a set of follicles and then applying an electric current. Depending on the nature of the device, the hair follicle is destroyed either by the production of heat or sodium hydroxide. This process is painful and requires consider a limited number of follicles so that it is quite time-consuming. Multiple treatments of a follicle are often necessary to achieve permanent destruction. Pigmentation at the site of treatment is common. Since considering of limited number of follicles, HFT of large areas is quite arduous.

Contra-indications to high-frequency treatments: cuts or abrasions to the skin in the area to be treated; skin diseases or disorders; highly vascular conditions; sensitive skin; highly nervous clients; excessive metal in the area; swellings in the area; very hairy areas; sinus blockages; heart conditions; epilepsy or diabetes; circulatory problems; pregnancy; asthmatics.

Laser hair removal. Laser hair removal is the process of removing unwanted hair by means of exposure to pulses of laser light that destroy the hair follicle (Fig. 3**)**. It had been performed experimentally for about twenty years before becoming commercially available in the mid-1990s. Many reviews of laser hair removal methods, safety, and efficacy have been published in the dermatology literature [1].

The primary principle behind laser hair removal is selective photothermolysis (SPTL), the matching of a specific wavelength of light and pulse duration to obtain optimal effect on a targeted tissue with minimal effect on surrounding tissue. Lasers can cause localized damage by selectively heating dark target matter, melanin, in the area that causes hair growth, the follicle, while not heating the rest of the skin. Light is absorbed by dark objects, so laser energy can be absorbed by dark material in the skin, but with much more speed and intensity. This dark target matter, or chromophore, can be naturally occurring or artificially introduced.

Melanin is considered the primary chromophore for all hair removal lasers currently on the market. Melanin occurs naturally in the skin and gives skin and hair their color. Because of the selective absorption of photons of laser light, only black or brown hair can be removed. Laser works best with dark coarse hair. Light skin and dark hair are an ideal combination, being most effective and producing the best results, but new lasers are now able to target black hair in patients with dark skin with some success.

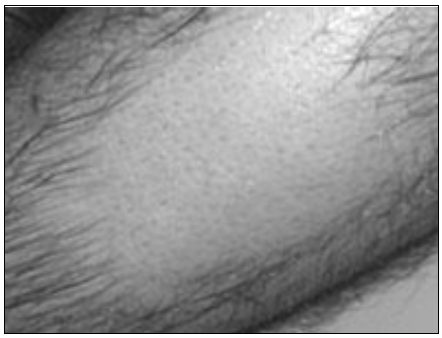

Fig. 3. Laser epilation

Under the FDA's definition, "permanent" hair reduction is the long-term, stable reduction in the number of hairs regrowing after a treatment regime. This means that although laser treatments with these devices will permanently reduce the total number of body hairs, they will not result in a permanent removal of all hair.

Laser hair removal has become popular because of its speed and efficacy, although some of the efficacy is dependent upon the skill and experience of the laser operator, and the choice and availability of different laser technologies used for the procedure. Some will need touch-up treatments, especially on large areas, after the initial set of 3-8 treatments.

The important output parameter when treating hair (and other skin conditions) is power density – this is a combination of energy, spot diameter and pulse duration. These three parameters determine what actually happens when the light energy is absorbed by the tissue chromophore be it melanin, hemoglobin or water, with the amount of tissue damaged being determined by the temperature/time combination. Hair grows in several phases (anagen, telogen, catagen) and a laser can only affect the currently active growing hair follicles (early anagen). Hence, several sessions are needed to kill hair in all phases of growth.

Multiple treatments depending on the type of hair and skin color have been shown to provide long-term reduction of hair. Most patients need a minimum of seven treatments. Current parameters differ from device to device but manufacturers and clinicians generally recommend waiting from three to eight weeks between sessions, depending on the area being treated. Some normal side effects may occur after laser hair removal treatments, including itching, pink skin, redness, and swelling around the treatment area or

swelling of the follicles (follicular edema). These side effects rarely last more than two or three days. The two most common serious side effects are acne and skin discoloration. Some level of pain should also be expected during treatments. Risks include the chance of burning the skin or discoloration of the skin, hypopigmentation (white spots), flare of acne, swelling around the hair follicle (considered a normal reaction), scab formation, purpura, and infection. These risks can be reduced by treatment with an appropriate laser type used at appropriate settings for the individual's skin type and treatment area.

Comparison with Intense Pulsed Light. A 2006 review article in the journal "Lasers in Medical Science" compared intense pulsed light (IPL) epilators and both alexandrite and diode lasers. The review found no statistical difference in short term effectiveness, but a higher incidence of side effects with diode laser based treatment. Hair reduction after 6 months was reported as 68.75 % for alexandrite lasers, 71.71 % for diode lasers, and 66.96 % for IPL. Side effects were reported as 9.5 % for alexandrite lasers, 28.9 % for diode lasers, and 15.3 % for IPL (see Table 1). All side effects were found to be temporary and even pigmentation changes returned to normal within 6 months.

Table 1

Lasers and their characteristics

Laser Used	Wavelength (nm)	Light Source	Type of Skin used on
Argon	488 nm or 514.5 nm	Turquoise/ Cyan or Green	No longer used
Ruby	694.3 nm	Deep red	Pale
Alexandrite	755 nm	Near-infrared	All skin types
Pulsed diode array	810 nm	Near-infrared	Pale to medium
Nd:YAG	1064 nm	Near-infrared	Darker complexion
Intense pulsed light (IPL is not a laser)	650 nm	Not a laser	Pale to medium

IPL, though technically not containing a laser, are sometimes incorrectly referred to as "laser hair removal". IPL-based methods, sometimes called "phototricholysis", or "photoepilation", use xenon flash lamps that emit full spectrum light. IPL systems typically output wavelengths between 400 nm and 1200 nm. Filters are applied to block shorter wavelengths, thereby only utilizing the longer, "redder" wavelengths for clinical applications. IPLs offer certain advantages over laser, principally in the pulse duration. While lasers may output trains of short pulses to simulate a longer pulse, IPL systems can generate pulse widths up to 250ms which is useful for larger diameter targets. Some current IPL systems have proven to be more successful in the removal of hair and blood vessels than many lasers.

Comparison with electrolysis. Unlike laser epilation, electrolysis can be used to remove 100 % of the hair from an area and is effective on hair of all colors, if used at an adequate power level with proper technique.

A study conducted in 2000 at the ASVAK Laser Center in Ankara, Turkey, comparing alexandrite laser and electrolysis for hair removal on 12 patients concluded that laser hair removal was 60 times faster, less painful and more reliable than electrolysis. It is important to note that the type of electrolysis performed in the study was galvanic electrolysis, rather than thermolysis or a blend of the two. Galvanic current requires 30 seconds to more than a minute to release each hair whereas thermolysis or a blend can require much less.

Adverse effects of laser. Laser treatments are basically burns. The following effects may occur:

- Temporary pain, redness, bruising, blistering and/or crusting;
- Infection, including reactivation of herpes simplex or folliculitis (Fig. 4);
- Pigment changes (brown and white marks), which may be permanent;
- Scarring.

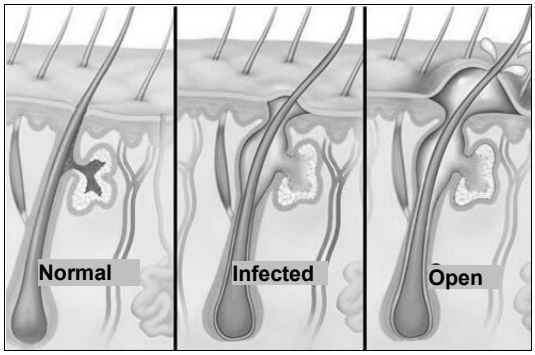

Fig. 4. Various types of hair with follicle

Folliculitis can be caused by a large number of infectious organisms. However, frequently folliculitis is sterile and seems to be induced by irritating chemical substances, drugs and physical irritants like shaving. Differentiating these causes is very important if the physician is going to be able to treat the condition successfully.

Novel plasma source for biological and medical applications. Nonthermal, low-temperature plasmas, having populations of high-temperature electrons and ions at or near room temperature mixed with a neutral gas background, are emerging as a novel tool for *in vivo* nondamaging treatment of living tissues in biological and medical applications. To be efficient for this purpose, plasma should meet the following criteria: it should significantly reduce bacterial density in the determinated area, cause a long-term post-irradiation inhibition of bacterial growth, without causing any negative effect on the natural living cells.

The sterilizing effect of the plasma source is mainly due to oxygen free radicals, like atomic oxygen O and hydroxyl group OH, other reactive oxygen species (ROS) and UV radiation have an essential role in the plasma germicidal effect. But, under the promise of sterilization effect, industrial applications can select their appropriate operating conditions. There are types of feeding gas and systems energy efficiency as the strong criterions among them. In order to satisfy these requirements of plasma characteristics and its production, a new generation of plasma sources specifically designed for this kind of application is being developed [3].

Microdischarges are direct current discharges that operate at a relatively high pressure of about 10–1000 Torr and geometric dimensions in the several hundred micrometer ranges. Microhollow cathode sustained discharge (MCSD) is a particular type of microdischarges configuration that uses microhollow cathode discharge (MHCD) as an electron source for sustaining larger volume plasma. At high gas pressure, microdischarges in these specific geometries possess several unique properties that can be very stable and useful tools for surface treatment, reduction of pollutants and generation of UV and VUV radiation. Limi-

tation of experimental data in conventional diagnostics due to small dimension a detailed study on this microdischarge relies on numerical analysis. Combined simulation of the MCSD and the MHCD is attempted and the corresponding simulation results of discharge properties such as electrostatic potential, electron density, atomic and molecular ion densities, excited species (metastables) densities, electron temperature, gas temperature etc.

Several atmospheric-pressure plasma jets at the microscale (micro-APPJs) have been developed by various groups and are widely used in applications ranging from thin film deposition to sterilization and biological decontamination to biomedical, medical, and dental applications and the treatment of temperature-sensitive substrates [7].

Charged species densities of order (10^{11} – 10^{15}) cm^{-3} and metastable species densities of order (10^{10} – 10^{15}) cm^{-3} are predicted for the condition investigated. Electron temperatures of several tens of eV near cathode sheath and ~1 eV in the remaining part of the discharge are predicted.

A distinct characteristic of a jet configuration is its ability to generate a stable discharge in a region of inert gas and then to transport the plasma to a separate region of reactive gas for processing applications, thus providing chemical reactivity without compromising plasma stability. This spatial separation of the plasma generation and surface processing regions allows for flexibility in jet designs to vary and control both plasma dynamics and reaction chemistry. At frequencies below 100 kHz, sub-microsecond pulsed is found to effectively reduce gas temperature.

A device and method to cause hair loss or prevent or inhibit hair growth were investigated in [5]. The CAP is used in this work. It was generated by flowing gas in proximity to an electrode that has a high potential applied to it. The result is a stream (~ 10 cm) of charged gas particles and active spices that are directed to the skin that contains hair. The flowing stream of gas is held above the surface of skin. Contact CAP and mice in [8] has duration one month. On day 30 the hair of animals in the no treatment group was almost completely regrown. In contrast, animals that received plasma treatment showed minimal hair regrowth on day 30.

Conclusions. The main benefits of Cold Plasma Treatment (CPT) with the supporting evidence of the clinical trials are:

- Anti-microbial – kills the bacteria in infected wounds/infections/ulcers leading to shorter healing time (reduced hospital costs)
- Reduces pain – relief for the patients/ reduces need for pain medicine.
- Safe treatment – CPT was used to treat more than 5 hundreds patients over a 2 year period with no side-effects reported.

In the past few years, plasma medicine has become an important field in medical science; as plasma has proven anti-inflammatory, antimicrobial, and antitumor efficacy, most topics are now focusing on immunologic disorders, infections, and dermatology. The non-thermal atmospheric pressure plasmas are adjustable in a wide array and can exhibit a multitude of activities depending on the design of the device. The breakthrough of plasma science into medical science came with the introduction of non-thermal plasma sources in the last years.

REFERENCES

1. *Goldberg D.J.* Laser Hair Removal. 2-nd Ed. / D. J. Goldberg. – CRC Press, 2008.

2. *Grabenhofer R.* Literature review: Damage, growth and conditioning in hair // Cosmetics & Toiletries, 2014. – Vol. 129(5). – P. 34–46.

3. *Graves D.B.* The emerging role of reactive oxygen and nitrogen species in redox biology and some implications for plasma applications to medicine and biology / D.B. Graves // Journal of Physics D: Applied Physics, 2012. – Vol. 45. – № 26. –P. 121–143.

4. Plasma medicine: Possible applications in dermatology / J. Heinlin, G. Morfill, M. Landthaler et al. // Journal der Deutschen Dermatologischen Gesellschaft, 2010. – B. 8.

5. *Jaroszeski M.J., Lopez-Diaz G.A., Connolly, R.J. and Hoff A.M.* // Device and method to prevent hair growth, 2013. USF Patents.-2013. – P. 190.

6. *Lin J.-T.* Progress of medical lasers: Fundamentals and applications / J.-T. Lin // Medical Devices and Diagnostic Engineering, 2016. – Vol. 1(2). – P. 36–41.

7. *Martysh Eu.V.* Peculiarities of plasma sources in plasma medicine / Eu.V. Martysh // Bulletin of Taras Shevchenko National Univ. Ser.: Radio-Physics & Electronics, 2013. – № 19 – P. 39–42.

8. Principles of Electrosurgery: Electrocautery : [electronic resource]. – URL: http://www.valleylab.com/education/poes/poes_02.html.

Submitted on 30.10.17

Є. Мартиш, д-р фіз.-мат. наук,
Ю. Веремій, канд. фіз.-мат. наук,
кафедра медичної радіофізики,
факультет радіофізики, електроніки та комп'ютерних систем,
Київський національний університет імені Тараса Шевченка

ПОРІВНЯЛЬНИЙ АНАЛІЗ МЕТОДІВ І ПРИСТРОЇВ ДЛЯ КОСМЕТИЧНОЇ ЕПІЛЯЦІЇ

Сучасні методи видалення волосся представлено такими косметичними операціями, як лазерна епіляція, електроепіляція, хімічна епіляція. Основним видом сучасної електроепіляції є термоліз, процес, при якому волосся знищується термічно, шляхом різкого нагрівання високочастотним змінним струмом. Термоліз використовується для всіх типів волосся, але вимагає ідеальної техніки, оскільки має відносно велику ймовірність отримання значних опіків. Цей метод також має велику кількість протипоказань і серйозних ускладнень. Більшість з них пов'язані з основним діючим фактором обох методів – тепловим шоком. Холодна атмосферна плазма забезпечує вибіркове застосування хімічної енергії до місця призначення на зовнішній поверхні тіла, наприклад, шкірну тканину для видалення волосся, запобігання або пригнічення росту волосся.

Ключові слова: епіляція, електротерапія, лазерна епіляція, мікророзряд, низькотемпературна плазма, обробка холодною плазмою.

Е. Мартыш, д-р физ.-мат. наук,
Ю. Веремий, канд. физ.-мат. наук,
кафедра медицинской радиофизики,
факультет радиофизики, электроники и компьютерных систем,
Киевский национальный университет имени Тараса Шевченко

СРАВНИТЕЛЬНЫЙ АНАЛИЗ МЕТОДОВ И УСТРОЙСТВ ДЛЯ КОСМЕТИЧЕСКОЙ ЭПИЛЯЦИИ

Современные методы удаления волос представлены такими косметическими операциями, как лазерная эпиляция, электроэпиляция, химическая эпиляция. Основным видом современной электроэпиляции является термолиз, процесс, при котором волосы уничтожаются термически, путем резкого нагрева высокочастотным переменным током. Термолиз используется для всех типов волос, но требует идеальной техники, поскольку имеет относительно большую вероятность получения значительных ожогов. Этот метод также имеет большое количество противопоказаний и серьезных осложнений. Большинство из них связаны с основным действующим фактором обоих методов – тепловым шоком. Холодная атмосферная плазма обеспечивает избирательное применение химической энергии к месту назначения на внешней поверхности тела, например, кожную ткань для удаления волос, предотвращения или подавления роста волос.

Ключевые слова: эпиляция, электротерапия, лазерная эпиляция, микроразряд, низкотемпературная плазма, обработка холодной плазмой.

UDC 535.36

O. Machulianskyi, Ph. D.,
Microelectronics department, Faculty of Electronics,
National Technical University of Ukraine Igor Sikorsky Kyiv Polytechnic Institute,
B. Babych, Ph. D. stud.,
Microelectronics department, Faculty of Electronics,
National Technical University of Ukraine Igor Sikorsky Kyiv Polytechnic Institute,
V. Machulianskyi, M. Sci.
Institute for Applied System Analysis,
National Technical University of Ukraine Igor Sikorsky Kyiv Polytechnic Institute

OPTICAL FILTERS ON THE BASIS OF COMPOSITE NANODIMENSIONAL STRUCTURES

Numerical modeling of the electromagnetic response of the metal nanodimensional films and composite metal-dielectric structures formed on their basis was conducted in the wavelength range of 0.2–1.9 microns. A comparative analysis of the calculated and experimental data was presented. Influence of parameters of the studied composites on their electromagnetic response was shown. The recommendations for the creation of optical filters with the set spectral and selective characteristics were proposed.

Keywords: metal nanodimensional films, composite metal-dielectric structures, spectral and selective characteristics, optical filters.

Introduction. Composite nanodimensional structures have a unique electromagnetic property that represents their perspective for various branches of the equipment, in particular for optoelectronics and power. Particular interest is given to transparent optical filters which are used as selective coverings for photoelectric and photothermal converters of energy, functional energy efficient coverings, etc. [5].

The analysis of scientific, technical and patent literature has shown that now for development of optical filters are generally used multilayered interferential structures. Such structures consist of serially located thin layers high-conductivity metals, and also dielectrics that transparent in the visible and infrared range of electromagnetic radiation. However such optical filters [1] have essential shortcomings, namely: complexity of manufacturing techniques and precision control of parameters of multilayered structures; insufficient mechanical durability; high prime cost of coverings; degradation of parameters.

The specified shortcomings can be avoided due to use of the composite metal-dielectric structures containing nanodimensional particles of metal which are distributed in a transparent dielectric matrix. These structures surpass difficult traditional multilayered systems [1, 7] in the properties. The purpose of this work is definition of a response of spectral characteristics of metal-dielectric nanodimensional structures to electromagnetic radiation in the optical range.

Main part. An optical filter based on a composite metal-dielectric structure consisting of a nanosized metal film of silver and a transparent layer (which uses materials with a refractive index of n = 1.7–2.2) is selected as a research object. In [8] it was shown that the operational stability of metal-dielectric structures with a nanosized metal component is determined by the properties of the dielectric component. In this regard, dielectric materials based on aluminum oxynitride, which have high protective properties and chemical resistance, are of particular interest. In addition, controlling the technological parameters of synthesis, you can change their optical properties [4].

In the manufacture of optical filters used barrier layers to eliminate the effects of degradation. They provide a connection between the constituent components and prevent interdiffusion of components. To determine the spectral characteristics of the electromagnetic response of optical filters was used a technique based on the transfer matrix method that presented by us in [2].

As input data for nanosized metal films used optical characteristics given in [6]. For the dielectric component – values of permittivity that determined in the study of the samples of aluminum oxynitride obtained by magnetron sputtering [4]. As a barrier layer – a nanosized film of nickel thickness is order 1 nm.

For calculation of spectral characteristics of nanodimensional films of metals usually use values of characteristic of macroscopic materials. However it is known that at such sizes optical parameters have proportional dependence. Therefore for the purpose of specification of legitimacy of use this approach for an assessment of an electromagnetic response of nanodimensional structures, we have made a model experiment which results are presented in Fig. 1. A curve 1 calculated on the basis of optical parameters of the nanodimensional films of nickel determined by us by an experimental-analytical method and presented in [3]. A curve 2 – coefficients of reflection R and transmission T of the model nanodimensional films estimated on the basis of optical parameters of macroscopic materials [6]. For comparison in Fig. 1 shows the experimental curve 3 – nanodimensional nickel film with structural parameters in accordance with the parameters used for the model experiment.

It can be seen that the difference between values calculated on the basis of optical parameters for nanoscale films and experimental ones lies within the limits of the calculation error. In turn, as expected, the result obtained using parameters characteristic of a massive metal differs from experiment up to 10 %. This confirms the reliability of the results obtained on the basis of the experimental-analytical method. An example of the spectral dependences of coefficients of reflection R and transmission T of composite nanosized metal-dielectric structures of the type "aluminum oxynitride – nickel bar-

rier film – nanosized silver film – nickel barrier film – aluminum oxynitride – glass substrate" at various values of their structural parameters are presented in Fig. 2. From the indicated spectral dependences it follows that by varying the thickness of the dielectric component, we can regulate the spectral selectivity of the optical filter (threshold wavelengths) in the range from 0.4 to 0.9 microns. In this case, the minimum and maximum values of the reflection and transmission coefficients vary from 0.2 to 0.9.

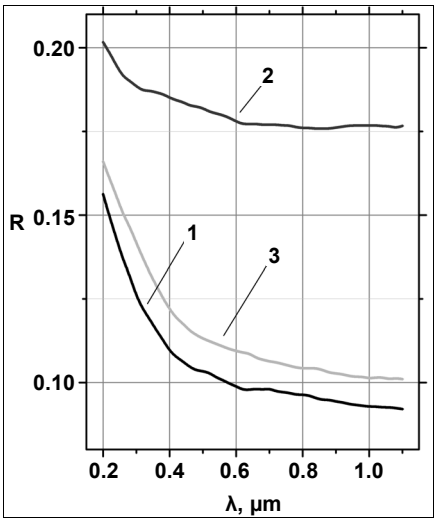

a)

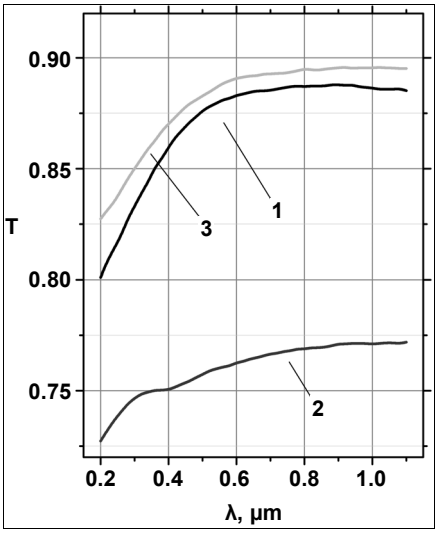

b)

Fig. 1. Spectral dependences of coefficients of reflection (a) and transmission (b) of model structure "nanodimensional film of nickel (5 nanometers) on SiO_2 substrate": 1 – curve calculated on the basis of the optical parameters determined by an experimental-analytical method; 2 – curve calculated on the basis of optical parameters of macroscopic materials; 3 – experimental curve

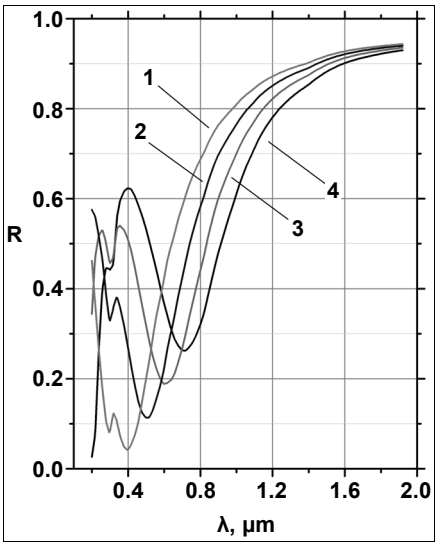

a)

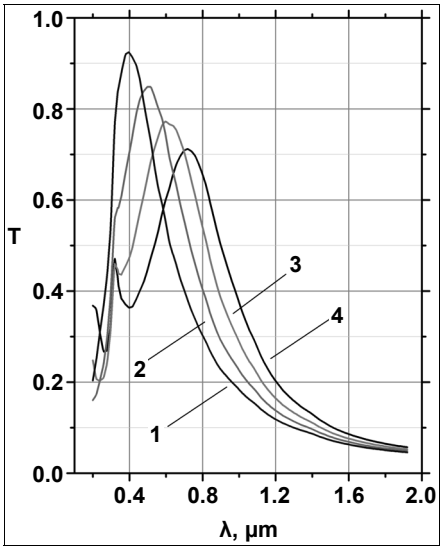

b)

Fig. 2. Spectral dependences of coefficients of reflection (a) and transmission (b) of a structures like "$Al_xN_yO_z$–Ni–Ag–Ni–$Al_xN_yO_z$–SiO_2" (b) at a thickness of a nanodimensional film of silver d_m = 20 nanometers for various thickness of a dielectric layer d_d: 1 – 20 nanometers; 2 – 30 nanometers; 3 – 40 nanometers; 4 – 50 nanometers

To evaluate the effect of changing the thickness of a nanosized silver film and dividing it in half by a dielectric layer, a model experiment was carried out, the results of which are presented in Fig. 3. As input data uses the results obtained earlier on the basis of the experimental-analytical method. Characteristic thickness of dielectric layers is 40 nm. In Fig. 3 curve 1 corresponds to a composite with nanosized metal layer d_m in thickness 10 nm, curve 2–20 nm. From the indicated spectral dependences it follows that changing the thickness of the metal layer we can regulate the spectral selectivity of the optical filter, shifting the

threshold values of the wave in the range from 0.8 to 1.2 microns. As you can see, with the increase in the thickness of the metal film, the threshold values of the reflection curve shifted to the short-wave region.

In addition, we calculated the nanocomposite structures in which the metal layer is divided into two parts by a dielectric layer in the thickness of 40 nm. The spectral characteristics of such structures correspond to curves 3 and 4. This design allows us to expand the spectrum of visibility.

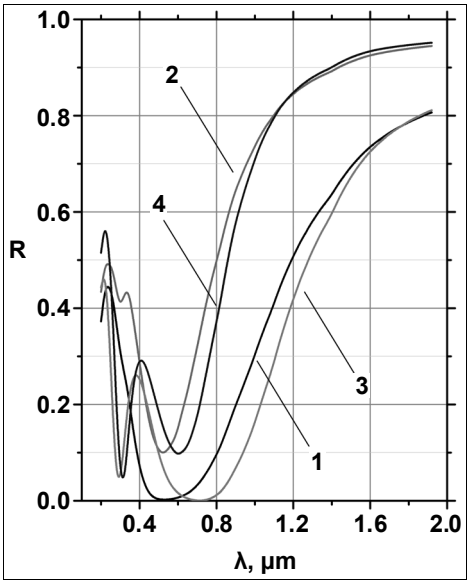

a)

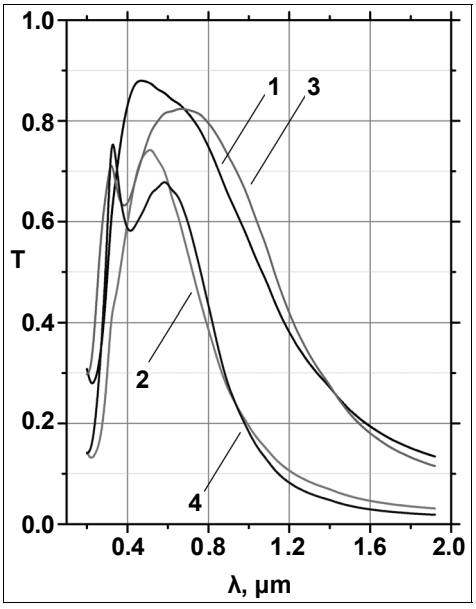

b)

Fig. 3. Spectral dependences of coefficients of reflection (a) and transmission (b) of a composite like "dielectric–barrier layer– silver nanodimensional film–barrier layer–dielectric–substrate" for various values of thickness of a nanodimensional silver film d_m: 1 – 10 nanometers; 2 – 20 nanometers; 3 – layer d_m (10 nanometers) is halved by a dielectric layer; 4 –layer d_m (20 nanometers) is halved by a dielectric layer

Conclusions. The correlation between optical characteristics of composite metal-dielectric structures and their structural and electromagnetic parameters is established. The response of the spectral characteristics of metal-dielectric nanosized structures to electromagnetic radiation in the optical range of the spectrum using the experimental-analytical method is calculated. It is determined that by varying the thickness of the dielectric component, it is possible to change the thresholds of the wavelength of the filter in the range from 0.4 to 0.9 microns.

In turn, the change in the thickness of the metal layer, regulates the spectral selectivity of the optical filter, shifts the threshold values of the wave in the range from 0.8 to 1.2 microns, and dividing it by two dielectric layers allows to expand the spectrum of transmission.

The values of optical parameters of nanosized metal layers are obtained by the authors with the help of the developed experimental-analytical method, with high accuracy correlating with experimental data, which makes it possible, when used, to increase the reliability of prediction of the characteristics of nanostructured systems.

The obtained results are of interest for predicting the selective characteristics of composite metal-dielectric structures for use as optical filters.

REFERENCES

1. *Agnihotri O.* Selektivnyie poverhnosti solnechnyih ustanovok / O. Agnihotri, B. Gupta. – M., 1984. – 273 p.

2. *Babych B.B.* Electrodynamic modeling of composites based on dielectric matrix with inclusions of ferromagnetic metals / B.B. Babych, A.V. Machulyansky, V.A. Machulyansky // Proc. of the 5th internat. sci.-practical conf. "Physical and technological problems of transmission, processing and storage of information in infocommunication systems", November 3–5, 2016, Chernivtsi, Ukraine, P. 165-166.

3. Dimensional dependencies of optical parameters of nanodimensional metal particles / A. Borisova, V. Verbitskiy, Y. Yakimenko et al. // IEEE 36th internat. sci. conf. electronics and nanotechnology (ELNANO), April 19–21, 2016, Kyiv, Ukraine, P. 140–143.

4. Properties of aluminum oxynitride films prepared by reactive magnetron sputtering / A. Borisova, M. Rodionov, Y. Yakimenko et al. // IEEE 34th internat. sci. conf. electronics and nanotechnology (ELNANO), April 16–19, 2014, Kyiv, Ukraine, P. 122–125.

5. Vyisokoeffektivnyie prosvetlyayuschie nanostrukturnyie opticheskie pokryitiya dlya solnechnyih elementov / O.N. Gadomskiy, K.K. Altunin, N.M. Ushakov et al. // ZhTF, 2010. – Vol. 80, № 6. – P. 83–89.

6. *Johnson P.B.* Optical constants of transition metals: Ti, V, Cr, Mn, Fe, Ni / P.B. Johnson, R.W. Christy // Phys. Rev. B, 1974. – Vol. 9, № 12. – P. 5056–5069.

7. Optical losses of multi component glasses for fibers and methods of their reduction / L.V. Maksimov, A.V. Anan'ev, V.N. Bogdanov et al. // Optics and Optoelectronics. Proc. SPIE, Vol. 5. – Warsaw, Poland, 2006. – P. 55–59.

8. *Zolotuhin I.V.* Nanokompozitnyie strukturyi na puti v nanoelektroniku / I.V. Zolotuhin, Yu.V. Kalinin, A.V. Sitnikov // Priroda, 2006. – № 1. – P. 11–19.

Submitted on 06.12.17

О. Мачулянський , доц., канд. техн. наук,
кафедра мікроелектроніки, факультет електроніки,
Національний технічний університет України "Київський політехнічний інститут імені Ігоря Сікорського"
Б. Бабич , асп.,
кафедра мікроелектроніки, факультет електроніки,
Національний технічний університет України "Київський політехнічний інститут імені Ігоря Сікорського"
Мачулянський В., магістр
Інститут прикладного системного аналізу,
Національний технічний університет України "Київський політехнічний інститут імені Ігоря Сікорського"

ОПТИЧНІ ФІЛЬТРИ НА ОСНОВІ КОМПОЗИТНИХ НАНОРОЗМІРНИХ СТРУКТУР

Проведено числове моделювання електромагнітного відгуку нанорозмірних плівок металів та композитних металодіелектричних структур, сформованих на їх основі, у діапазоні довжин хвиль 0,2–1,9 мкм. Здійснено порівняльний аналіз розрахованих даних з експериментальними. Показано вплив параметрів досліджуваних композитів на їх електромагнітний відгук. Надано рекомендації щодо можливості створення оптичних фільтрів з заданими спектрально-селективними характеристиками.

Ключові слова: нанорозмірні плівки металів, композитні металодіелектричні структури, спектрально-селективні характеристики, оптичні фільтри.

А. Мачулянский , доц., канд. техн. наук,
кафедра микроэлектроники, факультет электроники,
Национальный технический университет Украины "Киевский политехнический институт имени Игоря Сикорского",
Б. Бабыч, асп.,
кафедра микроэлектроники, факультет электроники,
Национальный технический университет Украины "Киевский политехнический институт имени Игоря Сикорского",
В. Мачулянский, магистр,
Институт прикладного системного анализа,
Национальный технический университет Украины "Киевский политехнический институт имени Игоря Сикорского"

ОПТИЧЕСКИЕ ФИЛЬТРЫ НА ОСНОВЕ КОМПОЗИТНЫХ НАНОРАЗМЕРНЫХ СТРУКТУР

Проведено численное моделирование электромагнитного отклика наноразмерных пленок металлов и композитных металлодиэлектрических структур, сформированных на их основе, в диапазоне длин волн 0,2–1,9 мкм. Осуществлен сравнительный анализ рассчитанных данных с экспериментальными. Показано влияние параметров исследуемых композитов на их электромагнитный отклик. Даны рекомендации по возможности создания оптических фильтров с заданными спектрально-селективными характеристиками.

Ключевые слова: наноразмерные пленки металлов, композитные металлодиэлектрических структуры, спектрально-селективные характеристики, оптические фильтры.

UDC 621.315.592

V. Mezhenskyi, Stud.,
O. Bauzha, Ph. D.,
Department of Electrophysics,
Faculty of Radiophysics, Electronics and Computer Systems,
National Taras Shevchenko University of Kyiv

THE DESIGN OF HARDWARE AND SOFTWARE COMPLEX FOR SELF-STUDYING BRAILLE

The research presents the method of realization of hardware and software complex for self-study of Braille. The result of the work is the development of the complex system that contains the hardware components for the reproduction of the Braille alphabet. The model WT020-SD-16P is used to play the audio information. This module is well-compatible with the platform Arduino Uno. The tactile module is implemented on electromagnet with a ferromagnetic core. The microcontroller ATmega328 is used to control audible and tactile modules. To power the system, the power supply of 12 V is used. Moreover, the board built on bipolar transistor switch is used for submission of the required current to electromagnets of the tactile module. The designed hardware and software complex can be used in specialized schools for visually impaired people and self-studying.

Keywords: Braille, WT020-SD-16P, Arduino, an electromagnet with a ferromagnetic core.

Introduction. Owing to sight, the human being perceives 80–90 % of information concerning the environment. As of 2016, there are approximately 300 thousands of visually impaired people in Ukraine. Instead, in the world, this figure reaches to 40 million of people who are blind and 246 million who are visually impaired. The annual growth in the number of visually impaired people in Ukraine reaches 12 thousand, in the world, this quantity is equal to 1 million. Every 5 seconds one adult loses sight but every second – one child. According to the forecasts of world health organization, these figures will have been increased in two times by 2020 [1].

World Braille Council which was established in 1950 had played a major role in adaptation of Braille for the most of the world's written languages, especially which are less common than English, French or Spanish. In 1953, Clutha Nantes Mackenzie was the Chairman of the World Braille Council. He published WORLD BRAILLE USAGE – a survey of efforts towards uniformity of Braille notation. This work includes the basic principles of World Blind Council and comprises of Braille alphabet for languages which were the most widespread. It should be admitted that World Braille Council was led by UNESCO as this organization appears to be the international organization best place to complete and apply the scheme World Braille Council has initiated. Later, World Braille Council became the part of World Braille Union which in 2008 established the objective-plan that was designed to implement its the most desirable goals. World Braille Union was eager to start its two main initiative which were rebuilding and strengthening the World Braille Council. Therefore, World Braille Council is a key organization which helps to satisfy the needs of visually-impaired people.

As for equipment designed to learning Braille, there are only manual devices such as cube-letter, line with Braille characters embossed or Braille alphabet. The disadvantage of these devices is its necessity for third-party assistance in learning, because using them independently is impossible.

For blind and visually impaired people the ability to write and read is a basis for living up to the hilt. Braille is a tactile writing system used by people who are blind or visually impaired. The basis of this system is a character which is depicted as a combination of embossed dots the height of which is 0.6 mm and the diameter is 1.4 mm. This character is written in a cell sized 4.2 mm * 7 mm. In the classic form of representation of the character, the cell has 6 dots with the appropriate numeration which is presented on the Fig. 1. The text written in this form is easily recognizable by touch. Easy reading of characters and their compactness allow blind to read the text quickly. This writing and reading system was created by French tyflopedahoh Louis Braille [2]. Latin and Cyrillic letters, Arabic numerals, musical notes and many other printed characters can be played in Braille by different combinations of dots in cells. Braille notations are used for writing mathematical symbols, equations, computer signs and also for writing in a foreign language.

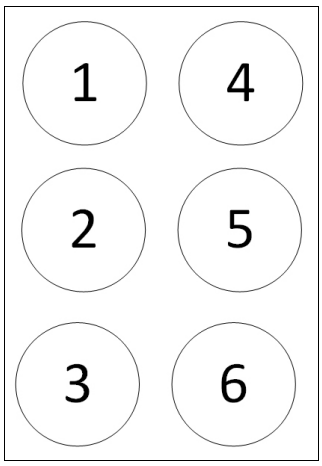

Fig. 1. The realization of Braille character in 6-dots system

Also, there are software and hardware systems for learning Braille independently, however, each of them has disadvantages. These disadvantages include support of languages of manufacturing country and manual control of restoration of tactile representation of the character. It should be also admitted that the cost of such devices is high and there is a lack of mass production of the most devices. As such, it could be concluded that the development of hardware and software complex which will enable people with visual impairments learn Braille independently is an urgent task.

A visually impaired person is unable to independently learn Braille. In this regard, the creation of hardware and software complex that will allow learning Braille independently is relevant and practically important technical issue.

There are hardware and software complexes for learning Braille, but they have disadvantages such as high commercial value. Moreover, their automation of tactile playback isn't full. Also, it is worth to note the lack of domestic devices and lack of support for localization of Ukrainian language.

The work presents hardware and software system for independent study Braille.

To hardware part the following requirements are:

- the existence of control panel that predicts the possibility of switching between characters;
- the existence of audible module for representing characters;
- the existence of tactile module of representing characters.

Software part serves for:

- tactile and audible representation of characters

The designed complex consists of the following components:

- control Panel;
- microcontroller Arduino Uno;
- audible module WT020-SD-16P;
- tactile module.

The general flowchart of hardware and software complex is shown in Fig. 2.

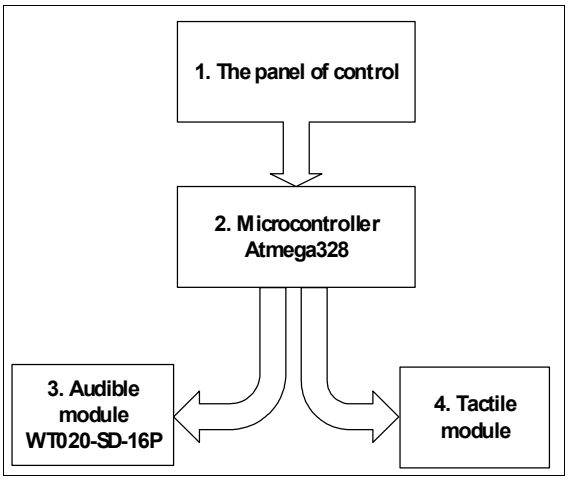

Fig. 2. Flowchart of hardware and software complex

The control panel consists of 4 buttons which have the following purpose:

Button "1" – switching to the previous character.

Button "2" – repeating the character.

Button "3" – switching to the next character.

Button "4" – switching to a different sequence of characters (letters, numbers etc.).

To control the audio and tactile module, the board for debugging Arduino Uno [3] based on the 8-bit microcontroller ATmega 328 is used. Arduino is an open hardware platform for rapid implementation of various electronic devices. The main components of the platform are the board of microcontroller with elements of I/O and development environment Processing / Wiring for programming by language C/C++. As a system of projecting for hardware platform Arduino, software Fritzing is convenient to use. The internal programmer is embedded in the microcontroller; therefore, the external programmer isn't required. As a programming environment, popular package Arduino IDE is appropriate to use.

The structure of board consists of 14 digital outputs (6 of which can be used as outputs for pulse width modulation, PWM outputs), 6 analog inputs, microcontroller Atmega 328, USB connectors, the power of internal circuit programming (ICSP) and a reset button. Recommended voltage is 7–12 V. The voltage can be served from the AC/DC-adapter or batteries, or through computer's USB-port.

For representation of audible information, audible module WT020SD16P [6], which has several advantages is used. Advantages:

- for collecting data SD- or micro-SD-card can be used;
- available commercial value;
- small size, 22*19 mm;
- does not require additional circuits;
- supports control commands made by the external microcontroller;
- a wide range of power: 2.7–5.0 V

Wiring to the microcontroller is shown in Fig. 3.

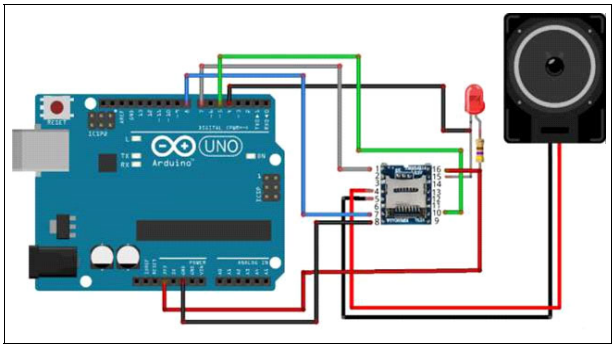

Fig. 3. Wiring of audible module WT020-SD-16P to the microcontroller

The tactile module is implemented with the use of electromagnets with the ferromagnetic core (see Fig. 4).

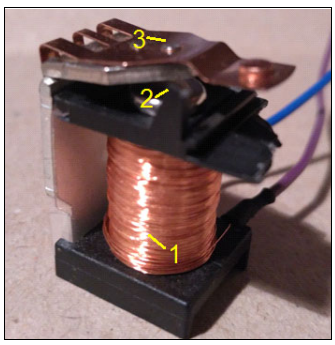

Fig. 4. Electromagnet with a ferromagnetic core (1 – coil, 2 – ferromagnetic core, 3 – elastic plate)

The principle of operation is the following: when the current does not run through the coil then the elastic plate is rejected and it indicates the presence of a relief point; when supplying current to the coil, elastic plate is attracted by a magnet that indicates the lack relief point. In this regard, the main advantages of using electromagnets with ferromagnetic core for implementing tactile module include low cost, stable and reliable operation and simple technical maintenance of module.

For full representation of cell, which consists of 6 relief points, 6 electromagnets are used. The tactile module is shown in Fig. 5.

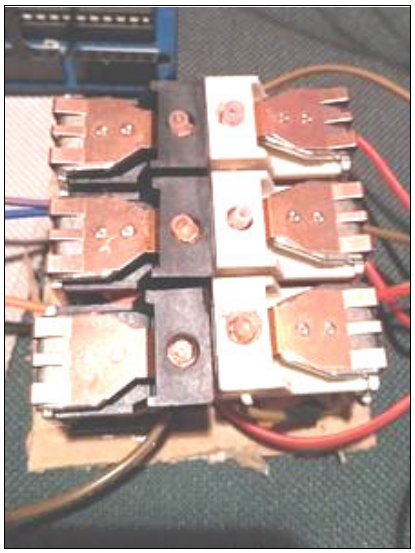

Fig. 5 The tactile module for representing the character of 6-dots Braille system

The physical characteristics of the developed tactile module are as follows:

– Width 4 cm;

– Height 1.5 cm;

– Length of 5 cm.

If it is necessary, the module listed above can be developed in smaller size by using smaller sized electromagnets with ferromagnetic center.

The designed complex is implemented using commonly used components among the experts, therefore, it is easily compiled in mass production. The cost of one device at small-scale manufacturing is about $15 that makes it affordable for most visually impaired people.

Conclusions. The presented software and hardware complex for learning Braille can open new opportunities for self-studying. Therefore, it will reduce the workload of teachers in special schools. To control the electrical components, popular hardware platform Arduino Uno characterized by small size and low power consumption is used. To play the audio information, the preference is given to audible module WT020SD16P because of its low cost, miniature size and simple management of commands made by the microcontroller. For tactile representation of characters, the tactile module using six magnets with the ferromagnetic core is manufactured.

The proposed software and hardware complex can be used both in special schools and for self-studying visually impaired people.

REFERENCES

1. World Health Organization. Visual impairment and blindness [elekrtronnyy resource], 2014, access : www.who.int/mediacentre/factsheets/fs282/en/index.html

2. *Synova E.P.* Relief-dot writing blind. Font L. Braylya. Tutorial, 2003. – 108 p.

3. *Jeremy Blum.* Learning Arduino. Tools and methods of technical wizardry / Jeremy Bloom. – Peterburg, 2015 – 336 p.

4. Atmega 328 [Datasheet, online] – 2016, – Available from: http://www.atmel.com/Images/Atmel-42735-8-bit-AVR-Microcontroller-ATmega 328-328P_Datasheet.pdf – 442 p.

5. WTV020SD [Datasheet, online] – 2014, – Available from: https://cdn.sparkfun.com/datasheets/Widgets/WTV020SD.pdf – 26 p.

6. *Brian W. Evans.* Arduino Programming Notebook. / B.W. Evans – 2007 – V 1.1 – 40 p.

7. *Dhogal P.S.* Basic Electrical Engineering, 1986. – Vol. 1. Tata McGraw-Hill Education. – 128 p.

Submitted on 01.06.17

В. Меженський, студ.,
О. Баужа, канд.фіз.-мат. наук, асист.,
кафедра комп'ютерної інженерії,
факультет радіофізики, електроніки та комп'ютерних систем,
Київський національний університет імені Тараса Шевченка

РОЗРОБКА ПРОГРАМНО-АПАРАТНОГО КОМПЛЕКСУ ДЛЯ САМОСТІЙНОГО ВИВЧЕННЯ ШРИФТУ БРАЙЛЯ

Представлено метод реалізації програмно-апаратного комплексу для самостійного вивчення шрифту Брайля. Розроблений пристрій має два способи представлення символів: звуковий і тактильний. Для відтворення звукової інформації використано модуль WT020-SD-16P, а тактильний модуль реалізовано на електромагнітах із феромагнітним осердям. Завдяки зазначеному комплексу слабозора людина зможе самостійно опанувати шрифт Брайля, що позитивно позначиться на освіті незрячих людей.

Ключові слова: шрифт Брайля, WT020-SD-16P, Arduino, електромагніт з феромагнітним осередком.

В. Меженский, студ.,
О. Баужа, канд. физ.-мат. наук, ассист.,
кафедра электрофизики,
кафедра компьютерной инженерии,
факультет радиофизики, электроники и компьютерных систем,
Киевский национальный университет имени Тараса Шевченко

РАЗРАБОТКА ПРОГРАММНО-АППАРАТНОГО КОМПЛЕКСА ДЛЯ САМОСТОЯТЕЛЬНОГО ИЗУЧЕНИЯ ШРИФТА БРАЙЛЯ

Представлен метод реализации программно-аппаратного комплекса для самостоятельного изучения шрифта Брайля. Разработанное устройство имеет два способа представления символов: звуковой и тактильный. Для воспроизведения звуковой информации использовано модуль WT020-SD-16P, а тактильный модуль реализован на электромагнитах с ферромагнитным сердечником. Благодаря указанному комплексу, слабовидящий человек сможет самостоятельно овладеть шрифт Брайля, что положительно скажется на образовании незрячих людей.

Ключевые слова: шрифт Брайля, WT020-SD-16P, Arduino, электромагнит с ферромагнитным центром

UDC 537.525:621.325

I. Melnyk, Dr. of Tech. Sci.,
I. Chernyatynskiy, Stud.,
N. Piasetska, Stud.
Electronic Instruments and Devices Department, Electronic Faculty,
National Technical University of Ukraine "Igor Sikorskiy Kiev Polytechnic Institute", Kyiv

SIMULATION OF FORM AND POSITION OF PLASMA BOUNDARY IN THE ELECTRODES SYSTEMS OF GLOW DISCHARGE ELECTRON GUNS WITH THE COMPLEX SPATIAL GEOMETRY FOR FORMING THE TUBE-LIKE ELECTRON BEAMS

The mathematical model of high-voltage glow discharge electrodes' systems with complex spatial geometry for forming of tube-like electron beams is presented in the article. The plasma boundary position is taking into account in the proposed model by providing calculations for simple plane electrodes system and by recalculation the volume of anode plasma corresponding to the real spatial geometry of electrodes. The results of calculation of electric field distribution in simulated electrodes' system are presented in the article.

Keywords: high voltage glow discharge, anode plasma, tube-like electron beam.

Introduction. High Voltage Glow Discharge (HVGD) electron sources, formed the electron beams with complex spatial geometry, like tube-like and disk-like, are widely used in industry for electron beam welding or annealing of cylindrical thin-wall items [6, 2]. The advantages of this type of electron-beam sources are follows:

– possibility of providing the technological operations in the soft vacuum in the medium of different gases, including noble and active ones, therefore choosing of suitable gas usually defined by the requirements of technological process;

– relatively low price both of the sources and of evacuation system of technological installation;

– high production rate of welding or annealing the tube-like items in the automation mode [6, 2].

General structure of high voltage glow discharge electrode system for forming the tube-like electron beam is presented at Fig. 1. For maintaining of high voltage glow discharge in the volume of electron source negative acceleration voltage range of few or tens of kV applied to the cathode. The operation pressure in the guns volume maintained in the range few Pa, up to tens Pa [6, 2].

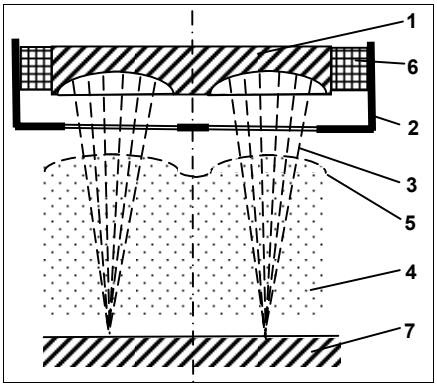

Fig. 1. Scheme of HVGD electron guns electrodes' system for forming tube-like electron beams. 1 – cathode, 2 – anode aperture, 3 – electron beam, 4 – anode plasma, 5 – plasma boundary, 6 – high-voltage insulator, 7 – treated item

The main problem for further development of HVGD electron sources with the complex spatial geometry of electrodes' systems for forming the tube-like electron beams is defining of plasma boundary position relatively to the cathode surface. This problem generally connected with the fact that plasma boundary take a grate influence to the complex discharge electron-ion optic as a source of positive ions and as a moving electrode with the small positive potential [6, 3]. In the paper [5] the analytical method for calculation the plasma boundary position in the HVGD electrodes systems with the complex spatial geometry was generally considered. Proposed method is based on calculation the plasma boundary position in the plane one-dimensional electrode system on the basis of analytical relations, obtained for HVGD [6], and on recalculation of this value with taking into account the real complex geometry of electrodes. In this paper this method is applied for the electrodes systems, formed the tube-like electron beams, and calculated distribution of electric field in such electrodes system is presented.

Geometrical parameters of considered electrodes system and analytical function for approximation of plasma boundary geometry. The constructive geometry parameters of considered HVGD electrodes' system are presented in Fig. 2. There are such parameters: R_c – radius of cathode torus surface, r_s – radial size of electrodes system, r_c – radial size of torus emission cathode surface, r_{d1} – internal diaphragm radius, r_{d2} – external diaphragm radius, d_p – anode plasma highest, R_p – radius of the torus part of plasma boundary.

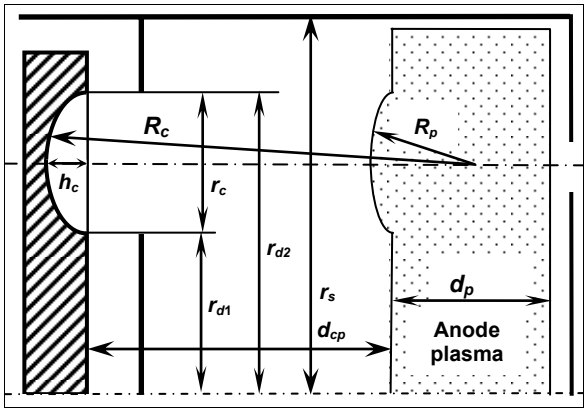

Fig. 2. Geometry parameters of HVGD electrodes system for forming tube-like electron beam

In considering case for finding analytical dependence $r(z)$, which described the geometry of plasma boundary by the analytical equation, we will to represent it as a rotation figure in cylindrical coordinate system, as shown at Fig. 2. In generally the next analytical dependences, characterized interconnections between EOS parameters, can be written

$$h_c = R_c - \sqrt{R_c^2 - r_c^2}\ ;\ \ r_c = \frac{d_p R_c}{R_c - h_c}\ . \qquad (1)$$

With taking into account equation (2) function $r(z)$, described torus surface of rotated body, presented at Fig. 3, can be written as follows:

$$r(z)=\sqrt{k_2+z^2+2k\sqrt{\left(\frac{d_pR_c}{R_c-h_c}\right)^2-z^2}}\ , \qquad (2)$$

where for simplifying the next coefficients are introduced:

$$k=r_{d1}-\frac{d_pR_c\sqrt{R_c^2-R_ch_c}}{(R_c-h_c)^2},\quad k_2=k^2-R_p^2=$$

$$=\frac{\left(r_{d1}(R_c-h_c)-d_pR_c\left(\frac{\sqrt{R_c^2-R_ch_c}}{(R_c-h_c)}-1\right)\right)}{(R_c-h_c)^2}\times$$

$$\times\frac{\left(r_{d1}(R_c-h_c)-d_pR_c\left(1-\frac{\sqrt{R_c^2-R_ch_c}}{(R_c-h_c)}\right)\right)}{(R_c-h_c)^2}. \qquad (3)$$

With known dependence (2) for the curve $r(z)$, which described by the equation (2), with known volume of anode plasma its highness can be calculated. Corresponded equations will be presented in the next part of the article.

Analytical relations for defining the anode plasma volume and square of emitted surface. For simplicity plasma boundary position firstly can be defined approximately on the base of more simple discharge models, and then recalculated for real electrodes' system geometry for the same volume, occupied by the anode plasma. Among such methods of calculation the simplest one was proposed in [6], where estimation of plasma boundary position is provided on the base of equivalent one-dimensional model of discharge gap from equation:

$$d_{\text{cp}}=L-\frac{I_{dp}}{Q_{e0}\left(\chi\gamma+\sqrt{\frac{m_i}{m_e}}\right)-\frac{5\mu_{i0}kT_e}{R^2p_{a0}^2e}\sqrt{\frac{m_i}{kT_i}}}, \qquad (4)$$

where I_{dp} is discharge current, L and R are the length and crosscut size of discharge gap correspondently, p_{a0} is reduced pressure in the discharge region, m_e and m_i is electron and ion mass correspondently, Q_{e0} is the mean value of electrons overcharge cross-section, χ is coefficient of mean enlarger of electrons trajectory in the anode plasma region and γ is the coefficient of electrons reflection from anode surface, μ_{i0} – mobility of ions in anode plasma. Then the plasma volume in one-dimensional plane electrodes' system calculated by the simple relation [1]:

$$V_p=\pi R^2d_{\text{p}}\,. \qquad (5)$$

For calculation of anode plasma volume in HVGD electrodes systems with cylindrical symmetry, like presented at Fig. 2, well-known relation from analytical geometry for calculation of rotation figure volume can be used [1]:

$$V_p=\int_a^b r^2(z)dx, \qquad (6)$$

where $r(z)$ is the analytical function, described by equation (2). With taking into account relations (2), (5) and (6), corresponded equation for calculation the volume of anode plasma in HVGD electrodes systems for forming tube-like electron beams can be written as follows [5]:

$$V_p=\pi r_s^2+\int_{\frac{d_p(R_c-h_c)}{R_c}}^{d_p}\left(k_2+z^2+2k\sqrt{\left(\frac{d_pR_c}{R_c-h_c}\right)^2-z^2}\right)^2dz=$$

$$=\pi r_s^2+k_2d_p\left(\frac{2R_c-h_c}{R_c}\right)+\frac{d_p^3}{3}-\frac{1}{3}\left(\frac{d_p(R_c-h_c)}{R_c}\right)^3-$$

$$-\frac{k}{2}\left(\frac{d_p(R_c-h_c)}{R_c}\right)^2\left(\arccos\left(\frac{Rc-h_c}{R_c}\right)-\arccos\left(\frac{h_c}{R_c}\right)\right)-$$

$$-kd_n^3\sqrt{\frac{R_c}{R_c-h_c}-1}. \qquad (7)$$

Another problem for the electrodes' systems with the complex spatial geometry is changing the square of emitted surface corresponded to the plane electrodes. It is well-known from analytical geometry, that the square of rotated surface, like presented at Fig. 2, generally defined as [1]:

$$S_p=\int_a^b r(z)\sqrt{1+(r'(z))^2}\ . \qquad (8)$$

It is clear, that $r(z)$ in equation (8) for considered electrodes' system, formed tube-like electron beam, defined by equation (2). Therefore equation (8) can be rewritten as follows [5]:

$$S_p=\int_{\frac{d_p(R_c-h_c)}{R_c}}^{d_p}\sqrt{k_2+z^2+2k\sqrt{\left(\frac{d_pR_c}{R_c-h_c}\right)^2-z^2}}\times$$

$$\times\sqrt{1+\left(\frac{2z\left(1+\frac{2k}{\sqrt{\left(\frac{d_pR_c}{R_c-h_c}\right)^2-z^2}}\right)}{\sqrt{k_2+z^2+2k\sqrt{\left(\frac{d_pR_c}{R_c-h_c}\right)^2-z^2}}}\right)^2}\,dz\,, \qquad (9)$$

where coefficients k and k_2 defined by equations (3).

Corresponded value of discharge current for electrodes systems with geometry, presented at Fig. 2, is obtained as:

$$I_{ds}=\frac{S_pI_{dp}}{2\pi Rd_p}\,. \qquad (10)$$

The highness of anode plasma d_p can be defined with using analytical equations (5) and (7) from graphic dependences $V_p(d_p)$. Corrected value of discharge current obtained from equations (8), (9). The results of numerical calculations for dependences $V_p(d_p)$ and $S_p(d_p)$ will be presented and analysed in the next part of this article.

Simulation results and its' analyse. Obtained as results of simulation graphical dependences $V_p(d_p)$ are presented at Fig. 3, and dependences $S_p(d_p)$ correspondently at Fig. 4. One can see, that all dependences are obtained for different cathode torus surface radius R_c. The main conclusion, which sequence from obtained results, is that corresponding to geometry of analyzed electrodes' systems the square of anode plasma emission part is decreased with enlarging of discharge current and with clos-

ing anode plasma to the cathode surface. Hence, current augmentation with the pressure boost caused only by increasing of ions concentration in a plasma volume, but not by the enlarging of its emission surface.

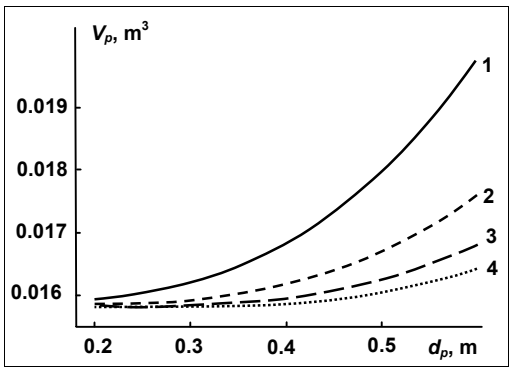

Fig. 3. Dependence of volume, occupied by anode plasma, from the plasma highest for different geometry parameters of electrodes system of HVGD electron guns, formed tube-like electron beam. r_{d1} = 0,2 m, r_c = 0,4 m, r_c = 0,7 m; 1 – R_c = 0,4 m, 2 – R_c = 0,5 m, 3 – R_c = 0,6 m, 4 – R_c = 0,7 m

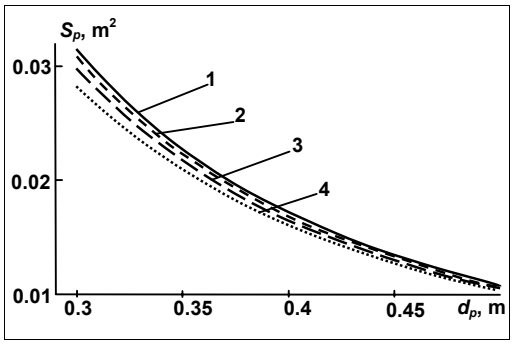

Fig. 4. Dependence of anode plasma emission surface from the plasma highest for different geometry parameters of electrodes system of HVGD electron guns, formed tube-like electron beam. r_{d1} = 0.2 m, r_c = 0.4 m, r_c = 0.7 m; 1 – R_c = 0.4 m, 2 – R_c = 0.5 m, 3 – R_c = 0.6 m, 4 – R_c = 0.7 m

Simulation results, presented at Figs. 3 and 4, shown that changing of emission plasma surface square with increasing of radius of plasma torus for small values of cathode torus size r_c is smaller the 10 %, and for grater values of r_c it can be changed at 2 or 3 times. Square of emission part of anode plasma and volume, occupied by plasma, decreased with enlarging of cathode torus radius, if other geometry parameters of electrodes are not changed. Therefore in electrodes systems with big values of cathode torus radius R_c and with small plasma height small contraction of plasma volume with increasing of its height is observed. This effect is caused by increasing of torus plasma radius R_p. Such discharge regimes (plasma height $d_p \approx 0.1$–0.3 m) are corresponded to very small discharge currents and usually are not considered in a preliminary analyzes. Furthermore, in small current discharge regimes plasma boundary is not parallel to the cathode surface, and estimations with using equations (7), (9) may be very rough [6, 3, 5]. Correct analyze of self-maintained electron-ion optics of HVGD electrodes systems for small discharge current can be provided only by analyzing discharge gap photographs [4].

However, because of small values of derivation for function $V_p'(d_p)$ for the big values of cathode torus radius R_c, correct choosing of range for finding the roots of equation (7) is necessary with using numerical methods to its' solving. In this procedure graphic dependences, are presented at Fig. 3, can be very useful. Furthermore, for providing the greater rate of convergence using of numerical methods without necessity calculation of derivations, for example simple iteration method or Stephenson method, is preferable. Since the Stephenson method has the second order rate of convergence, and the simple iteration method – first order, usually the Stephenson method will convergence faster.

With known position of plasma boundary relative to the cathode d_{cp}, marked at Fig. 2, and analytical dependence $r(z)$, defined by equations (2), (3), distribution of electric field in the simulated HVGD electrodes system also can be easy defined with using finite-difference method.

For example, in electrodes system, formed tube-like electron beams, cylindrical coordinate are considered, and finite-difference formula for the Poisson equation is written as follows [3, 5]:

$$U^n(i,k) = \omega\Big[C_a U^{n-1}(i+1,k) + C_b U^{n-1}(i,k+1) + C_c U^n(i-1,k) + C_d U^n(i,k-1) + \frac{C_\rho \rho^{n-1}(i,k)}{\varepsilon_0}\Big] \times (1-\omega) U^{n-1}(i,k), \quad (11)$$

where $C_a = C_c = \frac{1}{4h_z^2}$, $C_b = \frac{1+\frac{1}{2k}}{h_r^2}$, $C_d = \frac{1-\frac{1}{2k}}{h_r^2}$ for non-axial points, and $C_a = \frac{4}{6h_r^2}$, C_c = 0, $C_b = C_d = \frac{1}{6h_z^2}$ for axial points, n – number of current iteration by the potential, i and k – the numbers of current considered nodes by longitude and by radial coordinate correspondently, ω is a parameter, depended from electrodes' geometry, by using which the speed of convergence for iterations by the potential can be changed, h_r – step on r coordinate and h_z – step on z coordinate. Example of distribution of electric field in simulated electrodes systems is presented at Fig. 5.

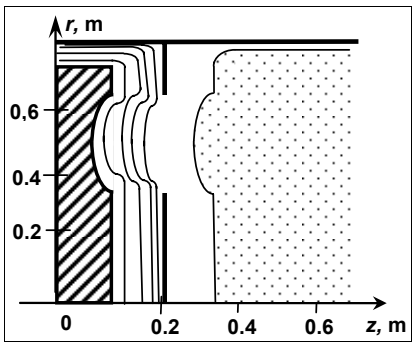

Fig. 5. Distribution of electric field in the simulated HVGD electrodes' system, formed the tube-like electron beam: R_c = 0.6 m, r_{d1} = 0.35 m, r_{d2} = 0.65 m, acceleration voltage – 15 kV, discharge current – 1.2 A, operation pressure 3.5 Pa

Comprising of results, presented at Figs. 3 and 4 with experimental data, shown, that for big values of d_p, which corresponded to maximal discharge currents, divergence of theory and experiments is not grater, then 10–15 %, and such accuracy is very fine in preliminary analyze of HVGD electrodes systems [5, 4]. Obtained analytical formulas and graphic dependences, characterized plasma boundary position for different geometrical parameters and discharge regimes, allows on the preliminary step of elaboration of

HVGD electrodes' systems, formed the tube-like electron beams, to estimate its electron-optical properties. Obtained value of parameter d_p, characterized the plasma boundary position, can also be used for the first iteration to more precision theoretical estimations. Information about the volume, occupied by the anode plasma, and about its emission surface square, also may be useful for further investigation of HVGD physics, for example, for estimation the level of ionization, electron and ion temperature in plasma, plasma density, and other physical parameters. Further analyzing and reviewing of finite-difference equations for current-tube method, obtained early [5], with taking into account peculiarity of geometry of HVGD electrodes' systems, formed profile electron beams, will allows to analyze the particles trajectories in the discharge gap and to find the electric field distribution with including consideration the space charge and elementary particles interactions.

Conclusion. Proposed method of simulation allows to estimate approximately the plasma boundary position in HVGD electrodes' systems with the complex spatial geometry, formed tube-like electron beams, and, correspondently, analysing the distribution of electric field. Comparising of theoretical and experimental results show, that difference between them by the anode plasma position and by the discharge current is not grater, than 15 %. Such precision of simulation can be considered as very fine for discharge systems. More precision estimations, especially for low pressure and low values of discharge current, can be given by making photograph of HVGD lighting and computer analysing of its' brightness.

Obtained results of simulation are very interesting and important for the further development of modern electron-beam technologies, connected with elaboration and applying in industry of advanced HVGD electron guns, formed tube-like electron beams.

REFERENCE

1. *Bronshtein I.N.* Spravochnik po matematike. Dlia inzhenerov i uchaschihsia vtuzov : Handbook on Mathematic for Engineers and Students of Higher Technical Institutions / I.N. Bronshtein, K.A. Semendiaev. – M. : Nauka, GRFML, 1986. – 723 p.

2. *Denbnovetsky S.V.* High voltage glow discharge electron sources and possibilities of its application in industry for realising of different technological operations / S.V. Denbnovetsky, V.G. Melnyk, I.V. Melnyk // IEEE Transactions on plasma science, 2003. – Vol. 31, № 5. – P. 987–993.

3. *Denbnovetsky S.V.* Model of beam formation in a glow discharge electron gun with a cold cathode. / S.V. Denbnovetsky, V.G. Melnyk, I.V. Melnyk // Applied Surface Science, 1997. – Vol. 111. – P. 288–294.

4. *Melnik I.V.* Issledovanie electronno-ionnoy optiki electrodnyh system vysokovoltnogo tleyuschego razryda s ispol'zovaniem metodov komp'uternogo analiza izobrazheniy. [Investigation of electron-ion optics of high voltage glow discharge electrodes' systems with using computers methods of images recognizing] / I.V. Melnyk // Elektronnoe modelirovanie, 2007. Vol. 29, № 1. – P. 45–58 (Published in Rus. language).

5. *Melnik I.V.* Simulation of geometry of high voltage glow discharge electrodes' systems, formed profile electron beams / I.V. Melnik // Proc. of SPIE. – Vol. 6278. Seventh Seminar on Problems of Theoretical and Applied Electron and Ion Optics. – P. 627809-1–627809-13.

6. *Novikov A.A.* Istochniki elektronov vysokovoltnogo tleyuschego razryada s anodnoy plasmoy : High voltage glow discharge electron sources with anode plasma / A.A. Novikov. – M. : Energoatomizdat, 1983. – 96 p. (Published in Rus. language).

Submitted on 16.10.17

І. Мельник, д-р техн. наук,
І. Чернятинський, студ.,
Н. П'ясецька, студ.,
кафедра електронних приладів та пристроїв, факультет електроніки,
Національній технічний університет України "КПІ імені Ігоря Сікорського", Київ

МОДЕЛЮВАННЯ ФОРМИ ТА ПОЛОЖЕННЯ МЕЖІ АНОДНОЇ ПЛАЗМИ В ЕЛЕКТРОДНИХ СИСТЕМАХ ЕЛЕКТРОННИХ ГАРМАТ ВИСОКОВОЛЬТНОГО ТЛІЮЧОГО РОЗРЯДУ З ПРОСТОРОВОЮ ГЕОМЕТРІЄЮ ЕЛЕКТРОДІВ ДЛЯ ФОРМУВАННЯ ТРУБЧАСТОГО ЕЛЕКТРОННОГО ПУЧКА

Описано математичну модель електродних систем високовольтного тліючого розряду зі складною просторовою геометрією електродів, призначених для формування трубчастих електронних пучків. У запропонованій моделі положення плазмової межі визначається через проведення розрахунків для простої геометрії електродної системи з плоскими електродами та перерахування отриманого об'єму анодної плазми для реальної просторової геометрії електродної системи. Наведено результати розрахунку розподілу електричного поля в електродній системі, яка моделювалася.

Ключові слова: високовольтний тліючий розряд, анодна плазма, трубчастий електронний пучок.

И. Мельник, д-р техн. наук,
И. Чернятинский, студ.,
Н. Пясецкая, студ.,
кафедра электронных приборов и устройств, факультет электроники,
Национальный технический университет Украины "КПИ имени Игоря Сикорского", Киев

МОДЕЛИРОВАНИЕ ФОРМЫ И ПОЛОЖЕНИЯ ГРАНИЦЫ АНОДНОЙ ПЛАЗМЫ В ЭЛЕКТРОДНЫХ СИСТЕМАХ ЭЛЕКТРОННЫХ ПУШЕК ВЫСОКОВОЛЬТНОГО ТЛЕЮЩЕГО РАЗРЯДА С ПРОСТРАНСТВЕННОЙ ГЕОМЕТРИЕЙ ЭЛЕКТРОДОВ ДЛЯ ФОРМИРОВАНИЯ ТРУБЧАТОГО ЭЛЕКТРОННОГО ПУЧКА

Описывается математическая модель электродных систем высоковольтного тлеющего разряда со сложной геометрией электродов, предназначенных для формирования трубчатых электронных пучков. В предлагаемой модели положение границы плазмы определяется путём проведения расчетов для простой геометрии электродной системы с плоскими электродами и перерасчета полученного объёма анодной плазмы для реальной пространственной геометрии электродной системы. Приведены результаты расчета распределения электрического поля в моделируемой электродной системе.

Ключевые слова: высоковольтный тлеющий разряд, анодная плазма, трубчатый электронный пучок.

UDC .537.60

R. Natarov, Stud.,
O. Sudakov, Ph. D., S. Radchenko, Ph. D.,
Department of Medical Radiophysics,
Faculty of Radiophysics, Electronics and Computer Systems,
Taras Shevchenko National University of Kyiv

COMPENSATION OF MAGNETIC FIELD SPATIAL HETEROGENEITY IN MAGNETIC RESONANCE IMAGING SYSTEM

Here we proposed the synthesis technique of a simple permanent magnet shimming system (SS) for magnetic resonance imaging (MRI) equipment. It is based on reduction of the second order magnetic field heterogeneity term in a specified plane. The system may be implemented with only two square coils. The author's software for automated calculation of the coils' parameters was developed. Computer simulations confirmed the efficiency of proposed SS. The achieved corrected magnetic field's inhomogeneity is 0.1 mT in the area of 20 mm is enough for construction of laboratory training magnetic imaging setup.

Keywords: magnetic resonance imaging, magnetic field, inhomogeneity, active shimming, coils.

Introduction. Today MRI is one of the leading methods for noninvasive diagnostic of living objects. This method is based on the nuclear magnetic resonance phenomenon i.e. sampling the electromagnetic response of atomic nuclei in the superposition of oscillating and static magnetic fields. Mostly hydrogen nuclei are used because on their high gyromagnetic ratio. The main component of magnetic resonance (MR) scanner is the polarizing magnet that provides a highly-homogeneous static magnetic field. This magnet regardless of type (permanent, resistive, superconducting), has magnetic field inhomogeneity, which leads to a distortion of a reconstructed image in pixels' values and spatial distribution. Decreasing of field's inhomogeneity leads to decrease of the effective spin-spin relaxation time that affects signal attenuation, broadening of spectral lines and deterioration of resolution in turn [7]. A spatial distortion rises from the fact that signal's frequency obtained from certain object's regions in the inhomogeneous magnetic field does not correspond to the expected frequency of excitation radio pulse, phase and frequency encoding. To avoid such distortion the inhomogeneity of static magnetic field B_0 in the magnets volume should be about 10^{-5} T [2].

Creation of large magnets with a specified level of inhomogeneity is a very difficult task. For correcting of the field's inhomogeneity passive and active shimming approaches are used. Passive shimming is performed by the placing of ferromagnetic plates inside the MRI system. This method has significant drawbacks: changing the magnetic properties of ferromagnetic under the influence of temperature and the impossibility of adjusting irregularities caused by the patient's body during his MR study. The idea of active shimming is in placing of coils with specific form and current inside the magnet for creation of magnetic field that compensates the inhomogeneity of B_0 field. The problem of shimming coils synthesis for known field distribution is fairly nontrivial. Several practical methods [1, 6] for synthesis of shimming coils exist. In this paper we simulated the shimming system for a permanent magnet with a high magnetic field inhomogeneity that is comparable with the magnetic field itself.

Methods. The permanent magnet (Fig. 1) has two poles with diameter and the distance between them – 7 cm. Magnetic field induction in center is 250 mT. The magnetic field distribution between the poles of a magnet is assumed to have an axial symmetry that was proved by measurements [4]. The proposed SS consists of two square coils placed inside the magnet (Fig. 1.) Square coils' form was chosen for development simplicity. According to [4, 5] the distribution of the magnetic field is:

$$B_M = 245.703 - 0.11x - 0.23z - 0.01xz - 0.04x^2 + 0.08z^2, \quad (1)$$

The field's induction is in mT, coordinates – in mm. The center of the coordinate system (CS) does not match the isocenter of the magnet. Thus displacement of the CS was applied. After that (1) was transformed to:

$$B_M = 245.634 - 0.01xz - 0.04x^2 + 0.08z^2. \quad (2)$$

The final field distribution along Z axis is:

$$B_{Mz} = 245.634 + 0.08z^2. \quad (3)$$

The inhomogeneity along Z axis is described by the second order polynomial:

$$B_{Sz} = B_S^{(0)} - 0.08z^2. \quad (4)$$

So the compensation coils should provide the corresponding special magnetic field dependence. The value of the coefficient $B_S^{(0)}$ is not essential.

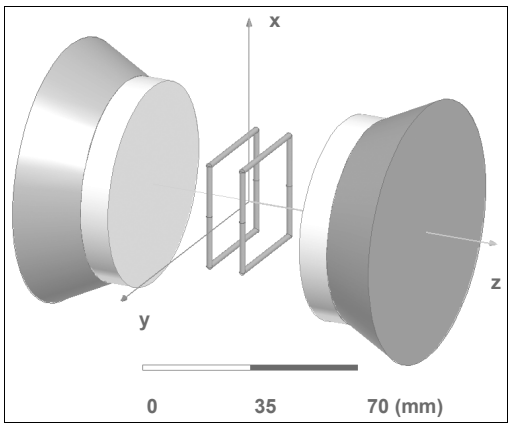

Fig. 1. Relative position of the magnet and coils

The field distribution of the single coil is the superposition of fields from four rectilinear wires with finite length. For simplicity the diameter of wires considers infinitesimal. Applying the Biot–Savart–Laplace law gives wire's spatial field distribution:

$$B_1 = \frac{I\mu_0\mu(\cos\varphi_1 - \cos\varphi_2)}{4\pi r_0}, \quad (5)$$

where r_0 – distance from point to wire, φ_1, φ_2 – angles between direction of current I and lines, that connect ends of the wire and spatial point. For the wire of length $2b$ and the spatial point equidistant to the wire's ends (Fig. 2) (5) can be rewritten:

$$B_2 = \frac{I\mu_0\mu b}{2\pi r_0\sqrt{b^2 + r_0^2}}. \quad (6)$$

Thus the magnetic field at the point A that is moved from center of CS at the distance s (Fig. 2) is as follows:

$$B_2 = \frac{I\mu_0\mu b}{2\pi\sqrt{s^2 + b^2}\sqrt{s^2 + 2b^2}}. \quad (7)$$

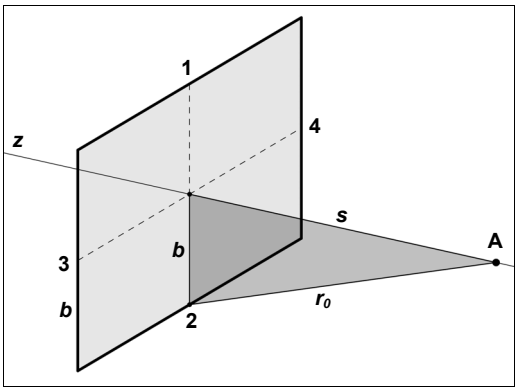

Fig. 2. Field from single wire of the coil

Considering that induction is a vector and its transversal components $\vec{B}_\perp$ are compensated (Fig. 3), the field from each wire is given by the equation:

$$B_i = \frac{\mu_0 \mu I b^2}{2\pi(s^2+b^2)\sqrt{s^2+2b^2}}. \quad (8)$$

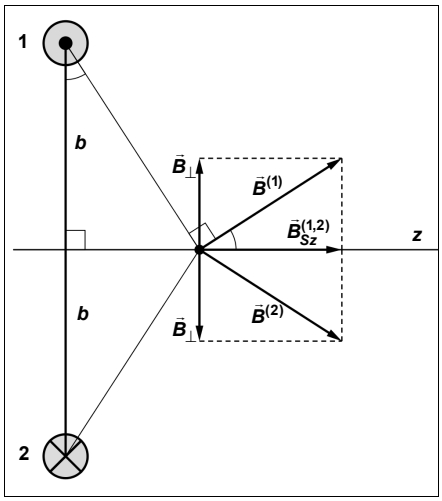

Fig. 3. Field from two wires of the coil

Field from the single coil is a superposition of the fields from all four wires:

$$B_{S1} = \frac{2I\mu_0 \mu b^2}{\pi(s^2+b^2)\sqrt{s^2+2b^2}}. \quad (9)$$

Described SS has several limitations:

- currents are low for heating prevention;
- small size, that is sufficient for a placing an object 10 × 10 × 10 mm, in the region of homogeneity;
- distance from isocenter to the center of the coil is less than 35 mm for avoid magnet poles effects.

The synthesis problem in analytic form is very complicated. We applied the much simpler "brute force" approach for coils parameters determination. Such parameters are: half-length of square coil's side *b*, distance from the coil to the center of coordinates *s* and current in each coil *I*.

Computing automation. Taking into account the large number of parameters' variations and the needs for approximation it was decided to create the software for automated calculation of SS parameters. The software was developed using Visual Studio 2010, programming language is C #. Software has user-friendly Graphical User Interface (Fig. 3) that allows interactive monitoring of the calculations' progress.

At the window user can set initial and final values of parameters and their step. In the box "Target 2" the value of the second term (3) with tolerance from the box "Tolerance 2" is given.

The algorithm has the following steps:

1. Shimming field distributions along Z-axis is calculated in 40 grid points located from –35 to 35 mm.
2. Data is approximated by 4÷8 degree polynomial using the ordinary least squares method.
3. Quadratic term of this polynomial is compared to the inhomogeneity term (3). If they match within tolerance, calculated parameters are added into the result area.
4. Parameters are increased by the step value. Calculation continues from the step 1 until the parameters reach their final values.

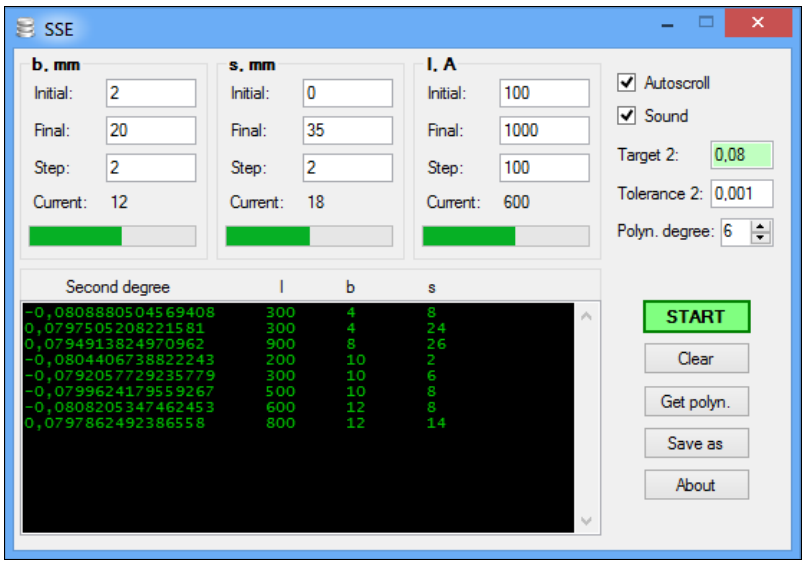

Fig. 4. The interface of the software

Results. For preliminary evaluation of the SS the parameters synthesis was performed in the wide range and with large step. The obtained parameters distribution is described on Fig. 5. Balls on the graph are at the correspond to parameters that meet (4). Also this graph shows the needs increasing the current while the coil is enlarged.

The optimal SS parameters that correspond to smallest current are as follows: I = 1076 Ampere-turns, b = 19.3 mm, s = 7.94 mm. Polynomial that describes the SS magnetic field is as follows:

$$B_{Sz} = 52.3 + 1{,}13 \cdot 10^{-16} z - 0{,}08 z^2 - 9{,}39 \cdot 10^{-19} z^3 + \\ + 5.46 \cdot 10^{-5} z^4 + 9{,}37 \cdot 10^{-22} z^5 - 1.4 \cdot 10^{-8} z^6. \quad (10)$$

Magnetic field along Z-axis after shimming is described in Fig. 6, line 2. Filed inhomogeneity obtained in present work (line 2) outperforms the previously obtained inhomogeneity for the same magnet (line 4) [3]. Thus inhomogeneity along Z-axis was decreased 45 times to $\Delta B \approx 0.1$ mT in area 20 mm, compared to magnet without SS (line 1).

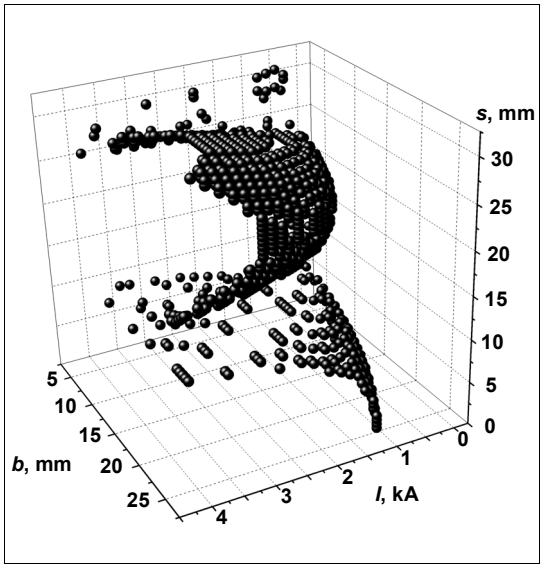

Fig. 5. Rough estimate of the parameters variation boundaries

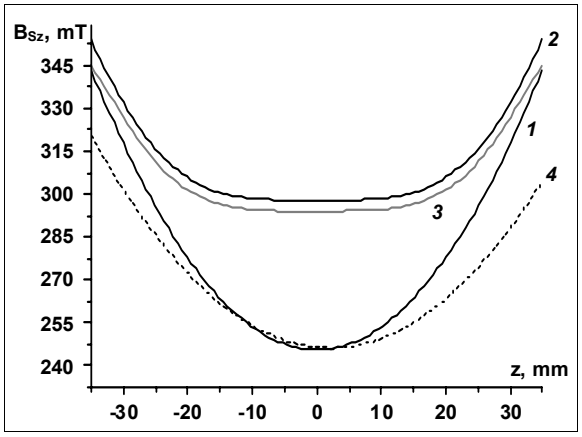

Fig. 6. Magnetic field inhomogeneity along the z-axis

The simulation in ANSYS Maxwell 3D 16.0 was performed to verify the obtained SS characteristics. Simulated magnetic field distribution proves field inhomogeneity (Fig. 6, line 3 and Fig. 7). Magnetic field distribution after compensation with the proposed SS was calculated and described on Fig. 7. Field distribution is rotated around the x-axes because polynomial (2) has term $-0.01xz$. Incompatibility between line 2 and line 3 (Fig. 6) is explained by the limitations of SS.

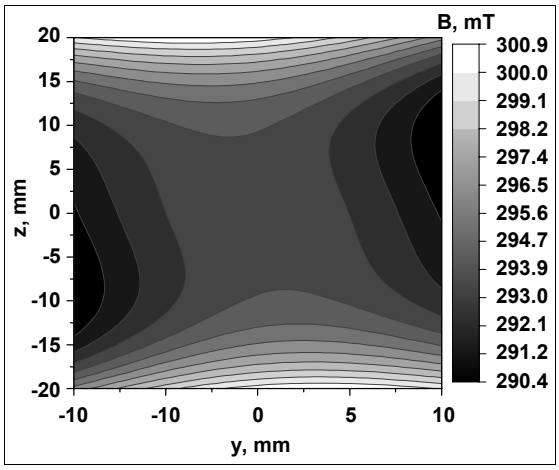

Fig. 7. Results comparison in plane yOz

Conclusion. Proposed simple active shimming system compensates the quadratic term inhomogeneity of permanent magnet's field. The achieved relative inhomogeneity is 10^{-4} that is enough for magnetic resonance imaging. Designed software can serve as a tool for design, calculation and optimization of shimming, gradient and other coils of MRI scanners. Described method can be used in X and Y-directions. The practical implementation of the coils should provide the possibility to move the coils along all axes in the range of ± 5 mm and the rotation around each axes in the range of ± 15°. The main shortcoming of this system is relatively large currents in the coils. Future work may be related to design the shimming system that compensates the higher order terms in magnetic field spatial dependence.

REFERENCES

1. *Jezzard P.* Shim coil design, limitations and implications / P. Jezzard // Abstracts from the International Society of Magnetic Resonance in Medicine (ISMRM) Annual Meeting, 2006.

2. *Kostyrin E.* Modeling the temperature fields in the working zone of magnetic resonance imaging in order to reduce magnetic field inhomogeneity / E. Kostyrin // Engineering Herald, 2013. – № 6. – P. 533–562

3. Compensated coils for reduction of magnetic field inhomogeneity / D. I. Maluk et al. // Proc. of the X Internat. Conf. "Electronics and Applied Physics", Kyiv, 2014.

4. *Соляник В.О.* Robotic system for measuring of heterogeneity of steady magnetic field in MRI system / В.О. Соляник, С.П. Радченко, О.О. Судаков // Proc. of the XIV Internat. young sci. conf. on applied physics Taras Shevchenko National University of Kyiv Faculty of Radiophysics 11–14 June, Kyiv. – P. 148–149.

5. *Natarov R.M.* System for correction of field heterogeneity in magnetic resonance system / R.M. Natarov // FRECS, T. Shevchenko Nat. Univ., Kyiv, 2016.

6. Расчёт и проектирование магнитных систем : учеб. пособ. – St. Petersburg, 2012.

7. The Physics of Medical Imaging / Ed. By S. Webb. – M., 1991. – Vol. 2.

Submitted on 08.09.17

Р. Натаров, студ.,
О. Судаков, канд. фіз.-мат. наук,
С. Радченко, канд. фіз.-мат. наук,
кафедра медичної радіофізики,
факультет радіофізики, електроніки та комп'ютерних систем,
Київський національний університет імені Тараса Шевченка

КОМПЕНСАЦІЯ ПРОСТОРОВОЇ НЕОДНОРІДНОСТІ РОЗПОДІЛУ МАГНІТНОГО ПОЛЯ В МАГНІТОРЕЗОНАНСНІЙ СИСТЕМІ

Запропоновано методику синтезу простої шимуючої системи постійного магніту для потреб магніторезонансної томографії. Методика базується на нівелюванні другого порядку неоднорідності в заданій площині. Система може бути реалізована лише за допомогою двох квадратних котушок. Для автоматизованого розрахунку параметрів котушок було розроблено програмний засіб. Ефективність пропонованої шимуючої системи підтверджено за допомогою комп'ютерної симуляції. Досягнуто неоднорідності корегованого магнітного поля 0,1 мТл в області розміром 20 мм, що достатньо для створення магніторезонансної томографічної лабораторної установки.

Ключові слова: магніторезонансне зображення, магнітне поле, неоднорідність, активне шимування, котушки.

Р. Натаров, студ.,
О. Судаков, канд. физ.-мат. наук,
С. Радченко, канд. физ.-мат. наук,
кафедра медицинской радиофизики,
факультет радиофизики, электроники и компьютерных систем
Киевский национальный университет имени Тараса Шевченко

КОМПЕНСАЦИЯ ПРОСТРАНСТВЕННОЙ НЕОДНОРОДНОСТИ РАСПРЕДЕЛЕНИЯ МАГНИТНОГО ПОЛЯ В МАГНИТОРЕЗОНАНСНОЙ СИСТЕМЕ

Предлагается методика синтеза простой шиммирующей системы для постоянного магнита для нужд магниторезонансной томографии. Методика основывается на нивелировании второго порядка неоднородности в заданной плоскости. Система может быть реализована при помощи всего лишь двух квадратных катушек. Для автоматизированного расчёта параметров катушек было разработано программное средство. Эффективность предлагаемой шиммирующей системы подтверждена с помощью компьютерной симуляции. Достигнута неоднородность корректированного магнитного поля 0,1 пространства размером 20 мм, которой достаточно для создания магниторезонасной томографической лабораторной установки.

Ключевые слова: магниторезонансное изображение, магнитное поле, неоднородность, активное шиммирование, катушки.

UDC 533.9.082.5

O. Turianska, Junior researcher,
M. Dreval, Senior researcher
Institute of Plasma Physics, National Science Center
"Kharkiv Institute of Physics and Technology"

PHOTODIODES SPECTRAL SENSITIVITY INFLUENCE ON THE TWO FOILS SOFT X-RAY TECHNIQUE IN THE URAGAN TORSATRONS

Soft X-ray (SXR) diagnostics is routinely used in URAGAN-3M and URAGAN-2M torsatrons. One of the SXR diagnostic applications is based on the plasma temperature estimation. The ratio of the SXR signals passed through two different foils is used for the temperature estimation. The spectral sensitivity of the photodiode itself can affect the temperature measurement in addition to the spectral dependence of the foil absorption function. Set of different modeling spectral sensitivity functions was used for numerical calculation of the SXR signals ratio. The influence is negligible in the case of the flat sensitivity in the energy range 5-500eV in the case of thin Al foils (for example in the AXUV-20EL photodiodes case).

Keywords: Soft X-ray, two foils technique, spectral sensitivity, torsatron.

Introduction. The diagnostics of the plasma in stellarators and tokomaks which is based on plasma radiation data in the Soft X-ray (SXR) range is an important tool for studying plasma confinement and heating, as well as plasma fluctuations. An important problem in fusion devices is the determination of the electron temperature T_e of the plasma. One of the SXR diagnostic applications is based on the plasma temperature estimation. A broadband light emission from plasma is filtered by fin beryllium or aluminum foil in order to separate SXR emission. The SXR energy spectrum, passed through the foil, depends on the foil thickness and material. The two foil technique used for the estimation of the electron temperature is based on the ratio R between the SXR brightnesses passed through different foils. The purpose of the work was to show how photodiodes spectral sensitivity influence on the electron temperature measurement.The ratios of the SXR signals passed through different foils R for different modeling dependences of the spectral sensitivity of the photodiodes F has been calculated numerically in our work.

Two Foils Technique. Let us consider the case of Bremsstrahlung radiation from the plasma only. The contribution of spectral lines under this assumption is negligible. The bremsstrahlung formula has the following form:

$$\frac{dW}{dE} \propto n_e(r) n_i(r) Z_{eff}^2(r) T_e^{-0.5}(r) e^{-\frac{E}{T_e(r)}}, \qquad (1)$$

where dW is the radiation power emitted in the photon energy interval dE and n_e, n_i, Z_{eff}, and T_e are electron and ion density, effective plasma charge and electron temperature, respectively.

The SXR emission is filtered by two aluminum or beryllium foils with different thickness. The foil material and thickness defines low energy absorption. If the SXR energy is higher, the emission is passed through the foil. Thus, the ratio of SXR emission measured by two different foils contains information about the electron temperature. The SXR intensity in the detector for the Maxwellian plasma is[7]:

$$I \propto \int_l \frac{n_e^2(l)}{\sqrt{T_e(l)}} Z_{eff} \int_E \xi(E) dE dl, \qquad (2)$$

where first integral along the line of sight path l represent ununiformed nature of the SXR emission from the plasma and second integral represent integration of local emission and absorption of the SXR emission by the foil versus energy. The function ξ is:

$$\xi(E) = \exp\left[-\frac{E}{T_e(l)}\right] \cdot \exp\left[-\frac{\mu}{\rho}(E)\rho \cdot t\right] \cdot F(E), \qquad (3)$$

where μ/ρ is the mass energy absorption coefficients of a foil, t is the foil thickness, $F(E)$ is a spectral sensitivity function of our photodiode. In previous work [2] constant spectral sensitivity was considered. We simulate various forms of spectral sensitivity function in our work in order to verify when it should be taken into account.

Generally, the problem is complex and needs inversion due to the first integral other line of sight. The temperature profile is peaked in Uragan-3M torsatron [4]. Let us assume that the major part of the SXR radiation comes from the plasma center. The contribution of the plasma periphery can be neglected under this assumption. In this case SXR signal in the detector is expressed as follow:

$$I \approx Z_{eff} \frac{n_e^2(l)}{\sqrt{T_e(l)}} \int_E \xi(E) dE. \qquad (4)$$

The integral part of this formula depends on the electron temperature only, Thus, the ratio of SXR signals passed through two foils depends on the temperature only:

$$R = \frac{I_1}{I_2} = R(T_e). \qquad (5)$$

This formula support the two foils technique applicability. Due to the complex $\mu(E)/\rho$ dependence the ration R of the signals is usually calculated numerically. Additional function is used in our numerical calculations in order to take into account spectral sensitivity of the photodiode.

Numerical calculations for two foils technique. Optimization of the foil thickness and material for the URAGAN conditions was done in previous work [2]. It was shown numerically that in assumption of the pure bremsstrahlung emission from the Maxwellian plasma the ration of signals passed through the 1.5 micrometer and 2.25 micrometer aluminum filters is weakly depends on the plasma temperature. Thicker second foil is required for the significant dependence of the ratio in the 0.1–1 keV temperature range, practically interesting for URAGANs plasma. Nonetheless, according to the experimental measurements in URAGAN-3M, the 1.5/2.25 μm signals ratio is substantially exceed predictions. One of the possible reasons of the discrepancy is based on the possible influence of the spectral sensitivity of the photodiodes, used in the SXR measurement systems. The uniform spectral sensitivity of the photodiode is used in the previous work. Real dependence of the sensitivity on the SXR wavelength can substantially modify the signals ratio, especially in the case than the difference of the foils thickness is rather low. The complete data of the spectral sensitivity of the even the AXUV photodiodes [2] and other photodiodes used in URAGANs is unknown (especially the sensitivity decay in the 10–30 keV range). The ratios of the SXR signals passed through different foils R for different modeling dependences of the spectral sensitivity of the photodiodes F has been calculated numerically in our work. For calculations, we use the formula in the form:

$$F(E) = \exp\left[-\left(\frac{E}{E_{\lim}}\right)^{\alpha}\right]. \qquad (6)$$

In this form the E_{lim} value define start of the spectral sensitivity decay and α define the decay speed. We calculated ratio of SXR signal intensities passed through two different foils *R* versus modeling photodiode sensitivity function *F* as it is shown in Fig. 1, Fig. 2. Numerical calculations was done for Al 0.9μm /6.15 μm and Al 1.5 μm /2.25 μm combinations, following to the Ref [2] logic.

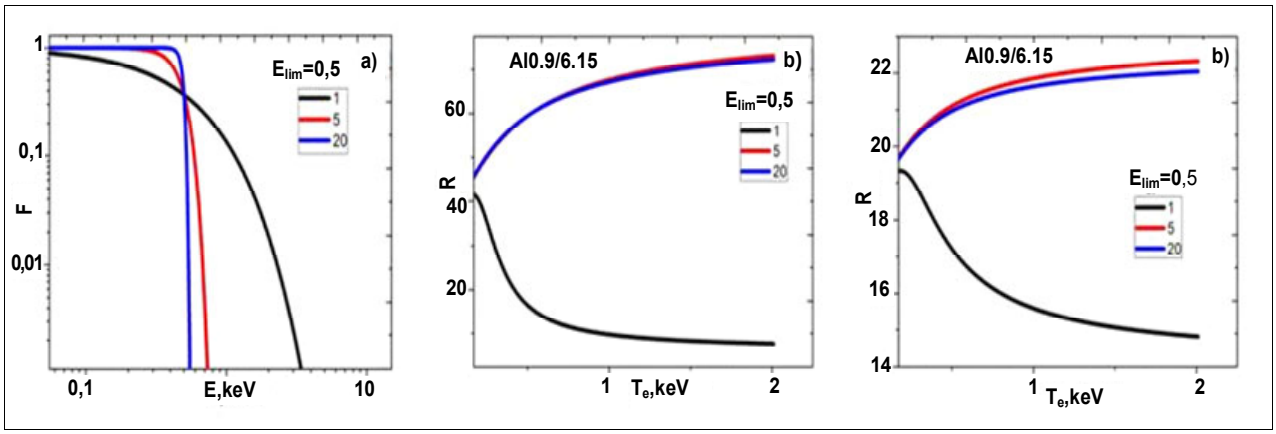

Fig. 1. a) Modeling functions E_{lim} = 0,5 values of α parameter are shown in the legends; b) SXR signals ratio for Al 0.9μm /6.15 μm and Al 1.5μm /2.25 μm

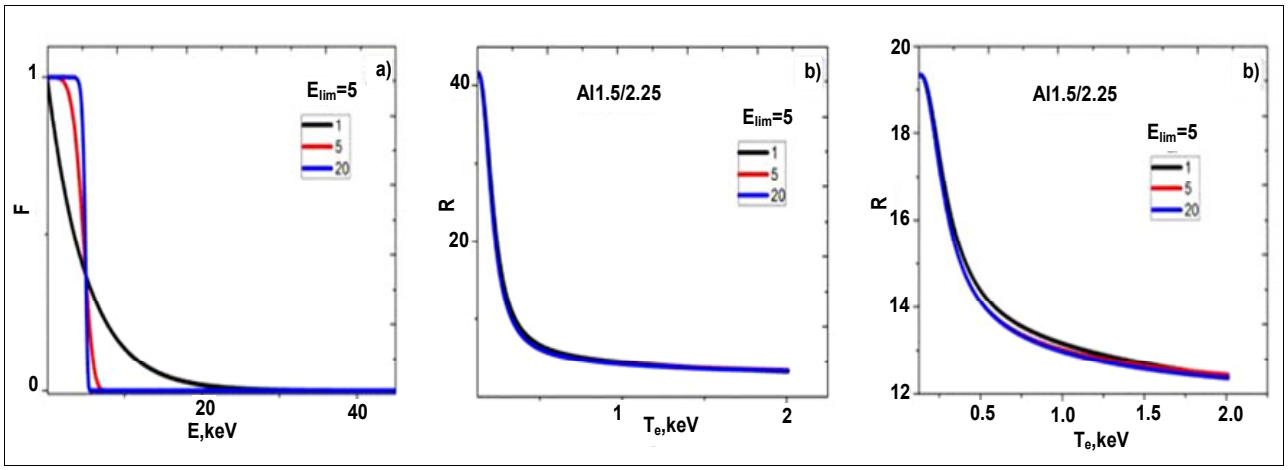

Fig. 2. a) Modeling functions E_{lim} = 0,5 values of α parameter are shown in the legends; b) SXR signals ratio for Al 0.9μm /6.15 μm and Al 1.5μm /2.25 μm

As it is seen from Fig. 1, in the case of the low the E_{lim} value the intensity ratio *R* is strongly depends on the coefficient α. In the case of low α, part of the sensitivity is still present in the energy range 0.5–2 keV. In this case *R* is not significantly different from the constant sensitivity case.

In the case of high E_{lim} (Fig. 2) the difference between constant sensitivity is almost absent. Thus, the low energy part (1–500 eV) of the spectral sensitivity of the photodiode can significantly modify the ratio of the SXR signals in the thing aluminum foils cases under consideration. In the AXUV-20EL photodiode case, spectral sensitivity is constant up to 5 keV, according to the datasheet of the manufacturer. This photodiode can be used for two foils technique application in U-3M torsatron. Another old photodiodes used in U-3M have not defined spectral sensitivity curves. Possible not flat shape of the sensitivity in the 1–500 eV energy range can explain practically observed discrepancy between constant sensitivity case calculations experimental measurements.

Conclusions. The ratios of the SXR signals passed through different foils *R* for different modeling dependences of the spectral sensitivity of the photodiodes *F* has been calculated numerically in our work. According to the AXUV specification [1, 3], its spectral sensitivity is almost flat up to 4 keV. In the case of thin foils, practically used in U-3M SXR diagnostics. The spectral sensitivity variation in the energy range above 4 keV practically is not modified initial ratio. The substantial modification is observed only in the low cutting energy case (0.5 keV), but this model is not represent spectral sensitivity of our AXUV20EL detector.

REFERENCES

1. *Dreval M.* Design and initial operation of multichord soft *X*-ray detection array on the U-3M torsatron / M. Dreval // Probl. Atom. Sci. Technol., 2014. – Vol. 6. – P. 250–253.

2. *Dreval M.* Design of multichord Soft *X*-ray detection arrays for the Uragan-2M stellarator / M. Dreval // Probl. Atom. Sci. Technol., 2010. – Vol. 6. – P. 11–13.

3. *Dreval M.* First results of multichord soft x-ray detection array on the U-3M torsatron / M. Dreval // Probl. Atom. Sci. Technol., 2015. – Vol. 1. –P. 8–11.

4. *Pavlichenko R.* Influence of suprathermal electrons on ece measurements in the Uragan-3M torsatron" / R. Pavlichenko // Probl. Atom. Sci. Technol., 2015. – Vol. 6. – P. 293–296.

5. Effects of light impurities on electron temperature measured by Soft *X*-Ray filter method / S. Morimoto, S. Okamoto et. al. // Japanese Journ. of App. Phys., 1986. – Vol. 25. – P. 120–123.

Submitted on 09.11.17

О. Турянська, мол. наук. співроб.,
М.Древаль, ст. наук. співроб.,
Інститут фізики плазми, Національний науковий центр,
"Харківський фізико-технічний інститут"

ВПЛИВ СПЕКТРАЛЬНОЇ ЧУТЛИВОСТІ ФОТОДІОДА НА МЕТОДИКУ ОБРОБКИ ДАНИХ М'ЯКОГО РЕНТГЕНУ З ВИКОРИСТАННЯМ ДВОХ ФОЛЬГ НА ТОРСАТРОНАХ "УРАГАН"

Діагностика за даними м'якого рентгенівського випромінювання використовується на торсатронах "Ураган-2М" і "Ураган-3М". Одне з діагностичних застосувань м'якого рентгену базується на оцінці температури плазми. Для оцінки температури використовують співвідношення сигналів м'якого рентгена, які проходять через дві фольги різної товщини. Спектральна чутливість самого фотодіода може впливати на вимірювання температури. Совокупність модельних функцій спектральної чутливості фотодіода використовувався для чисельного розрахунку співвідношення сигналів м'якого рентгену. У випадку тонких алюмінієвих фольг вплив незначний при плоскій чутливості фотодіода в діапазоні енергій 5-500 еВ (напр., у випадку фотодіодів AXUV-20EL).

Ключові слова: м'який рентген, техніка двох фольг, спектральна чутливість, торсатрон.

Е. Турянская, мл. научн. сотр.,
Н. Древаль ,ст. научн. сотр.,
Институт физики плазмы, Национальный научный центр
"Харьковский физико-технический институт"

ВЛИЯНИЕ СПЕКТРАЛЬНОЙ ЧУВСТВИТЕЛЬНОСТИ ФОТОДИОДА НА МЕТОДИКУ ОБРАБОТКИ ДАННЫХ МЯГКОГО РЕНТГЕНА С ИСПОЛЬЗОВАНИЕМ ДВУХ ФОЛЬГ НА ТОРСАТРОНАХ "УРАГАН"

Диагностика по данным мягкого рентгеновского излучения используется на торсатронах "Ураган-2М" и "Ураган-3М". Одно из диагностических применений мягкого рентгена основано на оценке температуры плазмы. Для оценки температуры используется соотношение сигналов мягкого рентгена, которые проходят через две фольги различной толщины. Спектральная чувствительность самого фотодиода может влиять на измерение температуры. Совокупность модельных функций спектральной чувствительности фотодиода использовался для численного расчета соотношения сигналов мягкого рентгена. В случае тонких алюминиевых фольг влияние незначительно при плоской чувствительности фотодиода в диапазоне энергий 5–500 эВ (напр., в случае фотодиодов AXUV-20EL).

Ключевые слова: мягкий рентген, техника двух фольг, спектральная чувствительность, торсатрон.

UDC 533.92

V. Chernyak, D. Sci.,
O. Tsymbaliuk, Ph. D.,
D. Chunikhina, Stud.,
I. Fedirchyk, Ph. D. Stud.,
O. Nedybaliuk, Ph. D.,
V. Iukhymenko, Ph. D.,
E. Martysh[1], D. Sci.,
Iu. Veremii[1], Ph. D.,
I. Prysiazhnevych, Ph. D.,
O. Prysiazhna[1], Ph. D.,
V. Prysiazhnyi, Ph. D.,
Department of Physical Electronics,
[1]Department of Medical Radiophysics,
Faculty of Radiophysics, Electronics and Computer Systems,
Taras Shevchenko National University of Kyiv

EXPERIMENTAL AND NUMERICAL RESEARCH OF PLASMA-CATALYTIC REFORMING OF HYDROCARBONS

This work is devoted to the exploration of the compatibility of the hybrid plasma-catalytic conversion of liquid hydrocarbons into syngas with the concept of sustainable development. The results of the experimental investigations indicate the high efficiency of plasma-catalytic conversion of ethanol to syngas and the small amount of waste (a few percent of feedstock weight). The results of the simulation of the kinetics using ZDPlasKin code for thermochemical and hybrid plasma-catalytic conversion.

Keywords: sustainable development, non-equilibrium plasma chemistry, rotating gliding discharge, conversion.

Introduction. The scale on which modern industry uses materials and energy not only led to the substantial depletion of fossil resources but also caused significant accumulation of waste, which is hazardous to the environment. In 1980 IUCN (The International Union for Conservation of Nature), UNEP (United Nations Environment Program) and WWF (World Wildlife Fund) approached this problem by developing the World Conservation Strategy for Sustainable Development. In September of 2015, the UN proposed 17 goals of sustainable development, which were adopted by 70 countries [26].

Among the goals of sustainable development, the minimization of the use of fossil fuels and their replacement with the renewable energy sources is one of the most important for ecology, society, and economics. The switch to the renewable biomass can lead to an ecologically beneficial reduction in the emission of carbon, chemicals, and liquid fuels. However, it is widely recognized that the use of first-generation biomass raw materials, such as corn or edible oilseeds, is not a sustainable solution overall because it competes directly or indirectly with the production of food. Therefore, the European Union is aimed at the use of second-generation biomass raw materials, which includes lignocellulose, waste oils and fats [22].

A major barrier to increasing the scale of biofuels production lies in the disadvantages of two main ways of processing lignocellulosic biomass: thermochemical and biotechnological. The biotechnical method of biofuel production is based on using the microorganisms for the processing of biomass into the desired product. This technology is used successfully to obtain ethanol from plant sugars and starches, but it faces significant challenges in the transition to the more complex raw materials, such as lignin and cellulose, and while attempting to produce more sophisticated biofuels than ethanol [27, 28]. At this stage of technological development, the performance of the biotechnical processing of lignocellulosic feedstock is low and is not able to offer the required rate of biofuel production growth.

The modern thermochemical technology of lignocellulosic biomass processing needs higher temperatures than biotechnological methods (over 700 °C for pyrolysis and 1000 °C for gasification). A significant disadvantage of the thermochemical technologies is low energy efficiency. In addition, the use of elevated temperatures not only complicates the design of processing devices and demands the increase of safety requirements, but also decreases the selectivity of the raw materials conversion and leads to the emergence of byproducts. Therefore, the traditional thermochemical (temperature > 700 °C) and traditional plasma-chemical (temperature > 1000 °C) (which is based on the ideas of thermochemical conversion using plasma torches) processing of biomass leads to the appearance of the unwanted byproducts and wastes. In the case of catalytic conversion, a high content of impurities in raw biomass negatively affects the yield and longevity of catalysts.

As of today, the discussion is open on the development of new principles behind the construction of technologies for the conversion of substances, which are known as "green chemistry". "Green chemistry" moves from the traditional evaluation of the effectiveness using the chemical yield to the assessment of the cost-effectiveness based on the lack of hazardous waste and non-toxic and/or hazardous substances. "Green chemistry" has to transform the raw materials (preferably renewable), exclude hazardous waste, and use no toxic agents in the production of chemical products and in their application [23]. There should be the development of processes involving H_2, O_2, CO, CO_2, NH as a direct source of atoms H, O, C and N in the production of fine chemicals. The quantitative measure of the environmental acceptability of chemical technology is E factor, which is defined as the ratio of waste weight to the weight of a target product. Waste includes everything that is not a target product [23].

This work is devoted to several topics: further experimental research of hybrid plasma-catalytic system with the gas discharge generator of the wide-aperture flow of non-isothermal plasma, the investigation of some features of the kinetics in a plasma of wide-aperture rotating gliding discharge using numerical modeling, the comparison of chemical kinetics during thermochemical reforming and experimental research.

Methods and experimental setup. Partial oxidation reforming of hydrocarbons is the most energy-efficient and economical reaction pathway for use in the conversion

methods that utilize electric energy. This is especially important for the plasma-chemical reforming methods that use electric energy. The reason for this is that in modern power plants the production of one unit of electrical energy needs three units of chemical energy. Fig. 1 shows the schemes of two hydrocarbon conversion approaches are present in plasma-chemistry: plasma reforming and plasma-catalytic reforming.

In plasma approach, the hydrocarbon and oxidant are introduced directly into the discharge area after which the activated mixture is injected into the reaction chamber. Such approach leads to the appearance of the exothermal reactions in the discharge area, which increase the rotational temperature of heavy plasma components and cause the decrease of plasma non-isothermality and drop in the yield of desired products [5, 6]. In plasma-catalytic approach, only a part of the oxidant is introduced into the discharge area and the activated oxidant is injected in a form of radicals into the reaction chamber, which has the separate injection of hydrocarbon. This approach results in the generation of the non-isothermal plasma, which provides the increased selectivity of desired product. Discharge can be used to activate a part of the oxidant while the rest of the oxidant is introduced into the reaction chamber together with the hydrocarbon. The plasma-catalytic approach uses the active species (OH, H, O), which are produced inside plasma from the non-toxic and/or safe reagents, to initiate the chain reactions of renewable biomass conversion at a low temperature (~ 250–350 °C).

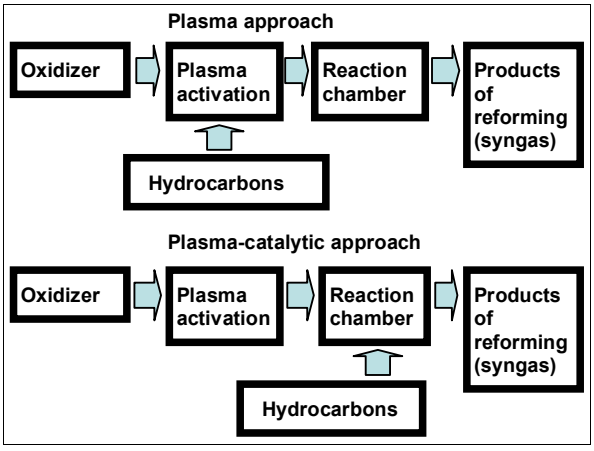

Fig. 1. Schematic representation of plasma and plasma-catalytic approaches to hydrocarbon conversion

A discharge chamber, which is attached to the reaction chamber [15], is designed for the plasma-catalytic approach to the hydrocarbon conversion. Plasma is generated using wide-aperture rotating gliding discharge [3, 4, 7]. The discharge is powered using DC power source. Fig. 2 shows the discharge chamber, gas flow directions, and wide-aperture rotating gliding discharge. 96 % ethanol was used as a model hydrocarbon during the plasma-catalytic reforming of hydrocarbons, atmospheric air, which was supplied using a compressor, was used as an oxidant. The system for plasma-catalytic reforming of hydrocarbons into the synthesis gas was designed for the output power of 25 kW and tested using 53.3 g min^{-1} (25 kW) ethanol flow. The experimental laboratory studies of hybrid plasma-catalytic reforming of ethanol were conducted at lower output power. Optical emission spectroscopy was used for the study of plasma. Gas chromatography was used for the study of gas-phase products.

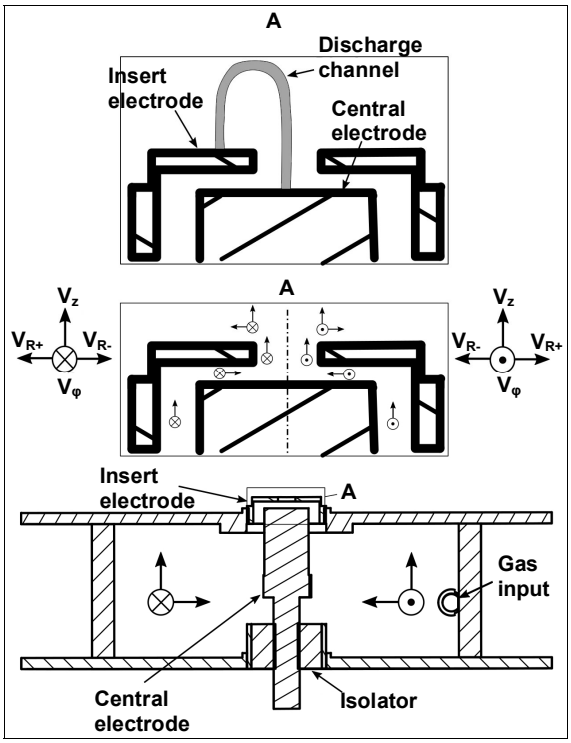

Fig. 2. Scheme of discharge chamber, directions of gas flows and wide-aperture rotating gliding discharge during plasma-catalytic reforming of hydrocarbons

Experimental results. The efficiency of the reforming system in terms of hydrogen production can be evaluated from its hydrogen energy yield. It corresponds to the flow of produced hydrogen divided by the electric power spent on plasma generation. Fig. 3 shows the comparison between the hydrogen energy yields of the hybrid plasma-catalytic reforming of ethanol (the best results of this work) and other methods of hydrogen production that utilize electrical energy: Water Electrolysis [17], Westinghouse [9], Laval Nozzle Arc [8], DBD [21], MW Discharge [13], Arc Discharge [19], GEN3 [11], Submerged Plasma [1].

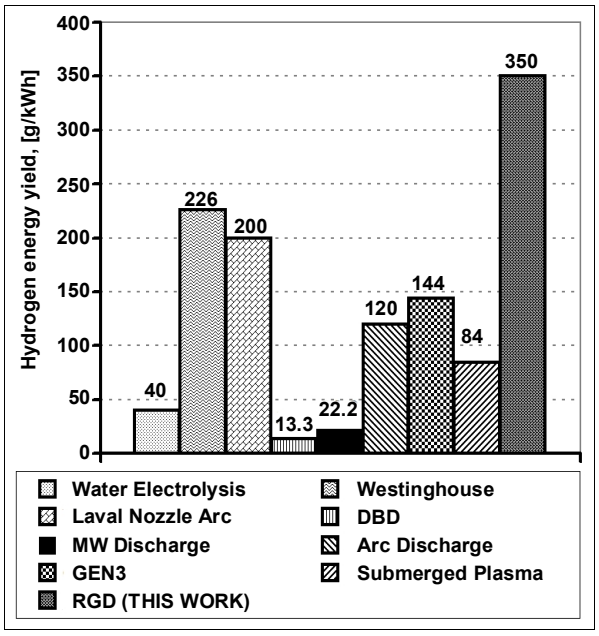

Fig. 3. The hydrogen energy yield of reforming of ethanol for different methods of hydrogen production using electrical energy

The hydrogen energy yield of hybrid plasma-catalytic ethanol reforming is the highest in comparison with the other methods [1,8,9,11,13,17,19,21]. The ratio of the reactor power output to its volume is approximately 100 kW l^{-1}. The hybrid plasma-catalytic approach can be used to solve the existing problems of the traditional renewable biomass reforming methods.

Physical modeling of calculations of plasma-catalytic reforming studied using numerical calculation methods. The numerical modeling of the kinetics was conducted for the ethanol reforming in plasma-catalytic systems. Fig. 4 shows the scheme of one of the experimental systems, which are used for the study of the liquid hydrocarbon reforming via the plasma-catalytic scheme [15].

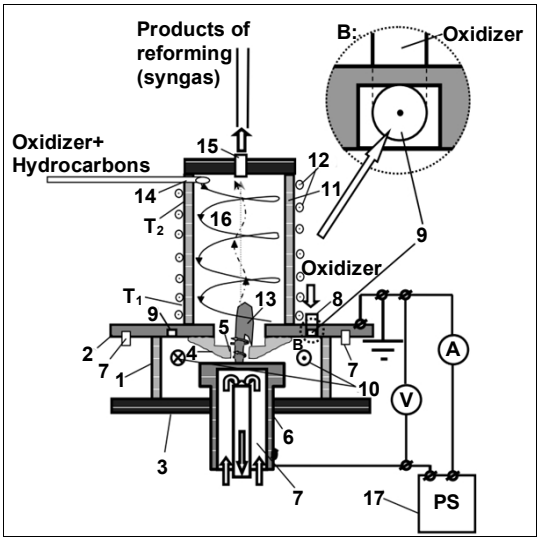

Fig. 4. Scheme of experimental setup: 1 – quartz chamber; 2, 3 – flanges; 4, 5 – inserts; 6 – T-shaped electrode; 7 – water cooling; 8 – oxidant input; 9 – directing channel; 10 – gas flow direction; 11 – pyrolytic chamber; 12 – heater; 13 – plasma torch; 14 – hydrocarbon input; 15 – reforming products outlet; 16 – gas flow direction; 17 – power supply

In several experiments, the quartz chamber (Fig. 4, 1) was filled with water and electrode (Fig. 4, 10) was completely submerged in the liquid. When electrode (Fig. 4, 10) was submerged, the electric field in plasma measured at 340 mA discharge current was approximately 700 V cm^{-1}.

The main goal of kinetics calculations is the study of the processes in the volume of the pyrolytic (reaction) chamber. The mixture of hydrocarbon vapors and oxidant was introduced into the chamber via the input (Fig. 4, 14) tangentially to the chamber wall and formed the "tornado" reverse vortex flow. Rotating mixture descends towards the bottom of the reaction chamber, moves towards the axis, where the plasma-activated oxidant is introduced into the reaction chamber, then the mixture moves upwards along the axis and flows out through the aperture 15. Therefore, the chemical reactor volume can be divided into several zones: I – chemical reforming process or pyrolysis zone; II – plasma zone; III – main reforming zone.

The first zone is the high-temperature area, into which the mixture of hydrocarbon and the part of the oxidant is injected. During the simulation, the temperature in this area is constant. The second zone is filled with the discharge plasma, into which the part of the oxidant (air) is injected and activated. The main parameter responsible for the kinetics in plasma is the reduced electric field E/N. E is an electric field and N is a concentration of neutral particles in the plasma. The specifics of the kinetics calculation in plasma zone is the ability to set reduced electric field based on the experimentally measured electric field and gas temperature obtained from the plasma emission spectra [16].

The third zone is the main reaction zone of the reactor, into which the end products of the first and second zones are introduced. The main hydrocarbon reforming processes with the possibility of the occurrence of the exothermic complete oxidation processes take place in this zone. These exothermic processes are the main source of thermal energy for the reforming processes. Fig. 5 show the scheme of the physical model used for the simulation of the kinetics of physical and chemical processes in the plasma-catalytic system.

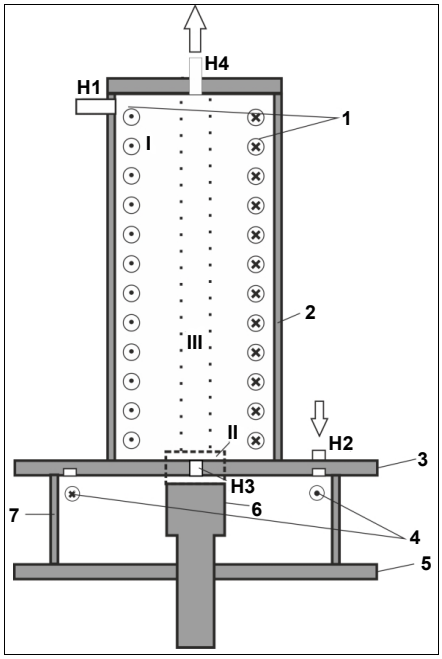

Fig. 5. Scheme of physical model used for calculations: H1 – inlet for the injection of oxidant and hydrocarbon mixture; H2 – inlet for the injection of the part of oxidant; H3 – outlet or the ejection of plasma torch; H4 – outlet channel for the reforming products; 1,4 – directions of the gas flow movement; 2 – pyrolytic chamber; 3,5 – flanges; 6 – T-shaped electrode; 7 – cylindrical chamber; I – first zone; II – second zone; III – third zone

Mathematical model of plasma-catalytic reforming study. This work presents the simulation of kinetics in all three reaction zones. The study of the first zone was done using the base with 130 chemical reactions between 30 components [12]. The goal of the conducted numerical experiments is the determination of the base kinetics mechanisms, the dynamics of the generation of active radicals and excited oxygen molecules and the kinetics of processes in which they participate. For the dependence on the absolute humidity, the range of the water content in plasma gas, for which the calculations were conducted, was from 1 % to 25 %.

In order to evaluate the dependence on the flow rate, the modeling was conducted for the arbitrarily large time interval, which allowed to make a "time cross-section" on any part of said interval. The time during which working gas was in the corresponding zone of the experimental reactor was equivalent to the modeling time.

Following parameters were set as base for the plasma of the second zone: 1) gas temperature T = 2500 K (corresponds to the rotational temperature determined from the experimental plasma emission spectra); 2) electric field 800 V/m, which corresponds to the maximum field from the investigated range of rotating gliding discharge. Plasma gas – air with water vapor. The modeling of the processes in the second zone (plasma, humid air) is based on the Capitelli mechanism, which is complemented with H_2O, CO_2 and partially N_2 reactions [2]. Because the experimental data confirms that the rotational temperature is high enough (~2500 K), all the reaction of the oxidation of atmospheric nitrogen were included to the list of reactions. The mechanism was complemented by the reactions, which involved such species as N_2O, NO_2, NO_3, N_2O_5, N_2O^+, NO_2^+, N_2O^-, NO_2^- NO_3^-, the rates of chemical and electron reactions were taken from [10]. According to the experiment, the electric field in the plasma zone varied in the range of 100-800 V/cm, which necessitated the addition of dissociation reactions by electron impact of such components as H_2O, NO_2, and HO. At the same time, in this type of conversion, the air with the addition of H_2O is the plasma gas, which is why the list of reactions involving H_2O and its derivatives was added to this mechanism. The list of reactions involving H_2O was composed using [14, 20].

Modeling was conducted from 10^{-6} s to 1 s, with the 10^{-6} s time step for the first and third zones and 10^{-8} s time step for the second zone. The kinetics of plasma-chemical processes in the plasma of wide-aperture rotating gliding discharge and chemical kinetics of ethanol conversion into synthesis gas were calculated via ZDPlasKin program code [18, 24]. ZDPlasKin allows the simulation of plasma kinetics from the preliminary set of input parameters of the studied system (temperature, pressure, the initial concentration of reagents etc.).

The program code allowed to solve the system of kinetic equations for r reactions between s components. Reactions can be presented schematically as:

$$c_{l_1 j}S_{l_1} + c_{l_2 j}S_{l_2} + \cdots + c_{l_n j}S_{l_n} \xrightarrow{k_j} c_{l_{n+1} j}S_{l_{n+1}} + c_{l_{n+2} j}S_{l_{n+2}} + \cdots + c_{l_{n+m} j}S_{l_{n+m}} \quad (1)$$

Where S_l is component with index l = 1,2,…,s. Each reaction has a characteristic rate constant k_j, where j = 1,2,…,r. For the zero-dimensional approximation (homogeneous space) model balance equations form a system of ordinary first order differential equations for the component concentrations:

$$\frac{d[S_i]}{dt} = \sum_j \pm c_{ij} k_j \prod_l [S_l]^{c_{lj}}, \quad (2)$$

where S_i is the stoichiometric coefficient of component i in reaction j and is a concentration of component with index l [24].

During the calculation fulfilled for the plasma of moist air (zone II on Fig. 5), the database used for the calculation comprised of 900 chemical and electron-molecular reactions involving 83 components. Time sampling step was 10^{-12} s. The time interval for the calculation of changes in the concentration of plasma components at the time evolution was 10^{-3} s. (It is significantly higher than the time of the exposure of gas to the current channel of gas discharge considering the experimental data: the rate of gas flow was ~ 10^3 cm s^{-1}, wide-aperture rotating discharge is a transverse discharge with the diameter of current channel ~ 10^{-1} cm, respectively the time of gas exposure to the current channel is ~ 10^{-4} s.

Results of numerical modeling. Typical time dependencies of the concentrations of N, O, O_3, H, OH, which are calculated for the plasma of gas discharge – [Ai](t), are shown in Fig. 6. Provided dependences [Ai](t) show that during the experiment the setting time of the fixed values [Ai] of O, H, and OH radicals corresponds to ~ 10^{-4} s, and the degree of the dissociation of molecular oxygen O_2 (Fig. 7) and water H_2O is ~ 10^{-2}.

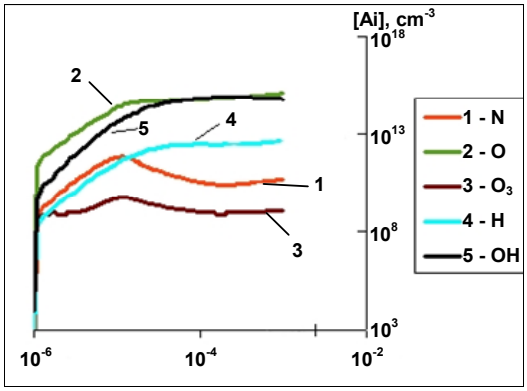

Fig. 6. Typical time dependencies of the concentrations of N, O, O_3, H, OH

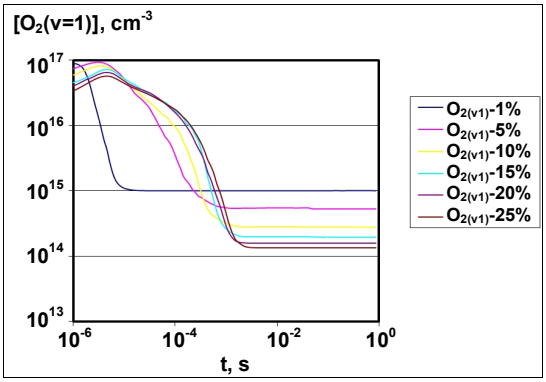

Fig. 7. Dependencies of changes of the concentration of oxygen molecules, excited to the first vibrational state, on the value of absolute humidity of plasma gas (air)

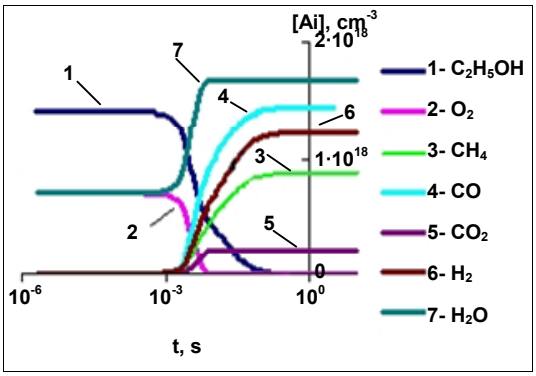

Fig. 8. Time dependence of concentrations for the thermochemical conversion of ethanol at 1300 K for $1C_2H_5OH/0.5O_2/0.5H_2O/2N_2$ initial mixture

The simulation of reforming kinetics was conducted for the zone of high-temperature ethanol conversion (Fig. 8), where thermochemical reforming takes place. Reforming takes place under the temperature influence via the interaction between the initial hydrocarbon (ethanol) with air (a mixture of molecular oxygen, nitrogen, which is chemically inert at the presented temperature T = 1100 K (Fig. 9), and water steam, which amounts to 10 % of the total volume of the mixture).

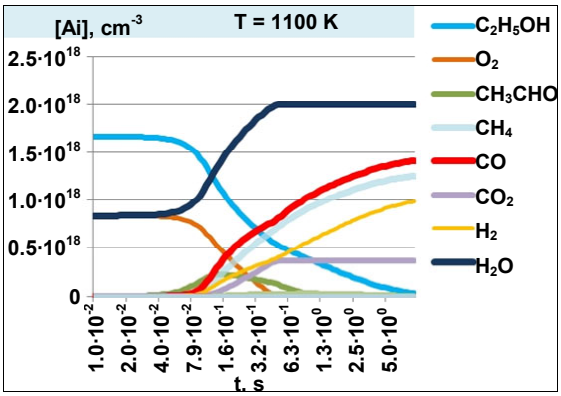

Fig. 9. The time dependence of the concentration of some component at atmospheric pressure and temperature T = 1100 K. Ratio between components in the initial mixture: $1C_2H_5OH/0.5O_2/0.5H_2O/2N_2$. Time range of simulation: [10^{-2} s; 10 s]. Sampling time step is 10^{-6} s. Air (nitrogen and oxygen mixture) humidity is 10 %, Water steam is present as neutral H_2O molecules

The next step in the study of ethanol conversion consisted of the kinetics simulation for the experimentally measured reforming temperature T = 523 K (Fig. 10). The aim of this numerical calculation was to prove the high efficiency of reforming, which was reached during the experiment. The initial calculation conditions remained unchanged relatively to the previously discussed model, calculations for which were conducted for the temperature of thermochemical conversion T = 1100 K.

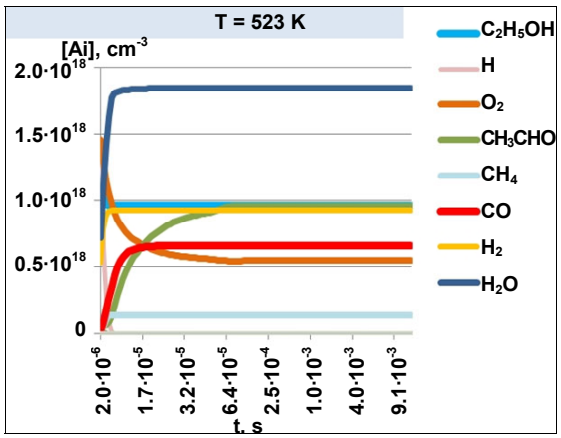

Fig. 10. Time dependencies of some of the components at atmospheric pressure and temperature T = 523 K. The ratio between the components in the initial mixture: $1C_2H_5OH/1O/0.5H/0.5OH/2N_2$. Time range of simulation: [10^{-6} s; 10^{-2} s]. Sampling time step is 10^{-6} s. Air (nitrogen and oxygen mixture) humidity is 10 %, water steam is present as neutral H_2O molecules

During the calculation of chemical kinetics in the reactor zone of the experimental system [7], the database contained 130 chemical reactions involving 30 components [25]. Time sampling step was 10^{-6} s. The time interval for the calculation of changes in the concentration of plasma components was 10^{-3} s. The time interval for the calculation of changes in the concentration of the gas components at the outlet of the reactor zone (Fig. 5) was equal to 10 seconds.

Time dependence of concentrations for the thermochemical partial oxidative conversion of ethanol indicates the existence of two conversion stages: oxygen and without oxygen.

Conclusions. The experimental and theoretical studies of plasma-catalytic and purely thermochemical conversions of ethanol show that:

1. The plasma-catalytic approach is an emerging alternative to the traditional conversion technologies. The plasma-catalytic approach uses active species generated in the plasma from non-toxic and/or non-hazardous reagents to initiate the chain reactions of renewable biomass conversion at low temperature (~ 500–600 K).

2. Plasma-catalytic approach confirms the concept of sustainable development with the production of small amounts of waste.

3. Studies of chemical kinetics revealed differences in the mechanism of the conversions that result in significant changes in syngas ratio ($[H_2]/[CO]$).

4. Partial oxidative conversion of ethanol has two conversion stages: with oxygen and without oxygen.

5. Temperature dependences of the conversion products concentrations show that syngas ratio changes in response to the rise of CO quantity in the system with the increase of reforming temperature. Additionally, CH_3CHO production correlates with a drastic decrease of oxidant (O_2) concentration in the system, which indicates that reforming is conducted through the chain reactions.

REFERENCES

1. *Bardos L.* Production of hydrogen-rich synthesis gas by pulsed atmospheric plasma submerged in mixture of water with ethanol / L. Bardos, H. Baránková, A. Bardos // Plasma Chemistry and Plasma Processing, 2017. – Vol. 37, №1. – P. 115–123.

2. Plasma kinetics in atmospheric gases / M. Capitelli, C.M. Ferreira, B.F. Gordiets, A.I. Osipov. – Berlin, Heidelberg : Springer Berlin Heidelberg, 2000. – 300 p.

3. *Chernyak V.* Gas discharge plasma in dynamics system as a non-equilibrium plasma sources / V. Chernyak // Proceedings of the 3rd Czech-Russian Seminar on Electrophysical and Thermophysical Processes in Low-temperature Plasma. – Brno, Czech Republic, 1999. – P. 94–99.

4. The rotating gliding discharge in quartz tube and open half-space at atmospheric pressure / V.Y. Chernyak, D.L. Chernolutsky, V.V. Kolgan et al. // Plasma Physics and Technology, 2015. – Vol. 2, № 2. – P. 116–119.

5. Plasma catalysis of chemical reactions / V.Y. Chernyak, O.A. Nedybaliuk, E.V. Martysh et al. // Problems of Atomic Science and Technology, 2014. – Vol. 94, № 6. – P. 124–129.

6. The problem of chemically active plasma nonequilibrium. review / V.Y. Chernyak, O.A. Nedybaliuk, E.V. Martysh et al. // Plasma Physics and Technology. – 2015. – Vol. 2, № 3. – P. 226-232.

7. *Chernyak V.Y.* Plasma-liquid system with rotational gliding arc with liquid electrode / V.Y. Chernyak, O.A. Nedybaliuk, O.V. Solomenko et al. // 20th Symposium on Physics of Switching Arc 2013, 2–6 September 2013. – Nove Mesto na Morave, Czech Republic. – 2013. – P. 112–115.

8. Hydrogen production by steam-oxidative reforming of bio-ethanol assisted by Laval nozzle arc discharge / C. Du, H. Li, L. Zhang et al. // International Journal of Hydrogen Energy, 2012. – Vol. 37, № 10. – P. 8318–8329.

9. *Ducharme C.* Technical and economic analysis of plasma-assisted waste-to-energy processes. – New York, USA : Columbia University, 2010. – 79 p.

10. *Flitti A.* Gas heating in fast pulsed discharges in N2–O2 mixtures / A. Flitti, S. Pancheshnyi // The European Physical Journal Applied Physics. – 2009. – Vol. 45, № 2. – P. 21001.

11. Hydrogen-rich gas production from plasmatron reforming of biofuels / K. Hadidi, L. Bromberg, D.R. Cohn et al. // World Renewable Energy Congress VIII and Expo. – Denver, CO, USA, 2004.

12. Plasma kinetics in ethanol/water/air mixture in a "tornado"-type electrical discharge / D. Levko, A. Shchedrin, V. Chernyak et al. // Journal of Physics D : Applied Physics, 2011. – Vol. 44, № 14. – P. 145206.

13. *Mizeraczyk J.* Plasma processing methods for hydrogen production / J. Mizeraczyk, M. Jasiński // The European Physical Journal Applied Physics, 2016. – Vol. 75, № 2. – P. 24702.

14. *Morgan L.* Plasma chemistry modeling – KINEMA research and software LLC [Electronic resource] / L. Morgan. – Access mode : http://kinema.com/plasma-chemistry-modeling/ (last access: 10.05.17).

15. Plasma-catalytic reforming of liquid hydrocarbons / O.A. Nedybaliuk, V.Y. Chernyak, V.V. Kolgan et al. // Problems of Atomic Science and Technology, 2015. – Vol. 95, № 1. – P. 235–238.

16. Plasma-liquid system with rotational gliding discharge with liquid electrode / O.A. Nedybaliuk, O.V. Solomenko, E.V. Martysh, I.I. Fedirchyk // Problems of Atomic Science and Technology, 2014. – Vol. 94, № 6. – P. 191–194.

17. NREL Current (2009) state-of-the-art hydrogen production cost estimate using water electrolysis (NREL/BK-6A1-46676) / NREL. – Golden, Colorado, USA : 2009. – 44 p.

18. Computer code ZDPlasKin / S. Pancheshnyi, B. Eismann, G.J.M. Hagelaar, L.C. Pitchford. – Toulouse, France: University of Toulouse, LAPLACE, CNRS-UPS-INP, 2008.

19. Ethanol and E85 reforming assisted by a non-thermal arc discharge / G. Petitpas, J. Gonzalez-Aguilar, A. Darmon, L. Fulcheri // Energy & Fuels, 2010. – Vol. 24, № 4. – P. 2607–2613.

20. An air breakdown kinetic model / A.E. Rodríguez, W.L. Morgan, K.J. Touryan et al. // Journal of Applied Physics, 1991. – Vol. 70, № 4. – P. 2015–2022.

21. Hydrogen production by reforming of hydrocarbons and alcohols in a dielectric barrier discharge / B. Sarmiento, J.J. Brey, I.G. Viera et al. // Journal of Power Sources, 2007. – Vol. 169, № 1. – P. 140–143.

22. *Sheldon R.A.* Green chemistry, catalysis and valorization of waste biomass / R.A. Sheldon // Journal of Molecular Catalysis A: Chemical, 2016. – Vol. 422. – P. 3–12.

23. *Sheldon R.A.* Green chemistry and catalysis / R.A. Sheldon, I. Arends, U. Hanefeld. – Weinheim, Germany : Wiley-VCH Verlag GmbH & Co. KGaA, 2007. – 433 p.

24. *Snoeckx R.* Plasma-based dry reforming: a computational study ranging from the nanoseconds to seconds time scale / R. Snoeckx, R. Aerts, X. Tu, A. Bogaerts // The Journal of Physical Chemistry C, 2013. – Vol. 117, № 10. – P. 4957–4970.

25. Influence of the gas mixture temperature on the efficiency of synthesis gas production from ethanol in a nonequilibrium plasma / A.N. Tsymbalyuk, D.S. Levko, V.Y. Chernyak et al. // Technical Physics, 2013. – Vol. 58, № 8. – P. 1138–1143.

26. UN SDGs.:. Sustainable Development Knowledge Platform [Electronic resource] / UN. – Access mode: https://sustainabledevelopment.un.org/sdgs (last access: 16.01.17).

27. U.S. GAO Renewable fuel standard: low expected production volumes make it unlikely that advanced biofuels can meet increasing targets (GAO-17-108) / U.S. GAO. – Washington, DC, USA, 2016.

28. *Veettil S.I.* Can microbially derived advanced biofuels ever compete with conventional bioethanol? A critical review / S.I. Veettil, L. Kumar, A.A. Koukoulas // BioResources, 2016. – Vol. 11, № 4. – P. 10711–10755.

Submitted on 02.06.17

В. Черняк, д-р фіз.-мат. наук,
О. Цимбалюк, канд. фіз.-мат. наук,
К. Чуніхіна, студ.,
І. Федірчик, асп.,
О. Недибалюк, канд. фіз.-мат. наук,
В. Юхименко, канд. фіз.-мат. наук,
Є.Мартиш[1], д-р фіз.-мат. наук,
Ю. Веремій*, канд. фіз.-мат. наук,
І. Присяжневич, канд. фіз.-мат. наук,
О. Присяжна[1], канд. фіз.-мат. наук,
В. Присяжний, канд. фіз.-мат. наук,
кафедра фізичної електроніки,
[1]кафедра медичної радіофізики,
факультет радіофізики, електроніки та комп'ютерних систем,
Київський національний університет імені Тараса Шевченка

ЕКСПЕРИМЕНТАЛЬНІ ТА ЧИСЛОВІ ДОСЛІДЖЕННЯ ПЛАЗМОВО-КАТАЛІТИЧНОГО РЕФОРМУВАННЯ ВУГЛЕВОДНІВ

Досліджено сумісність гібридної плазмово-каталітичної конверсії рідких вуглеводнів у сингаз з концепцією сталого розвитку. Результати експериментів вказують на високу ефективність плазмово-каталітичної конверсії етанолу в сингаз та на низьку кількість відходів (кілька відсотків від маси сировини). Наведено результати симуляції кінетики за допомогою коду ZDPlasKin для термохімічної та гібридної плазмово-каталітичної конверсії.

Ключові слова: сталий розвиток, нерівноважна плазмохімія, обертовий ковзний розряд, конверсія.

В. Черняк, д-р физ.-мат. наук,
О. Цымбалюк, канд. физ.-мат. наук,
К. Чунихина, студ.,
И. Федирчик, асп.,
О. Недыбалюк, канд. физ.-мат. наук,
В. Юхименко, канд. физ.-мат. наук,
Є. Мартыш[1], д-р физ.-мат. наук,
Ю. Веремий[1], канд. физ.-мат. наук,
И. Присяжневич, канд. физ.-мат. наук,
О. Присяжная[1], канд. физ.-мат. наук,
В. Присяжный, канд. физ.-мат. наук,
кафедра физической электроники,
[1]кафедра медицинской радиофизики,
факультет радиофизики, электроники и компьютерных систем,
Киевский национальный университет имени Тараса Шевченко

ЭКСПЕРИМЕНТАЛЬНЫЕ И ЧИСЛОВЫЕ ИССЛЕДОВАНИЯ ПЛАЗМЕННО-КАТАЛИТИЧЕСКОГО РЕФОРМИРОВАНИЯ УГЛЕВОДОРОДОВ

Посвящено исследованию совместимости гибридной плазменно-каталитической конверсии жидких углеводородов в сингаз с концепцией устойчивого развития. Результаты экспериментальных исследований указывают на высокую эффективность плазменно-каталитической конверсии этанола в сингаз и на низкое количество отходов (несколько процентов от массы сырья). Результаты симуляции кинетики с помощью кода ZDPlasKin для термохимической и гибридной плазменно-каталитической конверсии.

Ключевые слова: устойчивое развитие, неравновесная плазмохимия, вращательный скользящий разряд, конверсія.

80 РОКІВ ФІЗИЧНОЇ ЕЛЕКТРОНІКИ В КИЇВСЬКОМУ НАЦІОНАЛЬНОМУ УНІВЕРСИТЕТІ ІМЕНІ ТАРАСА ШЕВЧЕНКА: ОСНОВНІ ЕТАПИ

Член-кореспондент Академії наук УРСР, професор Н.Д. Моргуліс (1904–1976), засновник кафедри фізичної електроніки

Історія кафедри фізичної електроніки

1933 р. – організація спеціалізації "електрофізика" у складі фізико-математичного факультету відновленого Київського державного університету.

1937 р. – організація кафедри електрофізики на базі однойменної спеціалізації.

1940 р. – кафедра увійшла до складу новоствореного фізичного факультету.

1952 р. – перейменована на кафедру електроніки. Стала базою для організації радіофізичного факультету; початок 60-х років XX ст. – перейменована на кафедру фізичної електроніки.

1965 р. – на базі кафедри організовано проблемну лабораторію фізичної електроніки (зараз – науково-дослідницька лабораторія фізичної електроніки).

1973 р. – на базі кафедри організовано нову кафедру кріогенної та мікроелектроніки (зараз – кафедра нанофізики та наноелектроніки).

1996 р. – на базі кафедри організовано науково-дослідницький сектор теорії та моделювання плазмових процесів (спільно з Інститутом теоретичної фізики НАН України ім. М.М. Боголюбова).

2002 р. – на кафедру покладено викладання дисциплін радіоелектронного циклу для студентів молодших курсів.

2004 р. – урочисте відзначення 100-річчя від дня народження Н.Д. Моргуліса, випущено спеціальний номер журналу "Вісник КНУ. Радіофізика та електроніка".

2010 р. – на базі кафедри організовано нову кафедру радіотехніки та радіоелектронних систем.

2014 р. – урочисте відзначення 110-річчя від дня народження Н.Д. Моргуліса, відкриття меморіальної дошки.

Розвиток наукових досліджень на кафедрі

Дослідження в галузі фізичної електроніки в 1933–1964 рр. Першими дослідженнями в галузі фізичної електроніки, які проводились на кафедрі, були всебічні дослідження катодного розпорошення методами електронної емісії (Н.Д. Моргуліс, М.П. Бернадинер, іПотіоха, 1937–40 рр.; ці результати частково ввійшли до докторської дисертації Н.Д. Моргуліса). Вивчалися поріг та адсорбційна рівновага активних моноатомних плівок, присутність яких обумовлює високу електронну емісію і визначає можливість практичного використання катодів у різних приладах. Дослідження дії спеціально зробленої моделі для вивчення цього явища дозволило отримати вагомі дані щодо деталей статистичного характеру явища катодного розпорошення для побудови його теорії.

Ще в 1936 р. проф. Н.Д. Моргуліс уперше вказав на напівпровідникову природу оксидних катодів, які в той час почали широко застосовуватися в електронних лампах. Ця піонерська ідея мала надзвичайне значення для подальшого розвитку емісійної електроніки. Вона стала основою для створення першої теорії тунельної емісії з напівпровідників (задовго до робіт Р. Фаулера та Л. Нордгейма). Тоді ж Моргуліс разом зі співробітниками детально вивчили роботу оксидних катодів, застосувавши систему зондів у напівпровідниковому шарі катода. Таким шляхом уже тоді вдалося встановити наявність на межі катода з керном приграничного запірного шару, якому надалі надавалося дуже велике значення з огляду на його вплив на термоемісію катода. У той самий період розпочалися дослідження вторинної іонно-електронної емісії та компенсації об'ємного заряду електронів позитивними іонами (Н.Д. Моргуліс, М.Є. Гуртовий, Г.І. Коваленко). У результаті була створена одна з перших у світі теорій вторинної емісії. Пізніше (у 1950-ті рр.) М.Г. Находкін вказав на принципову роль кінетики електронів у цьому ефекті.

Ще в 1930-х рр. Н.Д. Моргуліс розпочав роботи з вивчення поверхневої іонізації (зокрема, експериментальні дослідження поверхневої іонізації атомів цезію на поверхні вольфраму) і створив одну з перших квантово-механічних теорій поверхневої іонізації. Зазначимо, що пізніше на основі цього ефекту були створені Q-машини, які знайшли широке застосування як джерела спокійної плазми.

При вивченні електричного розряду в парах цезію (проводилось на кафедрі під керівництвом Н.Д. Моргуліса в 1939–1940 рр. разом з М.Є. Гуртовим і Г.І. Коваленком) виявлено явище, яке лягло в основу термоемісійного методу безпосереднього перетворення теплової енергії на електричну. Дослідження продовжили в 1949-50 рр. Н.Д. Моргуліс зі співробітниками в ІФ АН УРСР, де він до 1961 р. працював завідувачем відділу.

Важливим етапом у становленні кафедри фізичної електроніки як наукового колективу було виконання урядової теми "Катод" (наук. керівник – Н.Д. Моргуліс, відп. вик. – М.Г. Находкін, 1954–57 рр.), яка ставила за мету розробку рекомендацій щодо збільшення строку служби оксидних катодів. При виконанні цієї теми була створена оригінальна методика дослідження стійкості оксидних катодів до іонного бомбардування з використанням газорозрядного джерела іонів (Є.Т. Кучеренко, В.П. Дем'яненко, Г.М. Тальнова).

У 1950-ті роки кафедра стала одним із перших колективів у Радянському Союзі, де почалися систематичні дослідження питань фізики і техніки високого й надвисокого вакууму. У ці роки Н.Д. Моргуліс і Г.Я. Пікус створили високовакуумний мас-спектрометр, який знайшов своє застосування в багатьох науково-дослідних і заводських лабораторіях. У 1962 р. за створення надчутливого мас-спектрометра Н.Д. Моргуліс, Г.Я. Пікус і В.Ф. Шнюков були нагороджені відповідно золотою, срібною та бронзовою медаллю ВДНГ СРСР. Цей мас-спектрометр був упроваджений у виробництво на Сумському заводі електронного машинобудування.

Принципово важливими були експериментальні дослідження дифракції повільних електронів, виконані Д.О. Городецьким та О.М. Корнєвим Їхня стаття була надрукована в 1959 р. одночасно з роботою К. Девідсона та Л. Джермера з цього питання. Однак в експериментах Девідсона та Джермера зняття однієї електронограми вимагало 48-годинних вимірювань, тоді як установка Городецького–Корнєва дозволяла спостерігати процес у реальному часі. Саме такий підхід з часом зробив дифракцію повільних електронів одним з найпоширеніших експериментальних методів діагностики поверхні.

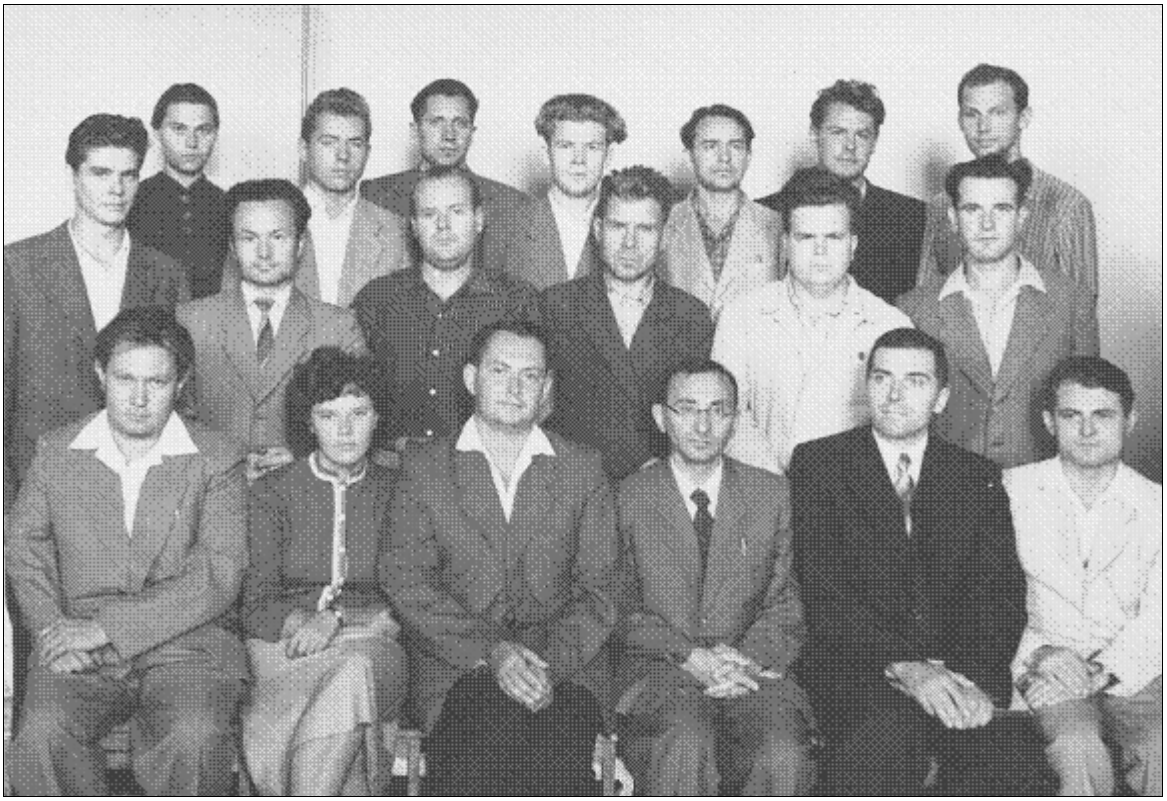

Кафедра фізичної електроніки 1959 р.

Дослідження в галузі фізики плазми в 1960–90-х роках. Дослідження з фізики низькотемпературної плазми на кафедрі в 1960-х рр. були нерозривно пов'язані з проблемою перетворення теплової енергії на електричну. Продовжуючи дослідження термоемісійного методу безпосереднього перетворення теплової енергії на електричну, розпочаті на кафедрі ще до війни, Н.Д. Моргуліс разом з Ю.П. Корчевим, Ю.І. Чутовим, І.М. Полушкіним, А.М. Пржонським, Д.Я. Дудком та О.І. Кравченком провели широкий спектр досліджень фізичних принципів, які лежать в основі цього методу.

Досліджено комплекс об'ємних та приелектродних явищ у дуговому розряді в парах цезію, природу іонізації в плазмі, особливості випромінювання інфрачервоного резонансного дублета тощо (Н.Д. Моргуліс, Ю.П. Корчевой, 1961–1965). Досліджено фізичні явища в "короткій" дузі в парах цезію, яка служить фізичною моделлю плазмового термоелектронного перетворювача (ТЕП) енергії (Н.Д. Моргуліс, Ю.П. Корчевой, Ю.І. Чутов, 1962–1965), а також емісійні властивості та продукти випаровування ряду матеріалів у зв'язку з їх використанням в цих перетворювачах (Н.Д. Моргуліс, Ю.А. Дядюн, Р.І. Марченко, Б.І. Михайловський).

Досліджено властивості плазми інертних газів при підвищеному тиску з домішкою легкоіонізованих парів лужних елементів за низького тиску як фізичної моделі домішкового газоплазмового напівпровідника (Н.Д. Моргуліс, І.М. Полушкін, 1962–1965). Визначені константи деяких елементарних процесів, зокрема, ефективний переріз розсіювання електронів атомами цезієвої та калієвої плазми за наявності інертного газу і без нього, ефективний переріз збудження та іонізації атомів калію і цезію в припороговій області, коефіцієнт рекомбінації при розпаді плазми в інертному газі з домішками парів цезію і калію (Н.Д. Моргуліс, Ю.П. Корчевой, І.М. Полушкін, 1962–1965).

Уперше було показано, що в міжелектродному проміжку термоемісійного перетворювача створюється плазма, яка визначає параметри ТЕПа в тих режимах його роботи, які відповідають реальним умовам експлуатації. У подальшому ці уявлення про роль плазми в ТЕПі стали загальновизнаними як серед вітчизняних учених, так і за кордоном.

Особливо слід відзначити відкриття явища фоторезонансної плазми в 1965 р. (Н.Д. Моргуліс, Ю.П. Корчевой, А.М. Пржонський). Воно було зареєстровано Міжнародною асоціацією авторів наукових відкриттів, яка видала Київському університету свідоцтво NA-118 від 4.08.1998 р.

Науковий напрям, пов'язаний з дослідженням НВЧ-властивостей плазми, у 1949 р. започаткував С.М. Левитський, коли працював на кафедрі як аспірант. У його кандидатській дисертації було вперше виявлено і досліджено явище катодного розпорошення у високочастотному розряді – процес, який згодом знайшов найширше застосування у технології виготовлення транзисторів і інтегральних мікросхем. Роботи Левитського з дослідження властивостей високочастотних розрядів (зокрема, відкриття α- та γ-режимів ємнісного ВЧ-розряду) здобули світове визнання і стали класичними, про що свідчать їх цитування як піонерських у численних наукових статтях, монографіях та довідниках.

Із 1957 р. С.М. Левитський разом з І.П. Шашуріним почали займатися розробкою нових надвисокочастотних методів діагностики плазми та її взаємодії з пучками електронів. Під його керівництвом співробітники кафедри М.С. Баранчук, І.П. Шашурін, В.З. Шаповал та К.Г. Філоненко в 1960–70 рр. дослідили динаміку розвитку плазмово-пучкової взаємодії та отримали цілу низку важливих даних про особливості поширення і нелінійної взаємодії різних видів спрямованих хвиль у плазмових хвилеводах. Під керівництвом Левитського його аспірант Ю.І. Буракін провів розробку плазмових випромінювачів – антени НВЧ-діапазону (1970-ті роки). У наступні роки робота НВЧ-випромінювачів у плазмі як діагностичних зондів була вивчена детально (С.М. Левитський, І.П. Шашурін, В.Ф. Вірко, Т.А. Грязнова, К.Ф. Галушкевич, О.П. Горчинська, О.В. Ісаров, К.С. Карплюк, Л.О. Малюк, В.М. Оленський, І.В. Тимощук, К.Г. Філоненко, О.З. Шаповал).

Було виявлене явище нелінійного самоузгодження плазми НВЧ-розряду з випромінювачами НВЧ-діапазону, яке є ефективним методом накачування енергії в НВЧ-розряд, що важливо при розробці та створенні високоефективних плазмотронів для плазмохімічних реакторів (С.М. Левитський, І.П. Шашурін, Т.А. Грязнова, К.Г. Філоненко).

На поч. 1960-х рр. на кафедрі проводилися дослідження пеннінгівського та плазмово-пучкового розрядів (В.А. Саєнко, І.А. Яворський). Вони стали базою для створення терміонного методу осадження тонких плівок (авт. св.1965 р.).

У 1960-ті рр. за ініціативи проф. Н.Д. Моргуліса його аспірант Ю.І. Чутов розпочав на кафедрі експериментальні дослідження однократної імпульсної рухомої плазми в електричних ударних трубках та її взаємодії з магнітним полем (новий науковий напрям досліджень – фізика плазми з рухомою межею). Під керівництвом проф. Ю.І. Чутова плідно працював науковий колектив: В.Й. Берко, Ю.В. Вовченко, В.А. Жовтянський, О.В. Королюк, О.І. Кравченко, О.Ю. Кравченко, Т.Є. Лиситченко, В.Л. Мельниченко, Ю.В. Міц, В.Ю. Палкін, В.М. Подольський, В.Я. Черняк, Д.Л. Чернолуцький та ін. У результаті всебічних експериментальних досліджень і комп'ютерного моделювання імпульсної плазми з рухомою межею, які провів цей колектив, з використанням оригінальних оптичних і зондових методик з високою просторовою та часовою роздільною здатністю, встановлені нові фізичні властивості обмежених плазмових згустків та струменів, а також нестаціонарних газових розрядів. Зокрема, було експериментально виявлено явище електричної детонації при поширенні ударних хвиль у газорозрядній плазмі та їх прискорення при переході межі поділу між плазмою та нейтральним газом, виявлено інтенсивне охолодження плазмових згустків унаслідок руху їхніх меж, встановлено умови виникнення ударних хвиль при взаємодії імпульсної плазми з нейтральним газом (Ю.І. Чутов, О.Ю. Кравченко, В.М. Подольський, 1980–1985). Окрім того, було розроблено ефективний ТЕП з додатковим пульсуючим розрядом (Ю.І. Чутов, О.І. Кравченко, Т.Є. Лиситченко, 1978–1980) і методику контролю якості виготовлення макетів і дослідних зразків плазмових індикаторів (Ю.І. Чутов, М.С. Баранчук, О.І. Кравченко, Т.Є. Лиситченко, Ю.В. Міц,1973–1976).

Була також виявлена й пояснена принципова відмінність впливу процесів перенесення на розпад розрідженої та щільної низькотемпературної плазми та метод подібності для визначення впливу самопоглинання випромінювання на заселення рівнів атомів інертних газів (В.А. Жовтянський, О.М. Новік), а також проведені дослідження пристінкових шарів у щільній плазмі за допомогою дифузійних зондів (В.А. Жовтянський, В.І. Кочетков, О.М. Новік, Б.Г. Ханько).

Стимулом для розширення зазначених напрямів наукових досліджень стало звернення ІЕЗ ім. Є.О. Патона до університету щодо діагностики плазми електричної дуги, що вільно підтримується в атмосфері між мідними електродами. Основна проблема полягала в тому, що дуга хаотично переміщується по поверхні електродів. Наявний потенціал швидкісних методів діагностики дозволив відносно легко вторгнутись з власне спектральними вимірюваннями такого нестаціонарного об'єкта (І.Л. Бабіч, А.М. Веклич, В.А. Жовтянський). Виявлена нерівноважність електродугової плазми, причиною якої є перенесення резонансного випромінювання (І.Л. Бабіч, А.М. Веклич, В.А. Головкіна, В.А. Жовтянський, А.І. Чередарчук). Моделювання процесів в електричній дузі підтвердило неістотність впливу деміксингу компонент у плазмі (В.А. Жовтянський, Е. Мерфі, В.М. Патріюк).

У 1996 р. відповідно до угоди між НАН України та Київським університетом імені Тараса Шевченка, на кафедрі було створено науково-дослідний сектор теорії та моделювання плазмових процесів (наук. керівник –Ю.І. Чутов , зав. сектора – Т.Є. Лиситченко), що водночас є складовою спільного науково-дослідного відділу теорії та моделювання плазмових процесів Інституту теоретичної фізики ім. М.М. Боголюбова (зав. відділу – А.Г. Загородній).

Особливого розвитку набуло на кафедрі комп'ютерне моделювання фізичних процесів у запорошеній плазмі (Ю.І. Чутов, О.Ю. Кравченко, В.С. Яковецький, В.М. Зюзь, Р.Д. Смірнов, 1997–2000)

У 1990-х роках на кафедрі під керівництвом доц. В.Я. Черняка у співробітництві з хімічним факультетом університету почали успішно розвиватися комплексні дослідження нерівноважної плазми газових розрядів у зв'язку з можливими застосуваннями в екології, зокрема, для очищення води. Були створені оригінальні експериментальні установки та вказана можливість керування іонізаційною і рекомбінаційною нерівноважністю плазми несамостійних розрядів.

На кафедрі були проведені теоретичні дослідження зв'язку елементарних та колективних процесів у нерівноважній плазмі. При цьому була створена теорія рекомбінації заряджених частинок з урахуванням внеску колективних процесів, проведено аналіз гетерогенної іонізаційної релаксації електронів на поверхні діелектриків, отримані її енергетичні та спектральні характеристики (Ю.Я. Коган, Є.В. Мартиш, 1978–1983).

У подальшому розвивалась теорія гетерогенної релаксації двоатомних молекул при високому рівні коливного збудження та її вплив на релаксацію молекулярної плазми (Є.В. Мартиш, А.В. Недоспасов, В.М. Мальнєв, С.М. Любка).

Дослідження з фізики поверхні та емісійної електроніки у 1960-х – 1990-х роках. Наукові дослідження з фізики поверхні та емісійної електроніки на кафедрі в 1960–1970-ті роки проводилися під керівництвом професорів М.Г. Находкіна, Г.Я. Пікуса та Д.О. Городецького. Великого практичного значення набули розпочаті ще в 1963 р. паралельні дослідження термоелектронної та термоіонної емісії кремнію (М.Г. Находкін, Г.О. Зиков). Ці дослідження, виконані у співдружності з Інститутом фізики НАН України, дозволили виявити в кристалах кремнію великі домішкові накопичення лужних металів, які суттєво впливають на роботу напівпровідникових приладів. Тим самим виникла надзвичайно важлива для сучасного напівпровідникового приладобудування проблема створення кристалів кремнію, вільних від домішок лужних металів.

Широке визнання одержали результати дослідження процесу взаємодії електронів середніх енергій із твердим тілом, які дозволили визначити важливі характеристики кінетики руху електронів у твердому тілі (М.Г. Находкін, П.В. Мельник, І.П. Коваль, Ю.М. Кринько та ін.). Ці роботи сприяли розкриттю механізму емісії нового класу ефективних емітерів із негативною спорідненістю з електроном і відіграли помітну роль у розвитку електронної спектроскопії твердого тіла та створенні нових її різновидів.

На основі дослідження механізму взаємодії електронів з діелектриками, виконаного під керівництвом проф. М.Г. Находкіна, були з'ясовані особливості процесу формування прихованого електростатичного зображення при термопластичному записі інформації. Ці роботи привели до створення систем для запису голограм у реальному масштабі часу в усій видимій області спектра, що сприяло створенню швидкодіючих напіваналогових оптоелектронних пристроїв. За ці та інші дослідження, які заклали фізичні основи запису інформації у фазових термопластичних середовищах, М.Г. Находкіну, М.Г. Кувшинському, В.П. Немцеву, І.Я. Подчерняєву в 1970 р. була присуджена Державна премія УРСР.

Ще в 1959 р. Д.О. Городецький разом із співробітниками (О.М. Корнєв, Ю.П. Мельник, В.К. Скляр, С.О. Шевляков, Ю.Г. Щудло, А.О. Ясько) розпочали вивчення структури адсорбованих на поверхні твердого тіла плівок методом дифракції повільних електронів. За допомогою розробленого на кафедрі оригінального приладу було проведено систематичне дослідження розміщення адсорбованих атомів на різних гранях монокристалів тугоплавких металів і кремнію. Результати цих робіт дозволили з'ясувати вплив різних факторів на структуру та електронні властивості моноатомних плівок. Був встановлений реконструктивний характер адсорбції кисню на вольфрамі та ренії.

За допомогою високовакуумної мас-спектрометричної методики було виконано широке коло досліджень фізики оксидного катоду (Г.Я. Пікус, В.Ф. Шнюков). У подальшому були з'ясовані загальні закономірності кінетики випаровування кристалів хімічних сполук у вакуумі (Г.Я. Пікус, Г.М. Тальнова). Дослідження випаровування іонних кристалів показали вирішальну роль електронної підсистеми кристала в процесі його випаровування та формування поверхневих шарів із заданими електронними властивостями за допомогою впливу на електронну підсистему, зокрема, шляхом нагрівання, зовнішнього опромінювання або накладання зовнішнього електричного поля, що відкрило нові перспективи для створення мікроелектронних пристроїв. Було розроблено метод виготовлення термокатодів на основі молекулярно напилених плівок оксидів лужноземельних металів зі значним строком служби (Г.Я. Пікус, Б.І. Михайловський, Г.М. Тальнова, В.П. Тетеря, В.Ф. Шнюков).

На основі узагальнення даних дослідження динаміки випаровування та зміни складу й електронних властивостей кристалів бінарних напівпровідникових сполук при високовакуумному відпалі було доведено, що в основі порушення стехіометрії лежить явище електронної саморегуляції ступеня відхилення від стехіометрії (Г.Я. Пікус, В.П.Тетеря, Г.М. Тальнова, В.Ф. Шнюков, Г.Є. Чайка). Розроблено теорію випаровування і формування складу бінарних напівпровідникових сполук з іонним зв'язком (Г.Я. Пікус, Г.Є. Чайка, В.Ф. Шнюков).

На основі твердих розчинів лужноземельних металів була розроблена нова технологія виготовлення високоефективного низькотемпературного термокатода, емісійна здатність якого в 3–5 разів перевищувала ефективність тогочасних вітчизняних та зарубіжних аналогів (Г.Я. Пікус, В.Ф. Шнюков, Б.І. Михайловський, О.Є. Лушкін, В.М. Телега). Були проведені комплексні дослідження впливу технологічних параметрів матриць металевопоруватих катодів на їхні фізико-хімічні та емісійні властивості з метою оптимізації експлуатаційних характеристик термоемітерів. Для з'ясування механізму емісії металевопоруватих катодів із домішками вивчалася взаємодія компонентів активної речовини звичайних металевопоруватих катодів зі скандієм (В.Ф. Шнюков, Г.Я. Пікус, Б.І. Михайловський, О.Є. Лушкін, В.М. Телега, І.І. Бех).

З приходом на кафедру в 1999 р. проф. В.В. Ільченка в науковій тематиці кафедри з'явилися нові напрями:

– дослідження фізичних властивостей гетерофазних сенсорних систем;

– дослідження адсорбційних та десорбційних явищ у гетерофазних сенсорних структурах та дослідження можливості використання сенсорних систем для діагностики хвороб людини за продуктами дихання.

Сучасні дослідження в галузі плазмової електроніки. Дослідження таких явищ, розпочаті свого часу на кафедрі С.М. Левитським зі співробітниками, тривають уже понад тридцять років. Серед останніх результатів досліджень у цьому напрямі можна назвати вивчення перехідного випромінювання електронних пучків в умовах активних експериментів у іоносфері та космосі (С.М. Левитський, І.О. Анісімов, О.І. Кельник та ін.). Виявлено ефект перенесення електромагнітних хвиль через шари щільної плазми за допомогою електронних пучків, що також заснований на перехідному випромінюванні (ефект був теоретично передбачений С.М. Левитським та І.О. Анісімовим, а пізніше виявлений і детально вивчений в експериментах Л.І. Романюка зі співробітниками (ІЯД НАН України) та за допомогою комп'ютерного моделювання (І.О. Анісімов, І.Ю. Котляров, Г.В. Лізунов, М.Й. Кіянчук (Соловйова)).

Запропоновано також метод діагностики неоднорідних плазмових утворень за перехідним випромінюванням коротких електронних згустків (І.О. Анісімов, К.І Любич) та за допомогою методів надширокосмугової радіолокації (С.М. Левитський)

Останнім часом розвивається комп'ютерне моделювання однорідних та неоднорідних плазмово-пучкових систем (С.М. Левитський, І.О. Анісімов, Т.В. Сіверський, О.І. Кельник, С.В. Сорока, Т.Є. Літошенко, М.Й. Соловйова, Ю.М. Толочкевич). Детально вивчено динаміку неоднорідної плазми в області локального плазмового резонансу, збуджуваній модульованим електронним пучком або високочастотним електричним полем накачування (І.О. Анісімов, Т.В.Сіверський, О.І. Кельник, С.В. Сорока, Т.Є. Літошенко)

Вивчено динаміку поперечно обмежених модульованих електронних пучків в однорідній та неоднорідній плазмі (І.О. Анісімов, Т.Є. Літошенко, М.Й. Соловйова) Досліджуються кінетичні ефекти, що супроводжують плазмово-пучкову взаємодію – розігрів плазми в області локального плазмового резонансу при її збудженні модульованим електронним пучком, утворення потоків частинок у фоновій плазмі в процесі розвитку плазмово-пучкової нестійкості (І.О. Анісімов, С.М. Левитський, Д.М. Танигіна). За допомогою комп'ютерного моделювання досліджено збудження кільватерних хвиль у плазмі електронними згустками, у тому числі, за наявності поздовжнього магнітного поля (І.О. Анісімов, Т.Є. Літошенко, Ю.М. Толочкевич, М.А. Щербінін).

Сучасні дослідження запорошеної плазми. Дослідження запорошеної плазми проводяться в рамках науково-дослідного сектору теорії та моделювання плазмових процесів у тісній співпраці з Інститутом теоретичної фізики ім. М.М. Боголюбова (акад. НАН України А.Г. Загородній). Ряд робіт було проведено з метою вивчення структури приелектродних шарів у запорошеній нерівноважній плазмі (Ю.І. Чутов, О.Ю. Кравченко, Р.Д. Смирнов, В.С. Яковецький), дослідження впливу пилових частинок на властивості радіочастотних розрядів (Ю.І. Чутов, О.Ю. Кравченко, Т.Є. Лиситченко, В.М. Зюзь), дослідження динаміки пилових згустків (О.Ю. Кравченко, М.М. Юрчук, І.С. Марущак) та структури плазмово-пилових кристалів (Ю.І. Чутов, О.Ю. Кравченко, Р.Д. Смирнов).

Останніми роками виконано ряд робіт з дослідження динаміки пилового компонента в радіочастотних розрядах низького тиску, у результаті яких було показано можливість утворення шаруватої структури розряду та запропонований фізичний механізм її формування (О.Ю. Кравченко, А.В. Вакуленко, Ю.А. Яструб, Г.І. Левада). Проведено моделювання різноманітних дисипативних структур у запорошеній плазмі, включаючи плазму радіочастотних розрядів та пристінкові області термоядерних реакторів, а також досліджено вплив на ці структури магнітного поля (О.Ю. Кравченко, Т.Є. Лиситченко, Ю.А. Яструб, І.С. Марущак).

За допомогою методу молекулярної динаміки проведено моделювання заряджання та екранування пилових частинок у нерівноважній плазмі за наявності іонного потоку та магнітного поля. Досліджено залежність сили взаємодії між пилинками, зумовлену ефектом екранування, від тиску нейтрального газу та величини магнітного поля (О.Ю. Кравченко, А.В. Вакуленко, Т.Е. Лиситченко, Г.О. Гавриш).

Сучасні дослідження з плазмохімії. У роботах проф. В.Я. Черняка зі співробітниками та аспірантами (І.Л. Бабич, Ю.П. Веремій, В.А. Зражевський, С.В. Ольшевський, І.В. Присяжневич, В.В. Юхименко, О.А. Недибалюк, С.М. Сидорук та ін.) було вперше:

– досліджено вплив розчиненого у воді повітря на фізико-хімічні властивості води після плазмової обробки, у результаті чого виявлена можливість прояву не тільки відомого "кислотного ефекту" плазмової обробки води (зменшення показника pH після обробки води в плазмово-рідинній системі), але й "лужного ефекту" такої обробки, тобто збільшення показника pH після обробки попередньо дегазованої води у плазмово-рідинній системі;

– виявлено ефект пам'яті води щодо її обробки в плазмово-рідинній системі, який може приводити протягом декількох діб залежно від умов обробки або до продовження деструкції вихідних органічних забруднювачів, або ж навпаки, до їх часткового відновлення;

– показано існування бактеріостатичного ефекту при стерилізації води у плазмово-рідинних системах на основі вторинного розряду;

– проведено дослідження ефективності деструкції органічних речовин у воді залежно від їхньої початкової концентрації, які показали перспективність використання плазмово-рідинних систем на основі вторинних розрядів для знешкодження токсичних відходів;

– виявлено умови як ефективного висадження іонів важких металів із водяних розчинів, так і розчинення слабко розчинних металів у водяних розчинах.

– розроблено ряд систем для ефективного стимулювання плазмою процесів спалення та реформування вуглеводнів у синтез-газ.

Сучасні дослідження термічної плазми дугового розряду. Науковою групою проф. А.М. Веклича – канд. фіз.-мат. наук І.Л. Бабіч, доц. В.Ф. Борецький, інж. В.Є. Осідач, канд. фіз.-мат. наук А.В. Лебідь, ас. С.О. Фесенко та ін. виконуються комплексні спектроскопічні та металографічні дослідження плазми електродугового розряду між електродами з композитних матеріалів. Серед наукових здобутків групи необхідно виділити такі:

– реалізована спектроскопічна методика діагностики квазістаціонарної плазми із застосуванням приладів із зарядовим зв'язком;

– виконані комплексні дослідження плазми електродугового розряду між електродами з композитних матеріалів на основі міді (Cu-W, Cu-Mo, Cu-Mo-LaB6) і срібла (Ag-Ni, Ag-C, Ag-CdO). Встановлений взаємозв'язок параметрів досліджуваної плазми (температури та електронної концентрації) зі станом робочого шару на поверхні електродів;

– розроблена спектроскопічна методика визначення вмісту домішок металів у плазмі електричної дуги, що горить у повітрі між багатокомпонентними електродами;

– виконані дослідження плазми електродугового розряду, що горить у потоці CO2 між мідними електродами. Встановлений взаємозв'язок стану досліджуваної плазми з теплофізичними характеристиками робочого газу.

Сучасні дослідження з емісійної електроніки. Основними напрямками емісійних досліджень (проф. В.В. Ільченко, доц. І.І. Бех та доц. О.Є. Лушкін) є:

– вивчення потужних термоемітерів електронів;

– аналіз процесів у електронних автоемітерах, які є основою сучасної вакуумної мікроелектроніки;

– дослідження впливу зовнішніх факторів на склад поверхні та продукти випаровування багатокомпонентних сполук з різним ступенем іонності.

Сучасні дослідження з фізики наногетерофазних структур. На кафедрі проводяться роботи, спрямовані на інтеграцію нанорозмірних систем у мікроелектронну технологію з метою створення газових та біосенсорів (проф. В.В. Ільченко, доц. І.І. Бех, доц. О.Є. Лушкін, ас. А.М. Горячко, зав. НДЛ, ст. наук. співроб. В.М. Телега, ст. наук. співроб. О.І. Кравченко та ін.). Проведені роботи показали, що на основі гетероструктур нанорозмірний

адсорбційно активний шар – кремній можуть бути створені нелінійні елементи газових та біосенсорів нового покоління. У ролі адсорбційно-активних шарів використовуються наноструктуровані оксиди металів. Виявлені в них ефекти, що зумовлені нанорозмірністю системи, дозволили побудувати алгоритми аналізу зміни їх електрофізичних параметрів при зміні навколишнього газового та біологічного середовищ. Система параметрів, яка визначає нелінійні властивості такої гетероструктури, може бути цілком визначена з електричних вимірювань.

Кафедра фізичної електроніки 2016 р.

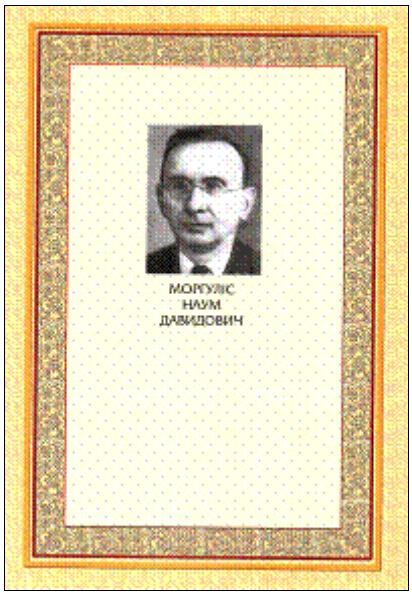

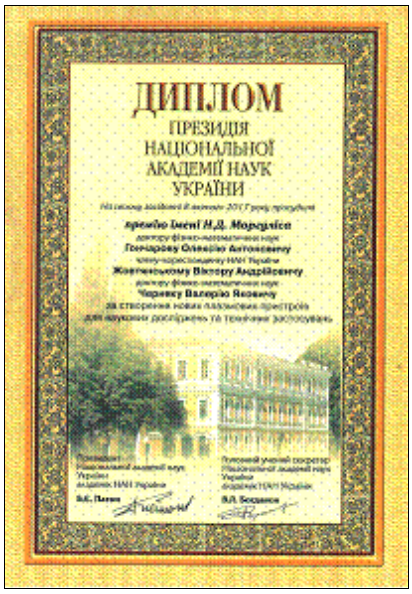

Кафедра пишається тим, що її співробітники двічі відзначені премією НАН України ім. Н.Д. Моргуліса:

2011 р. – І.О. Анісімов та В.В. Ільченко спільно з О.Г. Федорусом (ІФ НАН України) за роботи з генерування та динаміки електронних пучків у плазмі;

2017 р. – В.Я. Черняк спільно з О.А. Гончаровим (ІФ НАН України) та В.А. Жовтянським (ІГ НАН України) за створення нових плазмових пристроїв для наукових досліджень та технічних застосувань.

І. Анісімов, д-р фіз.-мат. наук,
А. Веклич, д-р фіз.-мат. наук,
кафедра фізичної електроніки,
факультет радіофізики, електроніки та комп'ютерних систем,
Київський національний університет імені Тараса Шевченка

Наукове видання

ВІСНИК

КИЇВСЬКОГО НАЦІОНАЛЬНОГО УНІВЕРСИТЕТУ ІМЕНІ ТАРАСА ШЕВЧЕНКА

РАДІОФІЗИКА ТА ЕЛЕКТРОНІКА

Випуск 1(25)

Статті подано в авторській редакції

Оригінал-макет виготовлено ВПЦ "Київський університет"

Формат 60x84$^{1/8}$. Ум. друк. арк. 7,5. Наклад 300. Зам. № 217-8513.
Гарнітура Arial. Папір офсетний. Друк офсетний. Вид. № Рф1.
Підписано до друку 11.10.17

Видавець і виготовлювач
Видавничо-поліграфічний центр "Київський університет"
01601, Київ, б-р Т. Шевченка, 14, кімн. 43
☎ (38044) 239 32 22; (38044) 239 31 72; тел./факс (38044) 239 31 28
e-mail: vpc_div.chief@univ.net.ua, redaktor@univ.net.ua
http: vpc.univ.kiev.ua
Свідоцтво суб'єкта видавничої справи ДК № 1103 від 31.10.02